EXPANDING NEUROCHEMICAL METHODS: IMPROVED DRUG DELIVERY AND MULTI-MODAL RECORDING

Douglas Charles Kirkpatrick

A dissertation submitted to the faculty at the University of North Carolina at Chapel Hill in partial fulfillment of the requirements for the degree of Doctor of Philosophy in the Department of Chemistry.

Chapel Hill
2016

Approved by:

R. Mark Wightman

Paul B. Manis

James W. Jorgenson

Royce W. Murray

Garret D. Stuber

ABSTRACT

Douglas Charles Kirkpatrick: Expanding Neurochemical Measurements: Improved Drug Delivery and Multi-Modal Recording
(Under the direction of R. Mark Wightman)

Neurochemical systems are studied by a variety of techniques in order to reveal information about physiological events such as cell firing, chemical changes, and vasoactivity. The aim of this dissertation is to improve upon the characterization ability of several existing methods through instrumental optimization and experimental design. First, microiontophoresis, a qualitative drug delivery technique which uses an electric current to eject drugs from a micropipette, is investigated for its quantitative capabilities. Factors underlying the volume affected by ejections and the concentration distribution of ejected species are determined. Next, the drug delivery rate during ejection from the micropipette is examined under a variety of conditions. From this, it is shown how the delivery rate can be modulated using the iontophoretic current and the concentration of the ejection solution. Further, controlled iontophoresis, which uses a carbon-fiber microelectrode to detect ejected electroactive species, is employed in an attempt to directly measure concentrations from ejections. To determine the accuracy, neurochemical responses following iontophoretic drug delivery are compared to responses from known drug concentrations. These studies reveal how systemic errors in ejection protocols can lead to inaccurate concentration evaluations. Practical experimental solutions to overcome these limitations are presented, and when instituted, lead to more accurate measurements. Lastly, a multi-modal recording method is demonstrated which combines patch

clamp electrophysiology and FSCV measurements in a brain slice. This is instituted with iontophoresis to provide a new way to simultaneously monitor cell behavior and chemical changes during drug delivery. In all, this work demonstrates how improvements in analytical methodologies can increase the power and scope of neurochemical investigations.

TABLE OF CONTENTS

LIST OF TABLES

LIST OF FIGURES

LIST OF ABBREVIATIONS AND SYMBOLS

A	Flow-injection analysis calibration factor
a	Radius of a perfect sphere
aCSF	Artificial cerebral spinal fluid
AP	Acetaminophen
C	Coulomb
CE	Capillary Electrophoresis
C_{int}	Concentration of iontophoresis barrel solution
C_m	Cell membrane capacitance
CV	Cyclic Voltammogram
D	Diffusion coefficient
DA	Dopamine
DF	Dilution factor
DHBA	3,4 - dihydroxybenzylamine
DOPAC	3,4 - dihydroxyphenylacetic acid
E	Electric field strength

EOF	Electroosmotic flow
F	Faraday's constant (96,485 C/mol)
FSCV	Fast-scan cyclic voltmmetry
g	Grams
HQ	Hydroquinone
Hz	Hertz
i	Current
IC_{50}	Concentration which minimizes response 50%
i_{ej}	Iontophoretic ejection current
J	Flux
J_o	Flux at boundary of a sphere
k_b	Boltzmann's constant ($1.38 \times 10^{-23} J \cdot K^{-1}$)
kg	Kilogram
LC	Liquid Chromatography
M	Molarity

mg	Milligram
min	Minutes
mM	Millimolar
mOsm	Milliosmoles
ms	Milliseconds
MSN	Medium spiny neuron
mV	Millivolts
N	Moles
n	Number of replicate trials
nA	Nanoamperes
NAc	Nucleus accumbens
NE	Norepinephrine
nM	Nanomolar
NPE	2-(4-nitrophenoxy) ethanol
Pe	Peclet number
Q	Charge

q	Elementary Charge ($1.6 \times 10^{-19} C$)
QP	Quinpirole
r	Distance from iontophoresis ejection origin
R_a	Access resistance
R_e	Carbon-fiber electrode resistance
R_i	Iontophoretic barrel resistance
R_m	Cell membrane resistance
R_s	Solution resistance
$Ru(bpy)_3^{2+}$	tris(2,2' - bipyridyl)dichlororuthenium(II)
s	Seconds
T	Temperature
t	Transport number
t_{ej}	Iontophoretic ejection time
V	Volts
V	Volume flow rate

v	Radial velocity
vBNST	Ventral bed nucleus of the stria terminalis
v_{ep}	Electroosmotic velocity
v_{mem}	Cell membrane potential
v_t	Velocity in an electric field
z	Molecular charge
ρ	Dimensionless distance ($\rho = r/a$)
µA	Microamperes
μ	Mobility in an electric field
μ_{ep}	Electroosmotic mobility
µm	Micrometers
µV	Microvolts

CHAPTER 1: INTRODUCTION: MICROIONTOPHORESIS AND PATCH CLAMP ELECTROPHYSIOLOGY

PART 1: MICROIONTOPHORESIS

Usage and Operating Principles

Iontophoresis describes the process by which an electric current is used to administer drugs from a solution. Many different modes of iontophoresis have been developed, and are further defined by their delivery method (Eljarrat-Binstock and Domb, 2006; Priya et al., 2006; Delgado-Charro, 2012). Microiontophoresis specifically refers to the ejection of a solution from a micropipette. This technique has been primarily used as a research tool in neurochemical investigations to deliver drugs and labeling agents to the brain. Figure 1.1 diagrams the delivery process. A constant current is driven through a micropipette barrel from a current source, which applies a voltage to the barrel solution based on its resistance. As a result, analytes are ejected by migration, which acts on ions, and electroosmotic flow (EOF), which affects all species (Herr et al., 2008).

Microiontophoresis has developed into a useful neurochemical drug delivery method for its ability to administer species quickly to a localized area (Herr and Wightman, 2013). Ejections can be performed in seconds, and unlike systemic delivery, drugs are confined to a small region of the brain. In addition, direct application ensures that drugs reach their target and are not inhibited by the blood brain barrier (Bloom, 1974). Despite these advantages, adoption of microiontophoresis as a neurochemical tool has been slowed by the inability to determine

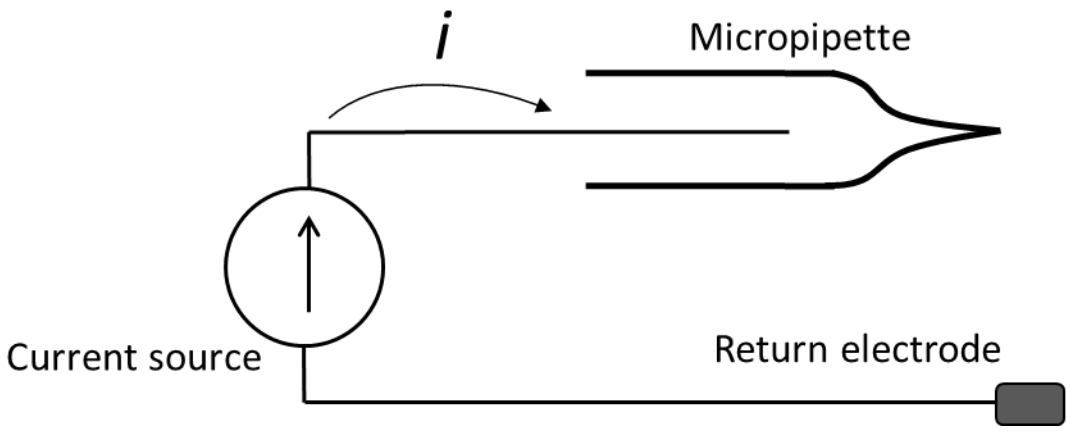

Figure 1.1 Representational diagram of microiontophoresis. An ejection current (*i*) is driven through a micropipette using a current source. A reference electrode placed in the ejection medium serves as a return for the current.

concentrations following ejections. In fact, delivery rates of species ejected from similarly fabricated barrels using identical currents and solutions result in concentrations spanning nearly an order of magnitude (Trubatch and Van Harreveld, 1972; Purves, 1980). Thus, there is no reliable method to calibrate ejections or compare delivery amounts between experiments. Additionally, no experimental strategy currently exists to accurately measure concentrations upon delivery. As a result, microiontophoresis has been largely excluded from quantitative applications.

Qualitative Use of Iontophoresis

Although the inability to administer drugs quantitatively has limited the impact of microiontophoresis, it remains a useful tool to probe qualitative aspects of neurochemical systems. Figure 1.2 demonstrates how iontophoresis was used to study the effect of norepinephrine (NE) on the local oxygen concentration in the brain of an anesthetized rat (Bucher et al., 2014). For this experiment, an iontophoresis probe containing a carbon-fiber microelectrode was inserted into the ventral bed nucleus of the stria terminalis (vBNST), a deep brain region with dense norepinephrine terminals. Here the electrode performed FSCV, which allowed it to detect concentration changes in NE and oxygen. Figure 1.2A displays the average FSCV color plot following stimulation of the ventral noradrenergic bundle, a group of cells with NE release sites in the vBNST. A horizontal cross section along the NE oxidation potential shows the time course of NE release (Figure 1.2A, panel II) (Bucher et al., 2013). Similarly, current generated along the oxygen reduction potential reveals that a biphasic oxygen change occurred following the stimulation (Figure 1.2A, panel I). To determine if the changes in oxygen were due to NE released from stimulation, exogenous NE was administered by iontophoresis while the oxygen response was examined. Figure 1.2B shows the color plot (lower) and oxygen

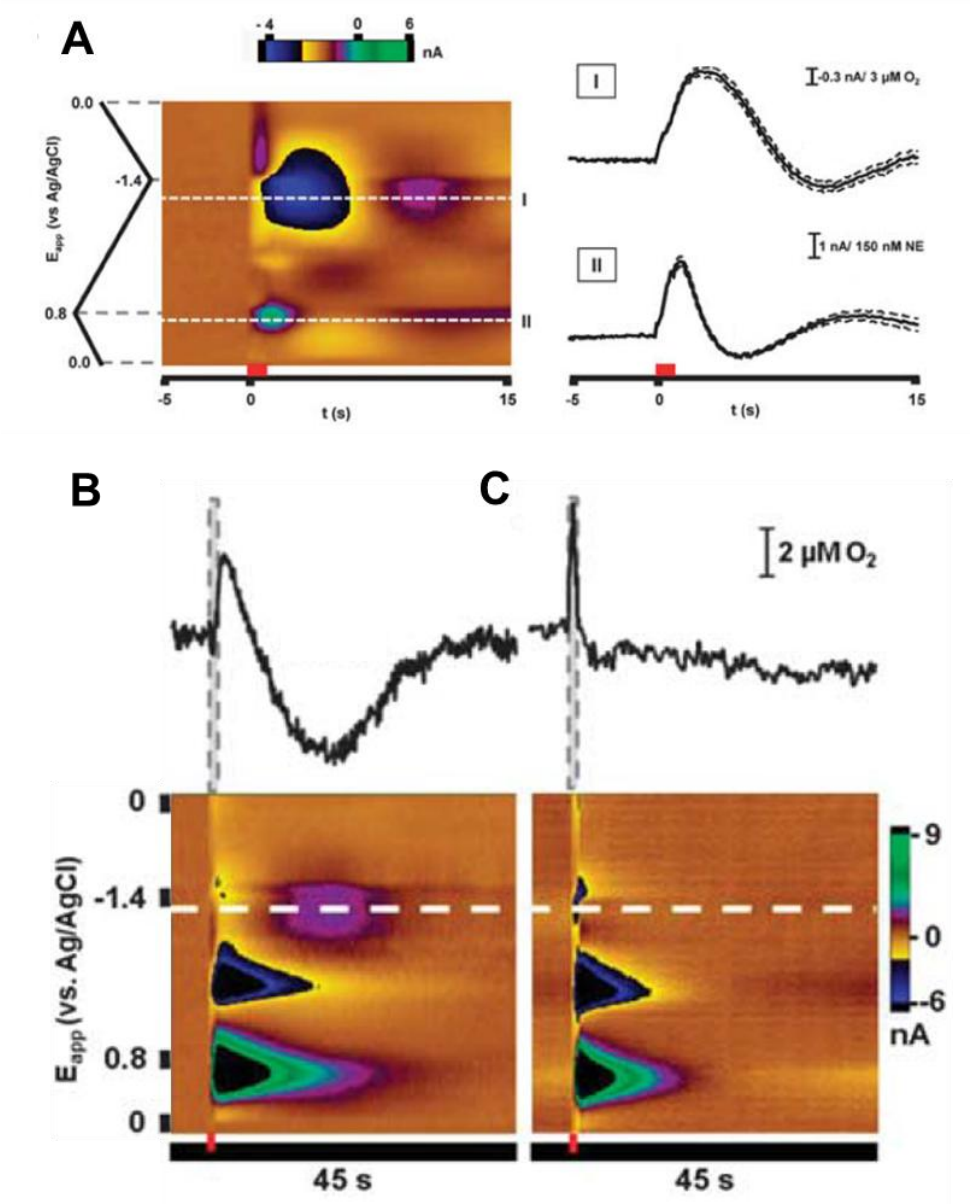

Figure 1.2. Effect of NE on oxygen concentration in the vBNST. (A) Average FSCV current following electrical stimulation of the ventral noradrenergic bundle (*n*=10 stimulations) *in vivo*. The time course of NE release is revealed by a horizontal cross-section of the FSCV current at the NE oxidation potential (0.75 V, panel II). Likewise, the oxygen concentration over time is obtained using the FSCV current along the oxygen reduction potential (-1.35 V, panel I). The red bars denote the time of stimulation. (B) Oxygen response (upper) and color plot (lower) to iontophoretically applied NE *in vivo*. The ejection (red bar) was performed in the vBNST. (C) Oxygen concentration (upper) and color plot (lower) for iontophoretic delivery of NE (red bar) to the vBNST in a brain slice.

concentration (upper) during iontophoretic administration of NE. Oxidation of NE administered by iontophoresis was detected by the carbon fiber, confirming its delivery to the region. Also detected was a biphasic oxygen change, which occurred without the stimulation. This indicated that the factors contributing to the oxygen response in 1.2A were at least partially triggered by released NE. Next, to determine if the cause of the oxygen changes was altered blood flow, the experiment was repeated in a slice preparation, where blood is absent. Figure 1.2C shows a color plot and oxygen trace following iontophoresis of NE in the vBNST of a brain slice. No oxygen change was observed, suggesting responses *in vivo* were due to altered blood flow. Thus the qualitative use of iontophoresis was able to determine that NE released in the vBNST causes changes in the local oxygen concentration, which result from vasoactivity.

A second example of qualitative iontophoretic delivery involves measuring the diffusion rate of ejected species to reveal structural information about the brain (Sykova and Nicholson, 2008). To accomplish this, ejections of tetramethylammonium were performed in brain tissue while an ion-selective electrode placed ~100 µm away was used for its detection. From the response at this electrode, the volume fraction and tortuosity of the brain were determined (Nicholson and Phillips, 1981; Rice and Nicholson, 1991). Thus, while providing quantitative results, this method does not require precise knowledge of the ejection quantity or concentration.

Methods to Measure Ejection Quantity

In order to improve the quantitative performance of iontophoresis, it is useful to understand how ejection conditions impact the delivery rate of ejected species. This includes factors such as the solution concentration, barrel width, and ejection current magnitude, all of which influence the ultimate ejection rate. Because of the low volume associated with ejections,

sensitive detection methods are required to quantify ejected species. One method that was incorporated previously in our lab for this purpose utilizes liquid chromatography (LC) with electrochemical detection (Herr et al., 2008). First, ejections of electroactive species are performed into small aliquots (~500 µL) of a buffered solution. Next, aliquots are injected onto a LC column, where separation and detection occur. Lastly, the concentration within each aliquot is determined by comparing the response at the detector with that of known standards. The total ejection quantity can be calculated from the volume of the aliquot, and the ejection rate is determined using the total time of the ejection. Due to the separation step on the LC column, this method is useful for comparing delivery rates of co-ejected species. A second method for determining ejection quantity utilizes fluorescence microscopy (Purves, 1979). This is performed by ejecting a fluorophore-containing solution ~50 µm below the surface of an agarose or polyacrylamide gel, while the fluorescence intensity of the ejected species is recorded. The use of a gel prevents convection from disturbing the natural spherical conformation of ejected species. After several minutes of continuous ejection, a steady-state around the pipette is achieved in which the fluorophore distribution is constant (Guy et al., 2012). Figure 1.3A shows a fluorescence image through the horizontal ejection plane following a 4 min ejection of fluorescein. Fluorescence intensities along each cross-section extending from the origin (dashed orange lines) are recorded and averaged to obtain a radial plot representing the concentration versus distance (Figure 1.3B). Total ejection quantities can be compared by integrating the radial distribution around a sphere, where the intensity at each distance is weighted by the volume it occupies. In addition to the ejection quantity, the fluorescence method is also useful for studying factors affecting the distribution of ejected species.

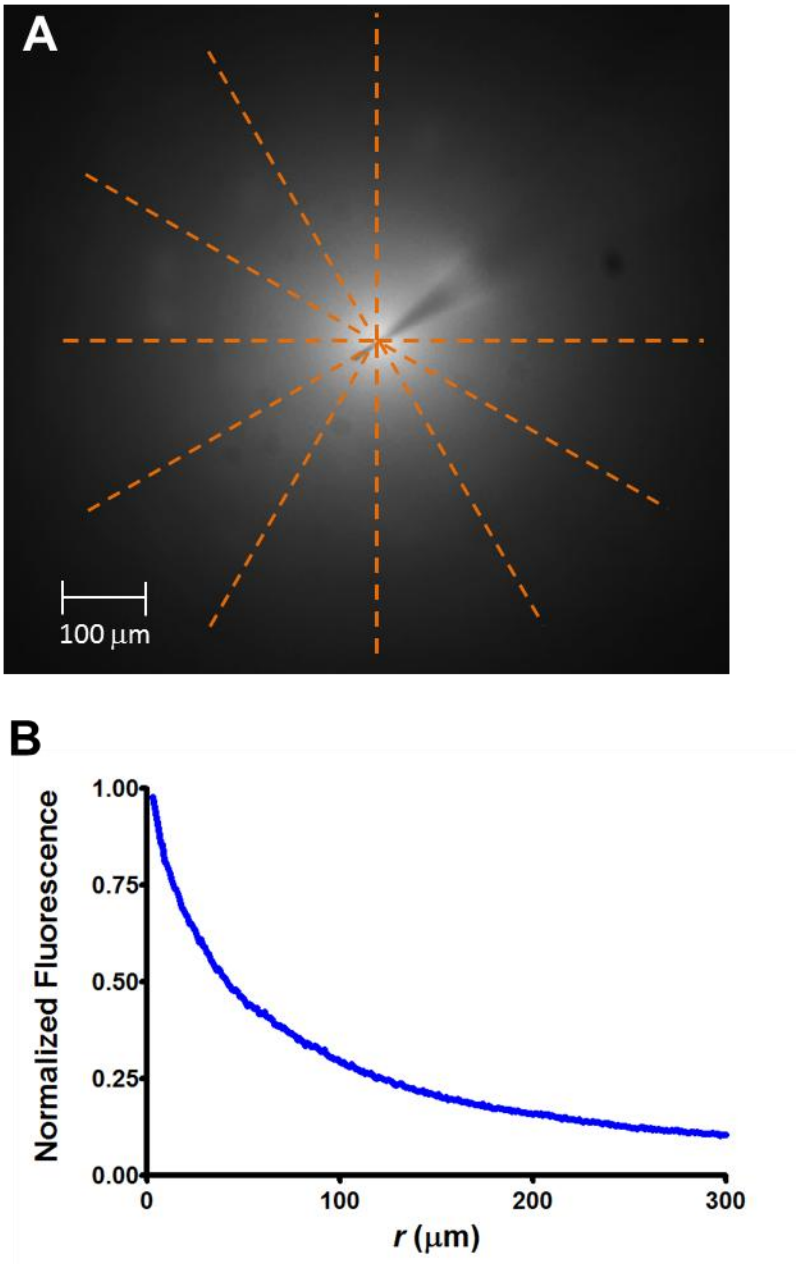

Figure 1.3 Determination of ejection quantity by fluorescence microscopy. (A) Fluorescence intensity following a 4 min ejection of a 5 mM fluorescein solution. Orange dashed lines represent cross-sections extending from the ejection origin. The intensities along cross-sections were averaged to generate (B), which shows the normalized fluorescence intensity versus distance from the ejection origin (r).

Factors Affecting Ejection Rates

Several studies have incorporated similar detection schemes to reveal how delivery rates are impacted by ejection conditions. A series of early reports following the development of microiontophoresis established that the ejection rate was proportional to the magnitude of the ejection current (Krnjevic et al., 1963; Purves, 1980; Hicks, 1984). Although different barrels ejected at different rates when similar currents were applied, each individual barrel resulted in a corresponding change to the ejection rate with the iontophoresis current. This provided a way to scale doses administered from a single barrel during experiments (Invernizzi et al., 2007). More recently, it was shown that much of the disparity between ejection rates of different barrels can be explained by variation in the tip diameter (Herr et al., 2008). Larger tip size leads to greater EOF, which in turn increases the ejection rate of all species. Also important to the delivery rate is the identity of the ejected species. Recall that in addition to EOF, migration acts on ionic species, which affects their ejection rates from the barrel. Species that have the same polarity as the voltage applied to the barrel solution will be ejected at faster rates than neutral molecules, while those of the opposite polarity will move slower. In addition to the molecular charge, the size of an analyte also affects its transport (Mudry et al., 2007). Larger species exhibit greater drag in solution, slowing their delivery relative to smaller compounds (Lee and Oh, 2014).

Compared to microiontophoresis, much more quantitative progress has been made in transdermal iontophoresis, which is used therapeutically to deliver drugs through the skin (Kasting, 1992). Here, multiple studies have examined how the delivery rate is affected by the concentration of the drug solution (Marro et al., 2001; Mudry et al., 2006b; Mudry et al., 2006a). These studies focus on the transport number, which represents the fraction of the current a species accounts for during ejection. Transport number theory predicts that when different ionic

species have comparable mobility rates in an electric field, the ejection quantity of each species will be proportional to the charge it accounts for in solution. In practice, this holds true for low molecular weight (< 250 g/mol) compounds, whose ejection rates can be modified by the inclusion of common salts to the drug solution. Importantly, this applies only to ions, since neutral species have no charge and do not contribute to the ejection current. Additionally, this relationship has yet to be demonstrated in microiontophoresis.

Controlled Iontophoresis

To further address the quantitative limitations of microiontophoretic drug delivery, several measurement strategies have been developed in attempts to measure concentrations upon ejection (Armstrong-James and Millar, 1980; Havey and Caspary, 1980; Ford et al., 2010). One such method, termed controlled iontophoresis, utilizes a carbon-fiber microelectrode inserted into a multibarreled probe, while the remaining barrels are used for ejections (Armstrong-James and Millar, 1979). As shown in Figure 1.4A, drug barrels terminate at the exposed surface of the carbon fiber, which allows electroactive species to be immediately detected upon ejection. Figure 1.4B displays the oxidation current of dopamine (DA) during a 60 s ejection, which was detected by FSCV performed on a carbon-fiber electrode. Upon initiation of the ejection, the FSCV current quickly rose to a steady-state value. In theory, the concentration from the ejection can be approximated by comparing the steady-state current with calibration by flow-injection analysis.

While controlled iontophoresis is useful for tracking ejections of electroactive species, not all drugs are electroactive. In these cases, markers are added to the drug solution to monitor ejection behavior. Markers are electroactive species that do not interfere with the neurochemical

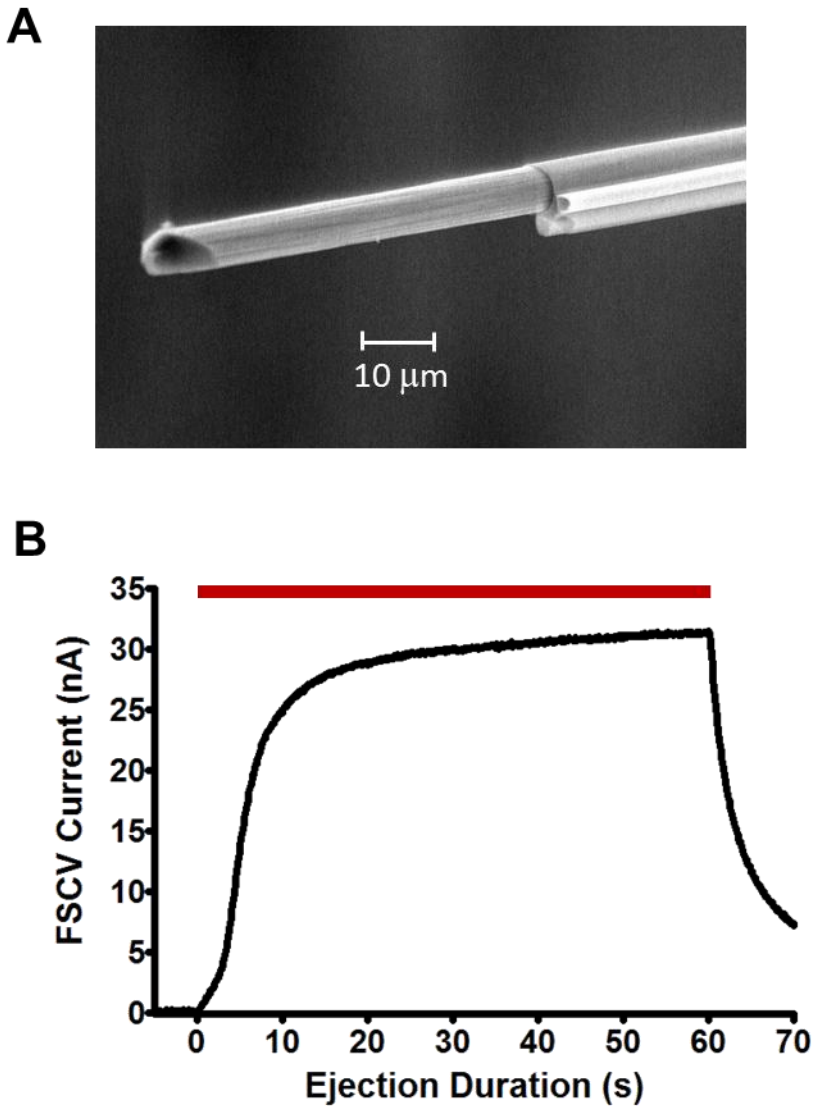

Figure 1.4 Controlled iontophoresis. (A) SEM micrograph of an iontophoresis probe containing a carbon-fiber microelectrode. (B) FSCV current of DA during a controlled ejection. An iontophoretic ejection (red bar) of a 5 mM DA and 5 mM NaCl solution was performed at +30 nA while the ejection was monitored by FSCV. The oxidation current along the DA oxidation potential reveals the time-course of delivery.

processes under investigation. Their detection on the carbon fiber reveals the time course of delivery, and may be used to determine the drug concentration from the ejection. A method to accomplish this has been previously developed in our lab, and is displayed in Equation 1.1 (Herr et al., 2010; Belle et al., 2013). The steady-state marker oxidation current (i_m) is used with the

$$[D] = i_m \times A_m \times \frac{[M]_b}{[D]_b} \times \frac{v_D}{v_M} \qquad \text{Equation 1.1}$$

flow-injection analysis calibration factor (A_m) to give the marker concentration. Next, the marker and drug concentrations of the ejection solution $\left(\frac{[M]_b}{[D]_b}\right)$ are applied with the electric field mobilities of the two species $\left(\frac{v_D}{v_M}\right)$, resulting in the steady-state drug concentration during the ejection ($[D]$). Importantly, the mobility terms correct for the difference in the delivery rates of the marker and drug. This implies that markers and drugs do not have to possess a similar molecular size and charge.

Specific Aim 1: Characterize spatial distribution of ejections

Previous work has shown how delivery rates are affected by certain ejection parameters. However, less attention has been paid to how these same factors impact the distribution of ejected species. This is important to understand in order to advance microiontophoresis as a quantitative method, since concentration is a function of the ejected quantity and the area in which it is contained. Therefore the first aim of this dissertation is to establish how the distribution of ejected species is affected by different ejection conditions. To study this, fluorescence microscopy is used to examine distributions following ejections. First, the magnitude of the ejection current is studied to determine if the distribution changes with different currents. Next, the influence of the charge of an ejected species is determined by comparing

distributions from differently charged fluorophores. From these experiments, a universal steady-state distribution is established and compared with a mathematical model, which was used to estimate concentration profiles of ejected species. This is the subject of Chapter 2.

Specific Aim 2: Determine how barrel concentration affects delivery rates

The next aim is to understand how the concentration of the barrel solution affects delivery rates of ejected species. To study this, ejections are performed from barrels containing different solution concentrations and ejection quantities were determined using LC and fluorescence microscopy. Results are compared with those observed in transdermal iontophoresis, in which the transport number successfully predicted changes in the delivery rate of ionic species. Additionally, principles governing the delivery rate of neutral molecules are established. It is then shown how the barrel solution composition will naturally change during experiments, which alters the delivery rate of all species. A strategy to measure and compensate for these changes is presented. This is the focus of Chapter 3.

Specific Aim 3: Improve concentration evaluations of iontophoretic ejections

Using controlled iontophoresis, a method to determine drug concentrations from the steady-state marker current has been proposed. In the third aim of this dissertation, the validity of this method is determined. To accomplish this, stimulated DA release is examined following administration of quinpirole (QP), a D2 receptor agonist. Responses to known concentrations are generated by perfusion of the drug to a brain slice. From this, a control dose-response curve is created which shows the inhibitory effect of QP on DA release. Next, iontophoretic ejections of QP and a marker are performed. An iontophoretic dose-response curve is generated and compared to the perfusion standard. On first attempt, the marker failed to provide an accurate

account of the drug concentration. To address this, additional iontophoretic dose-response curves were generated in which the ejection parameters were altered; this includes factors such as the molecular charge of the marker, the ejection duration, and the time between the end of the ejection and DA stimulation. In all, it is shown how optimized protocols greatly improve the ability of controlled iontophoresis to determine ejection concentrations. This is presented in Chapter 4.

PART II: MULTI-MODAL RECORDING IN BRAIN SLICES

Multi-Modal Recording

Multi-modal recording describes the simultaneous collection of information from multiple domains, and is advantageous for associating different varieties of events. For example, the previously described oxygen and NE experiment related changes in one domain, the chemical, to that in another, vasoactivity. While techniques such as FSCV are already capable of multi-modal measurements, such studies may be further enhanced by the addition of other independent methods (Moser et al., 1995; Galli et al., 1998; Sheth et al., 2004). Here it is described how information collected during FSCV can be used with electrophysiological patch clamp recordings to more powerfully characterize neurochemical systems.

Patch Clamp Electrophysiology

The patch clamp is a technique that allows investigations of individual cells and their components, and has been so integral to electrophysiological investigations that it was awarded the 1991 Nobel Prize in Physiology or Medicine (Neher and Sakmann, 1995). It is performed using a glass pipette pulled to a fine tip, which is then used to form a tight seal onto the exterior of a cell membrane. From here, one of several patch clamp varieties may be obtained. For this

study, the whole-cell patch is preferred for its ability to record activity from intact cells. This is achieved by applying suction to the pipette, which ruptures the small patch of membrane contained within the sealed tip. As a result, electrical contact between the cell interior and the internal pipette solution is obtained, which allows the behavior of the cell to be recorded. Measurements from a whole-cell patch clamp are made using one of two conventions. First, a whole-cell voltage clamp controls the potential of the cell while the current flowing to it is measured. This method is primarily used to study ion channel activity. Second, the whole-cell current clamp controls the current flowing into the cell while the membrane potential is measured. The current clamp method is useful for studying shifts in the membrane potential, and for recording cell firing. Using this method, spontaneous cell behavior can be observed by restricting current flow to the cell. Alternatively, injections of current can be administered to stimulate activity.

Medium Spiny Neurons

Medium spiny neurons (MSNs) account for nearly 95% of the total cell population in the dorsal striatum and nucleus accumbens (NAc) (Gerfen and Surmeier, 2011). Due to their suggested role in numerous neurological diseases, MSNs are highly studied and well characterized (Tozzi et al., 2011; Ehrlich, 2012). While principally excited by glutamatergic input, firing rates are also influenced by DA release from nearby terminals (Britt et al., 2012; Tritsch and Sabatini, 2012). Our lab has previously investigated MSNs in behaving animals during stimulated DA release and following iontophoretic administration of DA receptor agonists and antagonists (Belle et al., 2013). Studies were performed using a multi-modal recording method on a carbon-fiber electrode, where detection was alternated between electrophysiological single unit recording and FSCV (Takmakov et al., 2011). However, single

unit recording provides limited electrophysiological characterization, with information restricted to firing frequency. In contrast, the whole-cell current clamp can observe cell firing, measure the absolute membrane potential, and deliver stimulation to cells.

To study MSNs using the patch clamp method, correct cell identification must first be established. This was done by instituting a whole-cell current clamp protocol in which constant current steps were injected into cells while the potential response of the membrane was recorded. Figure 1.5A displays the potential of a cell in the NAc in response to current injections, which began at -200 pA and increased by 20 pA until firing was evoked. Characteristic of MSNs, the potential response was non-linear with current, and action potentials were preceded by a gradual voltage ramp (Ibáñez-Sandoval et al., 2010; Planert et al., 2010). Confirmation of cell identity was achieved using a staining procedure to view the membrane structure. To accomplish this, biocytin, a membrane staining agent, was added to the internal patch pipette solution. Upon forming a whole-cell patch, biocytin diffused throughout the interior of the cell and was naturally embedded within the membrane. After preservation in a paraformaldehyde solution, the cell-containing slice was incubated with a streptavidin-bound fluorophore. Association between biocytin and the fluorophore complex resulted in fluorescent labeling of the membrane. Confocal microscopy was utilized to reveal the structure of cells which gave MSN-like electrophysiological responses (Figure 1.5B). Characteristic of MSNs, cell bodies were approximately 10 μm in diameter, dendrites displayed extensive branching, and small spines were visible (Planert et al., 2010). Thus cells were confirmed as MSNs. Future cells could then be identified after observing similar electrophysiological responses.

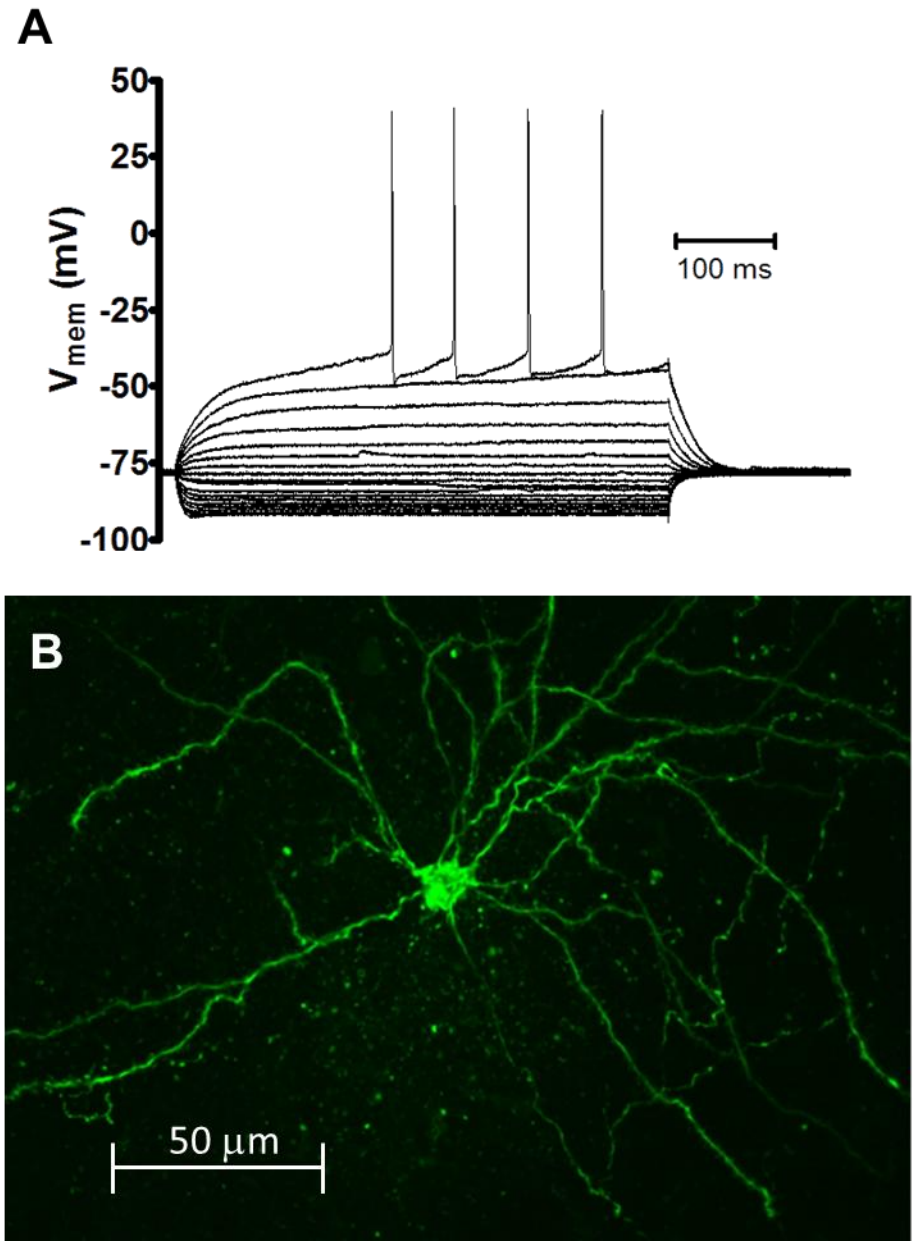

Figure 1.5 Characterization protocol of MSNs. (A) MSN response to intracellular current injections. A whole-cell current clamp procedure was used to characterize cell responses to current steps. Injections began at -200 pA and increased by 20 pA until cell firing occurred. (B) Fluorescence from a labeled MSN. Cell membranes were fluorescently labeled after patching. Confocal microscopy was used to reveal the structure of the cell.

Methods of Stimulation

MSNs oscillate between two states (Gerfen and Surmeier, 2011). In the down state, cells are highly polarized and inactive. In the up state, the membrane potential increases and cells fire at a rate of several Hz. Due to the lack of glutamatergic tone in brain slice experiments, MSNs naturally reside in the down state and require a depolarizing stimulus to fire (Vergara et al., 2003; Azdad et al., 2008). Thus in order to study how activity is modulated by transmitters such as DA, cells must first be transitioned to the up state. This can be accomplished several ways. First, cells can be stimulated by intracellular current injections. Figure 1.6A (left) shows the potential response of an MSN during the injection of current just strong enough to initiate firing. As the current was increased in subsequent steps, the firing frequency also increased (Figure 1.6A, center, right). At each step, firing occurred at a constant rate in accordance to the stimulus strength. A second way to stimulate cells involves the administration of glutamate. To accomplish this, an iontophoresis probe containing a 5 mM glutamate solution was positioned 30 µm from an MSN. A whole-cell patch was performed and the spontaneous membrane activity was monitored in current clamp mode during iontophoretic ejections (Figure 1.6B). As the magnitude of the iontophoretic current increased, the cell exhibited a greater degree of depolarization accompanied by faster firing rates. Presumably this was due to a higher ejected glutamate concentration. When extended ejections were performed using a constant iontophoretic current, cells fired at a steady rate (Figure 1.6C).

Specific Aim 4: Incorporate patch clamp and FSCV measurements with iontophoresis

Integration of simultaneous patch clamp and FSCV measurements would provide a powerful method to study how cell behavior is affected by chemical changes. However, these

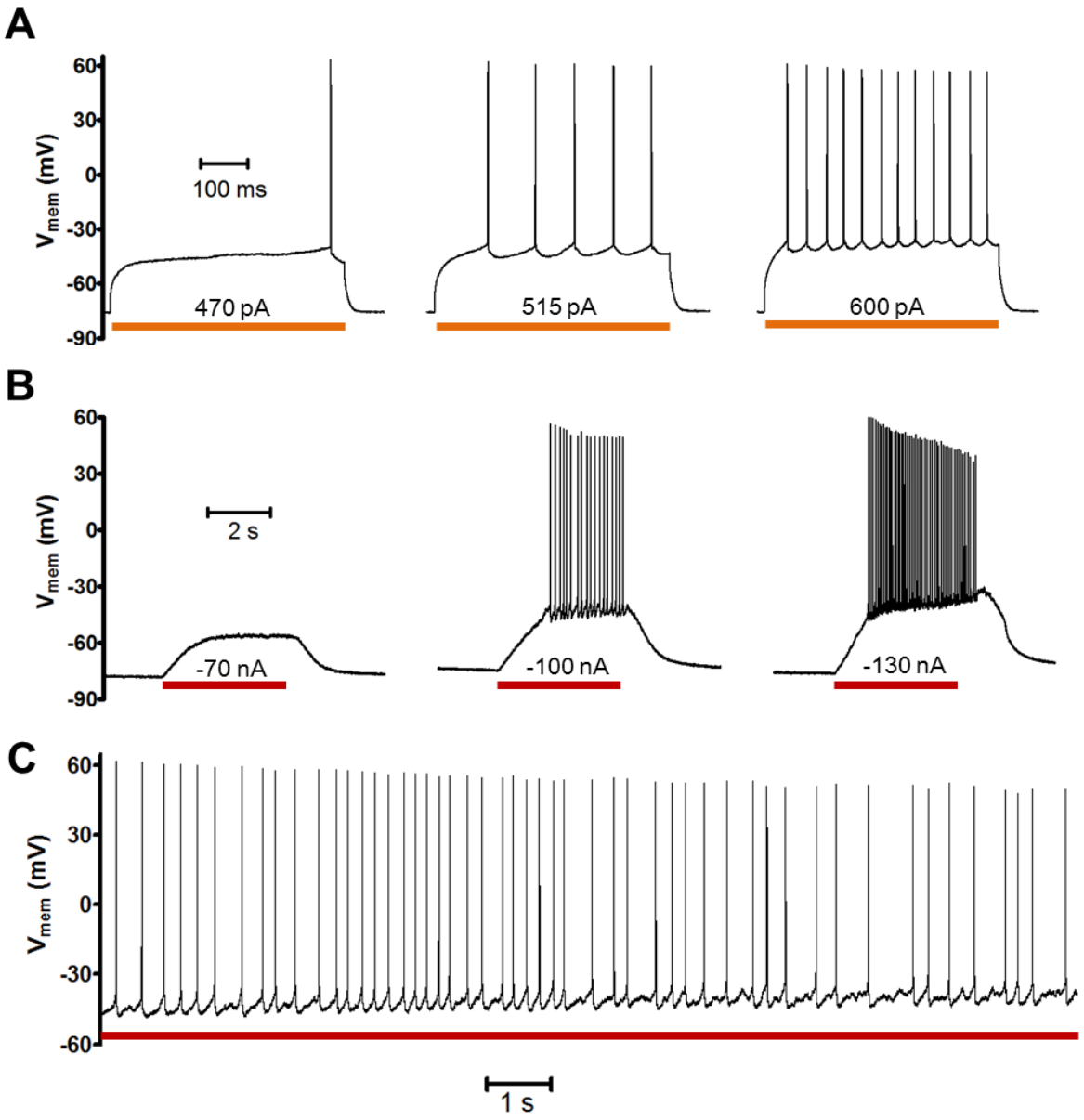

Figure 1.6. Methods of stimulating MSNs in brain slices. (A) Responses of an MSN to intracellular current injections (orange bars) delivered from a whole-cell current clamp. (B) MSN response to iontophoretic ejections of glutamate. Ejections (red bars) were 4 s and the magnitude is denoted by the current value. (C) MSN firing in response to a prolonged -75 nA ejection of glutamate.

techniques require precise measurements of voltage and current in order to properly function. Upon initial integration, electrical crosstalk between instruments prevented their concurrent use. The fourth aim of this dissertation is to successfully combine patch and FSCV instruments for synchronous measurements. Additional inclusion of iontophoresis is also desired. This is first explored by developing a model circuit which predicts the amount of crosstalk between instruments. Results are compared with those obtained experimentally. Once established as accurate, measurements of cell activity are recorded in the presence of exogenously applied potential and current to examine if operation of FSCV and iontophoresis impacted cell behavior. Lastly, cell activity is recorded during chemical changes resulting from iontophoretic drug delivery. This is presented as Chapter 5.

Dissertation Overview

The unifying theme of this dissertation is to further the analytical development of neurochemical methods. This is first accomplished through a vigorous characterization of microiontophoresis. Important concepts such as the area affected by ejections and the principles governing drug delivery rates are established. Next, controlled iontophoresis is examined for its ability to accurately evaluate ejection concentrations. From these studies, it is shown how to greatly improve the quantitative aspects of iontophoretic delivery. Lastly, existing electrophysiological and electrochemical techniques are combined with iontophoresis into a brain slice setup. This allows simultaneous recordings of cell activity and chemical changes following drug delivery.

REFERENCES

Armstrong-James M, Millar J (1979) Carbon fibre microelectrodes. J Neurosci Methods 1:279-287.

Armstrong-James M, Millar J (1980) Quantification of noradrenaline iontophoresis. Nature 288:181-183.

Azdad K, Gall D, Woods AS, Ledent C, Ferre S, Schiffmann SN (2008) Dopamine D2 and Adenosine A2A Receptors Regulate NMDA-Mediated Excitation in Accumbens Neurons Through A2A-D2 Receptor Heteromerization. Neuropsychopharmacology 34:972-986.

Belle AM, Owesson-White C, Herr NR, Carelli RM, Wightman RM (2013) Controlled iontophoresis coupled with fast-scan cyclic voltammetry/electrophysiology in awake, freely moving animals. ACS Chem Neurosci 4:761-771.

Bloom FE (1974) To spritz or not the spritz: the doubtful value of aimless iontophoresis. Life Sci 14:1819-1834.

Britt Jonathan P, Benaliouad F, McDevitt Ross A, Stuber Garret D, Wise Roy A, Bonci A (2012) Synaptic and Behavioral Profile of Multiple Glutamatergic Inputs to the Nucleus Accumbens. Neuron 76:790-803.

Bucher ES, Fox ME, Kim L, Kirkpatrick DC, Rodeberg NT, Belle AM, Wightman RM (2014) Medullary norepinephrine neurons modulate local oxygen concentrations in the bed nucleus of the stria terminalis. J Cereb Blood Flow Metab 34:1128-1137.

Bucher ES, Brooks K, Verber MD, Keithley RB, Owesson-White C, Carroll S, Takmakov P, McKinney CJ, Wightman RM (2013) Flexible Software Platform for Fast-Scan Cyclic Voltammetry Data Acquisition and Analysis. Anal Chem 85:10344-10353.

Delgado-Charro MB (2012) Iontophoretic drug delivery across the nail. Expert Opin Drug Deliv 9:91-103.

Ehrlich ME (2012) Huntington's Disease and the Striatal Medium Spiny Neuron: Cell-Autonomous and Non-Cell-Autonomous Mechanisms of Disease. Neurotherapeutics 9:270-284.

Eljarrat-Binstock E, Domb AJ (2006) Iontophoresis: a non-invasive ocular drug delivery. J Control Release 110:479-489.

Ford CP, Gantz SC, Phillips PEM, Williams JT (2010) Control of extracellular dopamine at dendrite and axon terminals. J Neurosci 30:6975-6983.

Galli A, Blakely RD, DeFelice LJ (1998) Patch-clamp and amperometric recordings from norepinephrine transporters: Channel activity and voltage-dependent uptake. Proc Natl Acad Sci USA 95:13260-13265.

Gerfen CR, Surmeier DJ (2011) Modulation of striatal projection systems by dopamine. Annu Rev Neurosci 34:441-466.

Guy Y, Faraji AH, Gavigan CA, Strein TG, Weber SG (2012) Iontophoresis from a micropipet into a porous medium depends on the zeta-potential of the medium. Anal Chem 84:2179-2187.

Havey DC, Caspary DM (1980) A simple technique for constructing 'piggy-back' multibarrel microelectrodes. Electroencephalogr Clin Neurophysiol 48:249-251.

Herr NR, Wightman RM (2013) Improved techniques for examining rapid dopamine signaling with iontophoresis. Front biosci (elite edition) 5:249-257.

Herr NR, Kile BM, Carelli RM, Wightman RM (2008) Electroosmotic flow and its contribution to iontophoretic delivery. Anal Chem 80:8635-8641.

Herr NR, Daniel KB, Belle AM, Carelli RM, Wightman RM (2010) Probing presynaptic regulation of extracellular dopamine with iontophoresis. ACS Chem Neurosci 1:627-638.

Hicks TP (1984) The history and development of microiontophoresis in experimental neurobiology. Prog Neurobiol 22:185-240.

Ibáñez-Sandoval O, Tecuapetla F, Unal B, Shah F, Koós T, Tepper JM (2010) Electrophysiological and Morphological Characteristics and Synaptic Connectivity of Tyrosine Hydroxylase-Expressing Neurons in Adult Mouse Striatum. J Neurosci 30:6999-7016.

Invernizzi RW, Pierucci M, Calcagno E, Di Giovanni G, Di Matteo V, Benigno A, Esposito E (2007) Selective activation of 5-HT2C receptors stimulates GABA-ergic function in the rat substantia nigra pars reticulata: A combined in vivo electrophysiological and neurochemical study. Neuroscience 144:1523-1535.

Kasting GB (1992) Theoretical models for iontophoretic delivery. Adv Drug Deliv Rev 9:177-199.

Krnjevic K, Mitchell JF, Szerb JC (1963) Determination of Iontophoretic Release of Acetylcholine from Micropipettes. J Physiol 165:421-436.

Lee SY, Oh SY (2014) Alteration of electroosmotic volume flow through skin by polyethylene glycols. Arch Pharm Res.

Marro D, Kalia YN, Delgado-Charro MB, Guy RH (2001) Optimizing iontophoretic drug delivery: Identification and distribution of the charge-carrying species. Pharm Res 18:1709-1713.

Moser T, Chow RH, Neher E (1995) Swelling-induced catecholamine secretion recorded from single chromaffin cells. Pflügers Archiv 431:196-203.

Mudry B, Guy RH, Delgado-Charro MB (2006a) Transport numbers in transdermal iontophoresis. Biophys J 90:2822-2830.

Mudry B, Guy RH, Begona Delgado-Charro M (2006b) Prediction of iontophoretic transport across the skin. J Control Release 111:362-367.

Mudry B, Carrupt PA, Guy RH, Delgado-Charro MB (2007) Quantitative structure-permeation relationship for iontophoretic transport across the skin. J Control Release 122:165-172.

Neher E, Sakmann B (1995) Single-Channel Recording, 2 Edition: Springer US.

Nicholson C, Phillips JM (1981) Ion diffusion modified by tortuosity and volume fraction in the extracellular microenvironment of the rat cerebellum. J Physiol 321:225-257.

Planert H, Szydlowski SN, Hjorth JJJ, Grillner S, Silberberg G (2010) Dynamics of Synaptic Transmission between Fast-Spiking Interneurons and Striatal Projection Neurons of the Direct and Indirect Pathways. J Neurosci 30:3499-3507.

Priya B, Rashmi T, Bozena M (2006) Transdermal iontophoresis. Expert Opin Drug Deliv 3:127-138.

Purves R (1979) The physics of iontophoretic pipettes. J Neurosci Meth 1:165-178.

Purves R (1980) Ionophoresis - progress and pitfalls. Trends Neurosci 3:245-247.

Rice ME, Nicholson C (1991) Diffusion characteristics and extracellular volume fraction during normoxia and hypoxia in slices of rat neostriatum. J Neurophysiol 65:264-272.

Sheth SA, Nemoto M, Guiou M, Walker M, Pouratian N, Toga AW (2004) Linear and Nonlinear Relationships between Neuronal Activity, Oxygen Metabolism, and Hemodynamic Responses. Neuron 42:347-355.

Sykova E, Nicholson C (2008) Diffusion in brain extracellular space. Physiol Rev 88:1277-1340.

Takmakov P, McKinney CJ, Carelli RM, Wightman RM (2011) Instrumentation for fast-scan cyclic voltammetry combined with electrophysiology for behavioral experiments in freely moving animals. Rev Sci Instrum 82:074302.

Tozzi A, de Iure A, Di Filippo M, Tantucci M, Costa C, Borsini F, Ghiglieri V, Giampà C, Fusco FR, Picconi B, Calabresi P (2011) The Distinct Role of Medium Spiny Neurons and Cholinergic Interneurons in the D2/A2A Receptor Interaction in the Striatum: Implications for Parkinson's Disease. J Neurosci 31:1850-1862.

Tritsch Nicolas X, Sabatini Bernardo L (2012) Dopaminergic Modulation of Synaptic Transmission in Cortex and Striatum. Neuron 76:33-50.

Trubatch J, Van Harreveld A (1972) Spread of iontophoretically injected ions in a tissue. J Theor Biol 36:355-366.

Vergara R, Rick C, Hernandez-Lopez S, Laville JA, Guzman JN, Galarraga E, Surmeier DJ, Bargas J (2003) Spontaneous voltage oscillations in striatal projection neurons in a rat corticostriatal slice. J Physiol 553:169-182.

CHAPTER 2: CHARACTERIZATION OF SOLUTE DISTRIBUTION FOLLOWING IONTOPHORESIS FROM A MICROPIPETTE[1]

INTRODUCTION

Iontophoresis is a drug delivery mechanism that uses a controlled current to eject solute from the tip of a pulled glass capillary. It was first utilized as a method to administer acetylcholine at a neuromuscular junction and was eventually adopted for a similar purpose at synaptic sites (Del Castillo and Katz, 1955; Hicks, 1984). This technique has proved beneficial for applications in neuroscience as it provides several distinct advantages over more traditional methods of drug delivery, including local and rapid application, bypassing of the blood brain barrier, and avoiding interference with the behavior of animals (Bloom, 1974; Purves, 1980a; West and Woodware, 1984; Pierce and Rebec, 1995).

Iontophoresis has proved useful in modern studies as a tool to investigate a host of neurological properties such as receptor dynamics and location (Overton and Clark, 1992; Herr et al., 2010; Belle et al., 2013; Bucher et al., 2014). Despite its advantages, more widespread adoption of iontophoresis has been limited due to the inability to monitor and quantify ejections (Bloom, 1974; Purves, 1976, 1980b). This has been partially addressed through various measurement strategies including electrochemical, radiometric, and fluorescent based techniques (Dionne, 1976; Purves, 1979; Bevan et al., 1981; Chen and Nicholson, 2002). Notably the addition of a carbon fiber to an adjacent barrel on the iontophoresis probe allows for the

[1] This chapter previously appeared as an article in *Analytical Chemistry*. The original citation is as follows: Kirkpatrick DC, Edwards, MA, Flowers, PA, Wightman, RM (2014) Characterization of Solute Distribution Following Iontophoresis from a Micropipette. Anal Chem 86:9909-9916.

electrochemical detection of an electroactive solute while also providing an estimate of the ejection quantity (Armstrong-James and Millar, 1980; Kruk et al., 1980; Armstrong-James et al., 1981). However, obtaining precise drug concentrations from iontophoretic ejections remains difficult (Herr et al., 2010).

While much of the attention regarding the quantification of iontophoresis has focused on ejection amount, the spatial distribution of ejected solute plays an equally important role on establishing the concentration of a delivered species. In contrast to pressure-based ejections, the electric field induced by the ejection current has been posited to facilitate electroosmosis in the tissue surrounding the ejection point (Trubatch and Van Harreveld, 1972; Guy et al., 2012). However, this view is not shared by some who argue that the current density outside the barrel is too low to significantly contribute to mass transport (Norman, 1975). In either case the velocity of the ejected barrel solution may also be sufficient to displace previously delivered solute, adding an advective component to the mass transport. This is made possible by the presence of electroosmosis within the barrel, resulting in the transport of bulk solution from the tip (Bevan et al., 1981; Bath et al., 2000; Herr et al., 2008). Migration of charged ions within the barrel can also play an important role on the ejection rate (Curtis, 1964). However a drop in the current density outside the barrel also raises questions regarding the influence of charge on the mass transport of ions following ejection.

In this study we establish the velocity range for iontophoretic ejections from barrels formed from micropipettes and use these values to predict how advection affects the distribution of an ejected species. Concentration distributions are derived from steady state fluorescence measurements and were compared with the theoretical predications. Additionally, the effect of migration on the solute distribution was examined by comparing fluorescence intensity profiles

of oppositely charged fluorophores. Finally, we constructed a simple model to approximate the concentration during and following an iontophoretic ejection. This model was used with experimental measurements to aid in the design of more effective protocols for iontophoretic experiments.

THEORY

To predict the distribution of substances ejected by iontophoresis from micropipettes, we used a mathematical model to describe this process once steady state had been achieved. We assumed the ejected species is a neutral substance transported by convection and diffusion only. The source was assumed to be a sphere of radius *a*, and mass transport was considered to be spherically symmetric. Lastly, the concentration was presumed to go to zero at distances far from the source. The differential equation to be evaluated is:

$$J = C(r)v(r) - D\nabla C(r) \qquad \text{Equation 2.1}$$

Where *J* is the flux of the ejected species, *C* is its concentration, *v* is the radial velocity of the solution, *D* is the diffusion coefficient, and *r* is the distance from the barrel tip. We define *V* as the volume flow rate from the barrel which gives:

$$v(r) = V/4\pi r^2 \qquad \text{Equation 2.2}$$

We only consider the solution at steady state requiring evaluation of:

$$0 = \frac{\partial C(r)}{\partial t} = D\frac{\partial^2 C(r)}{\partial r^2} + \frac{\partial C(r)}{\partial r}\left(\frac{2D}{r} - \frac{V}{4\pi r^2}\right) \qquad \text{Equation 2.3}$$

Introducing the dimensionless distance ρ ($\rho = r/a$), this can be written using the Peclet number in a similar manner to Weber and coworkers (Guy et al., 2012):

$$\frac{dC(\rho)}{d\rho}\left(\frac{Pe}{\rho^2}-\frac{2}{\rho}\right)=\frac{d^2C(\rho)}{d\rho^2} \qquad \text{Equation 2.4}$$

where the Peclet number (*Pe*) is a dimensionless value, which for the present work is given by:

$$Pe=\frac{V}{4\pi aD} \qquad \text{Equation 2.5}$$

This equation was solved previously using the boundary conditions that $C(\rho\rightarrow\infty) = 0$ and $J(\rho=1)$ are constant. The solution is then:

$$C(\rho)=\frac{J_0 a}{PeD}\left[1-exp\left(\frac{-Pe}{\rho}\right)\right] \qquad \text{Equation 2.6}$$

where the flux at the boundary of the sphere, J_o, can be described by:

$$J_o=\frac{C_{int}V}{4\pi a^2}=\frac{DC_{int}Pe}{a} \qquad \text{Equation 2.7}$$

where C_{int} is the concentration of the ejected substance in the interior of the barrel. Substitution of this value into the previous equation yields:

$$C(\rho)=C_{int}\left[1-exp\left(\frac{-Pe}{\rho}\right)\right] \qquad \text{Equation 2.8}$$

At small values of *Pe* (mass transport dominated by diffusion) this relationship collapses to:

$$C(\rho)=\frac{C_{int}Pe}{\rho} \qquad \text{Equation 2.9}$$

that can be rewritten as:

$$C(r)=\frac{C_{int}V}{4\pi D}\left(\frac{1}{r}\right) \qquad \text{Equation 2.10}$$

This equation reveals that, with *Pe* <<1, normalized concentration responses should superimpose and have shapes that are independent of *a* and are linear with 1/*r*.

EXPERIMENTAL

Chemicals and Solutions

All chemicals were used as received from Sigma Aldrich (St. Louis, MO) unless otherwise noted. Artificial cerebral spinal fluid (aCSF) was prepared with 126 mM NaCl, 2.5 mM KCl, 1 mM NaH_2PO_4, 26 mM $NaHCO_3$, 1.2 mM $MgCl_2$, 2.4 mM $CaCl_2$, and 11 mM glucose in deionized water with the pH adjusted to 7.4 using HCl. Fluorophore stock solutions were 10 mM for disodium fluorescein, tris(2,2' –bipyridyl)dichlororuthenium(II) ($Ru(bpy)_3Cl_2$), and rhodamine B, all in 5 mM NaCl. The stock of 7-amino-4-methylcoumarin (coumarin 120) was a saturated solution that was prepared by stirring with low heat for 20 min, resulting in a concentration near the solubility limit (low mM)(Nowakowska et al., 2001). Before addition to the iontophoresis barrel, all stock solutions were diluted 1:1 with 5 mM NaCl and filtered using a 0.20 µm PTFE filter (EMD Millipore, Billerica, MA).

Iontophoretic Ejections

Iontophoresis probes were fabricated from four-barreled pre-fused glass (Friedrich & Dimmock, Millville, NJ) as previously described (Herr et al., 2008; Belle et al., 2013). One barrel contained a carbon fiber for electrochemical measurements. To minimize natural convection during imaging, iontophoretic ejections were made into a 1% (wt/vol) agarose block (Promega, Madison, WI) prepared with aCSF. Low percentage agarose was used to minimize its hydraulic permeability (Johnson and Deen, 1996). The agarose (~ 2 cm thickness) was placed on a glass coverslip inside a rectangular barrier of Vaseline which contained aCSF. A Ag/AgCl

pellet reference (World Precision Instruments, Sarasota, FL) was placed within the barrier to support the iontophoretic current. Using a micromanipulator, the tip of the iontophoresis barrel was carefully inserted into the agarose until it was approximately 500 µm beneath the surface. Ejections were initiated using a homemade current source (UNC Electronics Facility, Chapel Hill, NC) and controlled with customized software.

Amperometry and Liquid Chromatography

Ejections of 20 mM hydroquinone in 5 mM NaCl were performed into 1.5 mL Eppendorf polyethylene test tubes containing 100 µL aliquots of phosphate buffered saline (140 mM NaCl, 3 mM KCl, 10 mM NaH_2PO_4) adjusted to pH 7.4 with 3 M NaOH. The carbon fiber was used for amperometric oxidation of ejected hydroquinone at +0.9 V relative to a Ag/AgCl reference with a UEI current transducer (UNC Chemistry Electronics Facility, Chapel Hill, NC). The amperometric current was integrated with respect to time to determine the total amount detected electrochemically by Faraday's law. The amount of hydroquinone that was not amperometrically oxidized was determined using liquid chromatography (HP Series 1050, Hewlett Packard, Palo Alto, CA). Injections (20 µL) were made onto a C18 reverse phase column (5 µm, 4.6 x 250 mm, Phenomenex, Torrance, CA) with a mobile phase consisting of 100 mM citric acid, 1 mM sodium hexyl sulfate (Research Plus, Barnegat, NJ), and 0.1 mM EDTA (pH=3), with 10% added MeOH. Amperometric detection at the end of the column employed a glassy carbon thin layer radial cell (Bioanalytical Systems, West Lafayette, IN) held at +0.8 V relative to a Ag/AgCl reference. Data were recorded on customized LabVIEW software (Jorgenson Lab, UNC) using homebuilt electronics. The number of moles injected for each sample was determined by integration of the peak area and comparison to similarly prepared standards.

Fluorescence Measurements

Epifluorescence microscopy was performed using an Eclipse FN1 microscope (Nikon Instruments) with illumination from a Xenon halide source (X-Cite 120, EXFO). Filter cubes (Nikon Instruments) were used to select excitation and emission wavelengths specific to each fluorophore. Images were captured using a Retiga Exi camera (QImaging, Surrey, BC, Canada) and recorded with QCapture software (QImaging). For confocal imaging, an SP2 Laser Scanning Confocal Microscope (Leica, Wetzlar, Germany) was used with assistance from the Michael Hooker Microscopy Facility at the University of North Carolina Chapel Hill.

Data Analysis

To obtain fluorescence intensity-distance profiles for ejections performed on the epifluorescence setup, images were analyzed using a custom Matlab script (Figure 2.1A). Overlaid on the fluorescence intensity are 11 cross-sections (dashed lines) that span outwards from the tip of the iontophoresis barrel at 30˚ intervals. The twelfth cross-section nearest the barrel was omitted due to optical distortion. The fluorescence intensity along each line was subtracted from the background and averaged together, resulting in the final distribution profile for the ejection (Figure 2.1B). For ejections on the confocal microscope a similar analysis was employed that utilized the microscope associated software (LAS-AF lite v 2.6, Leica, Wetzal, Germany).

Brain Slice Experiments

Coronal brain slices of the dorsal striatum from male Sprague-Dawley rats were prepared. The animal was anesthetized with urethane (1.5 g/kg) and decapitated. Following immediate removal of the brain and immersion into oxygenated (95% O_2/5%CO_2) chilled aCSF,

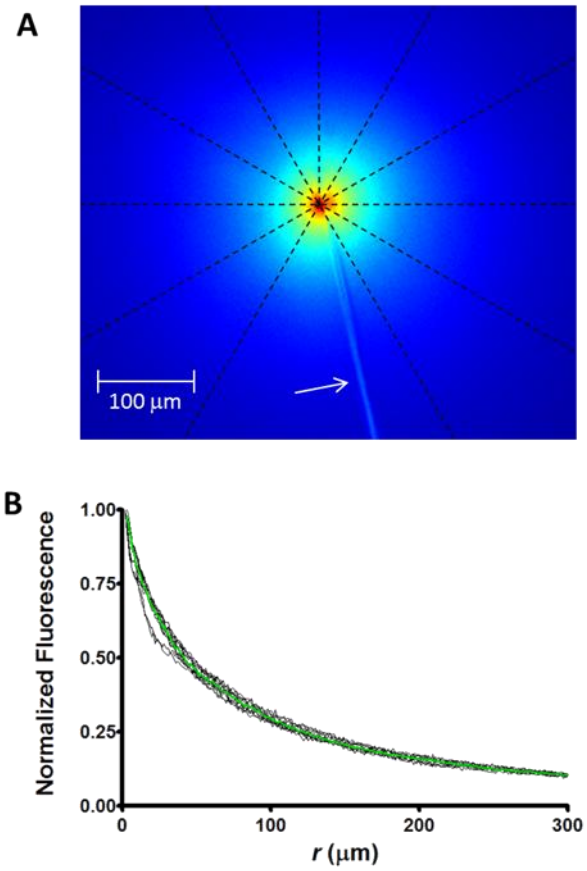

Figure 2.1 Determination of fluorophore distribution for iontophoretic ejections. (A) Matlab false color plot of fluorescence intensity for an ejection of fluorescein into 1% agarose. The dashed black lines depict 11 cross sections which extend from the origin at 30° intervals along which the intensity was recorded. The iontophoresis barrel is indicated by an arrow. (B) Background subtracted fluorescence intensity versus distance along each cross section (black) and average trace of all cross sections (green).

a vibratome (VF-200, Precisionary Instruments, San Jose, CA) was used to cut 300 µm thick sections. The slices were stored at room temperature in oxygenated aCSF and transferred to a perfusion chamber (RC-22, Warner Instruments, Hamden, CT) for measurements during perfusion with a constant stream of oxygenated aCSF at 37˚ C. The iontophoresis barrel was placed just below the surface of the cortex where the tissue contrast was determined to be most uniform. During ejections, the perfusion was temporarily stopped. Animal procedures were approved by the Institutional Animal Care and Use Committee at the University of North Carolina at Chapel Hill. Special care was taken to reduce the number of animals used for this study and to minimize any suffering.

RESULTS AND DISCUSSION

Range of Ejection Velocities

To compare our experimental results to the theory, we needed to know the iontophoretic ejection velocities due to electroosmosis so that the Peclet numbers could be evaluated. To accomplish this, hydroquinone, a neutral molecule, was ejected into 100 µL aliquots of PBS. A carbon fiber on an attached barrel was used to quantify and monitor the ejection by amperometric oxidation (Figure 2.2A). The amount of hydroquinone oxidized by the carbon fiber, *N*, was determined by Faraday's law, $N = \frac{Qn}{F}$, where *n* is the number of electrons (2) transferred in the oxidation step and *F* is Faraday's constant. The charge *Q* was determined from integration of the oxidation current with respect to time. The amount of hydroquinone ejected, but not oxidized and thus remaining in the PBS aliquot, was determined using liquid chromatography with comparison of peak area to known standards. The total number of moles of hydroquinone ejected was calculated as the sum of the moles oxidized at the carbon fiber and

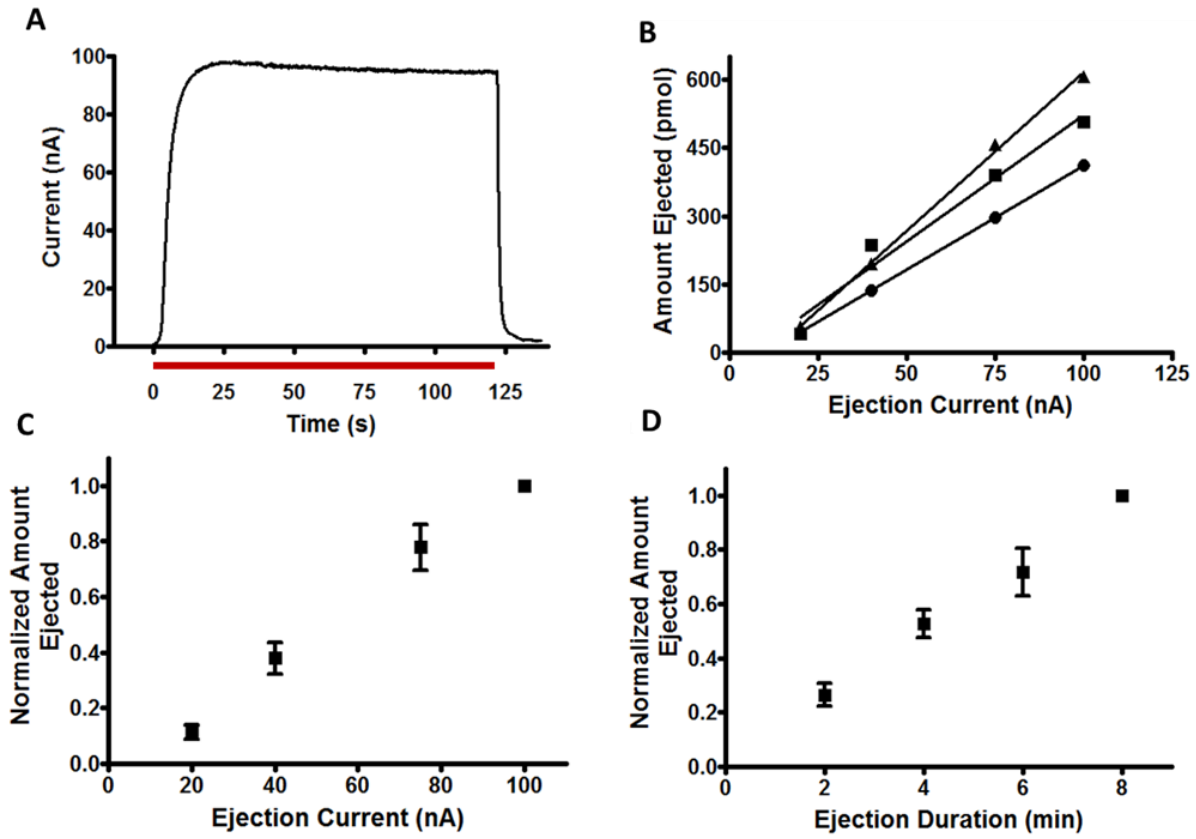

Figure 2.2 Determination of the velocity range for iontophoretic ejections. (A) Amperometric current versus time trace for a two minute, 50 nA ejection of 20 mM hydroquinone into PBS. (Red bar represents ejection time) (B) Amount ejected versus ejection current for 3 min ejections of three different barrels. The ejection quantity is linear with ejection current, but the sensitivity varies between barrels. (C) Normalized amount of hydroquinone ejected versus ejection current for 3 min ejections (n=5). Here and throughout the work error bars represent ±1 standard deviation. (D) Normalized amount of hydroquinone ejected versus ejection duration for 50 nA ejections (n=5).

that determined by liquid chromatography. The collection efficiency, defined as the fraction of hydroquinone detected by the fiber compared to the total amount ejected, ranged from 18 to 60%. This value was dependent on the amount of hydroquinone ejected and varied between barrels. While each barrel showed a linear response of the amount ejected versus ejection current (3 min ejections), the sensitivity differed (Figure 2.2B). The amount of hydroquinone ejected from five barrels normalized to the amount ejected at 100 nA is plotted versus the magnitude of the ejection current in Figure 2.2C. This shows that an increase in the ejection current resulted in a proportional increase in the ejection amount, indicating the flux and ejection velocity of the barrel solution can be scaled by the ejection current. Further analysis of ejections in Figure 2.2C revealed that the volumetric flow rate was between 10 and 175 pL/s for ejection currents from 20 to 100 nA. Using this range, typical barrel dimensions (a = 0.5 – 1 μm), and a diffusion coefficient typical of small molecules we were ejecting (7.5×10^{-6} cm^2/s), Equation 2.5 predicts *Pe* values between 1.1 and 37. We also examined the flux of ejections for different times (2 to 8 minutes) at a constant ejection current (50 nA). The amount of hydroquinone ejected normalized to the amount ejected in 8 minutes was linear with time, indicating a constant flux from the barrels (Figure 2.2D).

Effect of Velocity on Steady-State Distribution

To examine the concentration distribution at the tip of the iontophoresis barrel at different ejection rates, steady-state epifluorescence images of $Ru(bpy)_3^{2+}$ were recorded at different ejection currents. Steady state was achieved within 2-3 minutes. We confirmed that the epifluorescent microscope had sufficient depth of field for these measurements by comparing results with those obtained from a confocal microscope. As the ejection current increased, so did the steady-state $Ru(bpy)_3^{2+}$ concentration using 4 min ejections (Figure 2.3A). Due to the higher

ionic strength of the $Ru(bpy)_3^{2+}$ solutions that were used, it could support larger currents compared to barrels that contained neutral hydroquinone and 5 mM NaCl. The total fluorescence from $Ru(bpy)_3^{2+}$ within 500 µm of the barrel tip was determined by effective spherical integration of the concentration profiles, assuming spherical symmetry in non-imaged planes. These values were linear with ejection current when results were averaged from six barrels (Figure 2.3B). Once again there was linearity between the total amount and the ejection current, consistent with the previously established relationship between velocity and the ejection current.

If the diffusion-limited, steady-state condition is approached (*Pe* < 1), then the normalized concentration distribution should be independent of ejection velocity. To test this, the fluorescence curves from Figure 2.3A were normalized by the fluorescence intensity at a similar distance from the barrel and compared. When the amplitudes were normalized to their values measured 1 µm from the barrel tip, the distributions were similar at the lower range of ejection currents, the expected condition for small values of *Pe* (Figure 2.3C). However, at larger ejection currents the curves diverged. Under these conditions advection from the velocity of the barrel solution is sufficient to move previously ejected solute, indicating *Pe*>1. The fluorescent measurements in agarose thus agree with the liquid chromatographic results that the *Pe* values are low for ejection currents < 50 nA with the conditions employed.

To examine the impact of advection on the steady state distribution at distances further from the ejection origin, the distributions in Figure 2.3A were normalized by the intensity 100 µm from the barrel (Figure 2.3D). The close alignment of these curves demonstrates that advective convection has little effect on the distributions far from the origin. Although the normalization distance required to see a convergence varied, distributions obtained from other

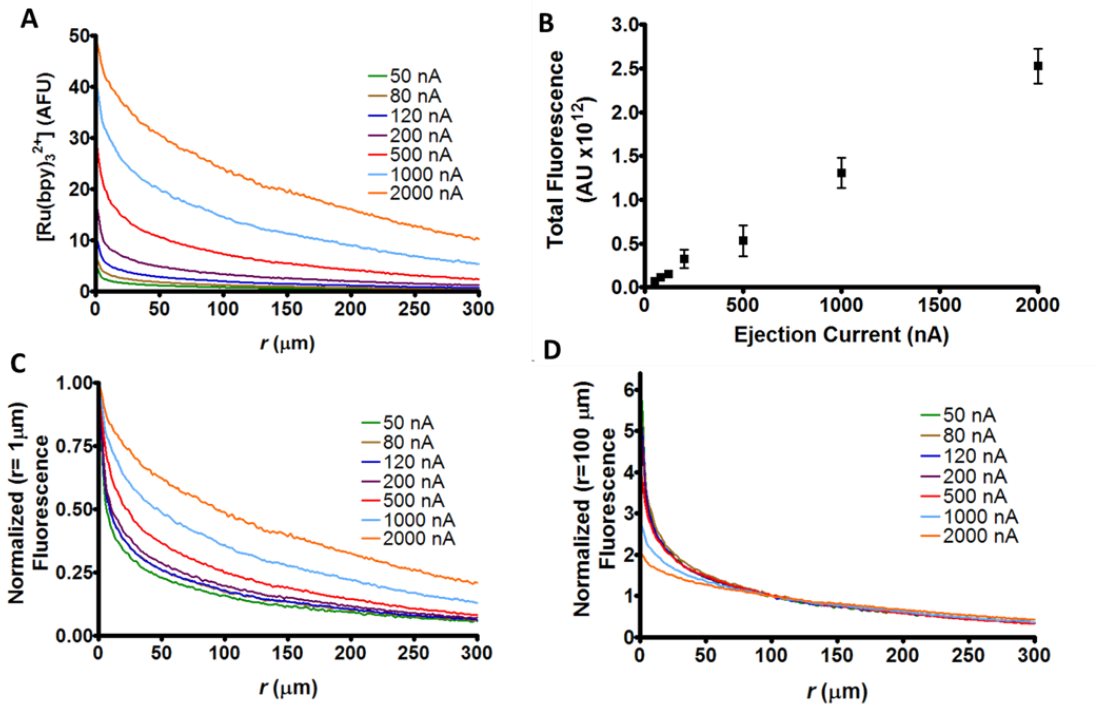

Figure 2.3 $Ru(bpy)_3^{2+}$ fluorescence at steady state for different ejection currents. (A) The steady-state fluorescence intensity for ejections ranging from 50 to 2000 nA. (B) The total fluorescence intensity of $Ru(bpy)_3^{2+}$ within 500 μm of the origin versus ejection current. Steady-state distributions (n=7) were integrated about a sphere to determine the total fluorescence. (C) Steady-state fluorescence profiles from A normalized at the ejection origin. (D) Steady-state fluorescence profiles from A normalized at 100 μm from the origin.

barrels (n = 7) behaved similarly when normalized within 100-200 μm of the tip (data not shown). Thus, even when *Pe*>1, the total volume affected by an ejection at steady-state can be approximated independently of the ejection current using the apparent diffusion rate of the ejected species. Spherical integration of the intensity for normalized distributions displaying the smallest dependence on ejection current revealed that ~10% of the ejected solute at steady state was within 100 μm of the barrel.

Effect of Molecular Charge on Steady State

To examine whether the molecular charge of an ejected species influences the concentration distribution using solutions that approximate physiological conditions, steady state profiles of fluorophores with different charges were compared. The steady-state distributions of ejected fluorescein, rhodamine B, coumarin 120, and $Ru(bpy)_3^{2+}$, which possess charges at pH 7.4 of -1, 0, 0, and +2, respectively, overlay when normalized by the intensity 30 μm from the barrel (Figure 2.4A). These measurements are the average from at least 12 barrels for each compound. Clearly, the differently charged fluorophores have similar concentration distributions, indicating that mass transport by migration away from the barrel tip does not play a role under these conditions. Additionally, ejections from barrels containing multiple fluorophores showed no difference in the steady-state distribution when each was separately imaged (data not shown).

In these experiments, the normalization distance of 30 μm was selected to minimize errors in specifying the center of the ejection that often was distorted by the carbon fiber. There also exists the possibility of fluorophore self-quenching, which would be most prevalent in the concentrated region near the origin. Additionally although these ejections employed moderate

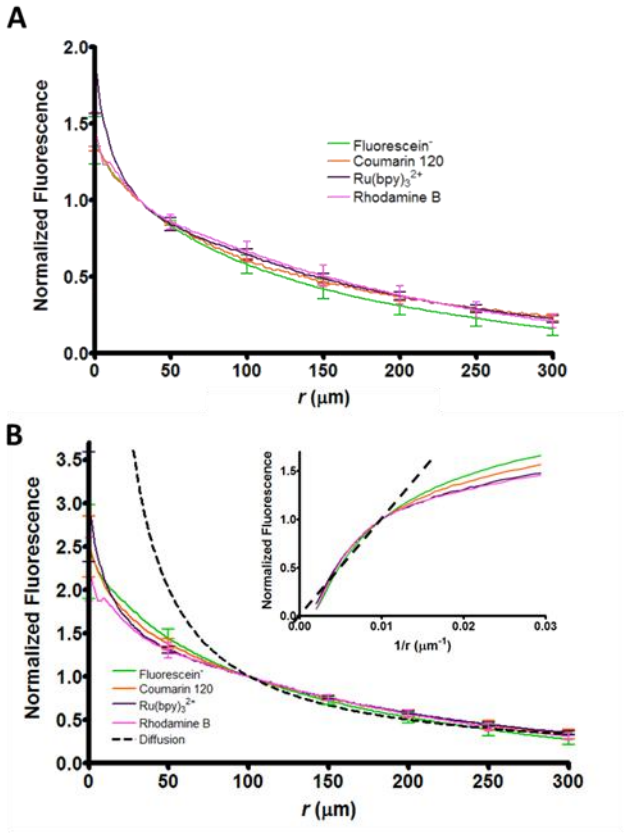

Figure 2.4 Effect of molecular charge on steady-state fluorescence distribution. (A) Average steady state fluorescence profiles (n=12) normalized at 30 μm for $Ru(bpy)_3^{2+}$ (purple), coumarin 120 (orange), rhodamine B (pink), and fluorescein (green) into 1% agarose (B) Comparison of steady-state distributions from A to the diffusion-limited case (dashed) predicted by Equation 2.10. A plot of the intensity versus 1/r (inset) highlights the transition to diffusion-limited behavior away from the origin.

ejection currents (<85 nA), there is still an advective component that was previously shown to be minimized by normalization further from the origin. Lastly, Weber and coworkers showed that a zeta potential mismatch between the glass barrel and the surrounding medium can induce radial electroosmotic transport and increase the rate of mass transport of ejected solute (Guy et al., 2012). To examine whether this was occurring in our gel, the zeta potential of the glass was altered by raising the ionic strength of the barrel solution. However ejections performed of $Ru(bpy)_3^{2+}$ in 5 mM and 150 mM NaCl displayed no difference in the steady state conformation (data not shown), indicating that this additional electroosmotic force was not a factor within the agarose. Thus, we conclude that under the conditions used in this work migration away from the barrel tip is minimized. However, both electroosmosis and migration contribute to the rate of ejection out of the barrel tip as shown previously (Herr et al., 2008).

To examine further whether the steady-state profiles were diffusion-limited away from the origin, the fluorescence distributions were compared to a theoretical diffusion curve calculated from Equation 2.10. In this case, the steady state distributions from Figure 2.4A and the $1/r$ curve were normalized 100 μm from the barrel (Figure 2.4B). Consistent with the fact that the experimental distributions were obtained with $Pe>1$, there is a noticeable deviation from the diffusion-limited case near the ejection origin. After the first 100 μm however, the distribution follows the $1/r$ model. To highlight the transition to diffusion-limited transport, the curves were replotted on a 1/r axis, shown in the inset of Figure 2.4B. Here the distributions at distances further from the barrel ($0 < 1/r < 0.01$ μm^{-1}) are linear and track the diffusional result curve, demonstrating that mass transport of ejected solute >100 μm from the barrel is diffusion controlled.

Steady-State Ejections in Brain Slices

The steady-state distribution following ejections into brain tissue is expected to have differences from those measured in agarose due to different structural and electrical properties. Brain slices exhibit tortuosity in diffusion pathways that lowers the apparent diffusional rate (Sykova and Nicholson, 2008). Furthermore, as Weber demonstrated (Xu et al., 2010) negative membrane charge may introduce an additional electroosmotic component not present in the gel. Therefore, we made iontophoretic ejections of coumarin 120 (neutral) into the cortex of rat brain slices and compared the concentration profiles to ones obtained in agarose for the same substance (Figure 2.5A). When the fluorescence intensities were normalized to the values 30 μm from the barrel origin, there was very little difference between the two profiles. Similarly, the steady-state distribution of $Ru(bpy)_3^{2+}$ in a brain slice also showed only small differences to the responses in agarose (data not shown). To ensure that the molecular charge of an ejected species does not influence the distribution in brain slices, ejections of fluorescein were performed in brain slices and compared to the coumarin 120 and $Ru(bpy)_3^{2+}$ distributions in the same preparation (Figure 2.5B). As in the agarose gel, the distribution of any ejected species in brain tissue was not influenced by the charge.

Modeling of Time-Dependent Diffusive Distribution from an Iontophoretic Barrel

A description of the diffusion limited distribution was constructed in LabVIEW for spherically divergent diffusion using a convolution method established by Engstrom and coworkers (Engstrom et al., 1988; Kawagoe and Wightman, 1994). From the step-response function for spherically divergent diffusion, the impulse response function was derived, and it was convoluted with the Heavyside step function that approximates the flux at the origin. Using

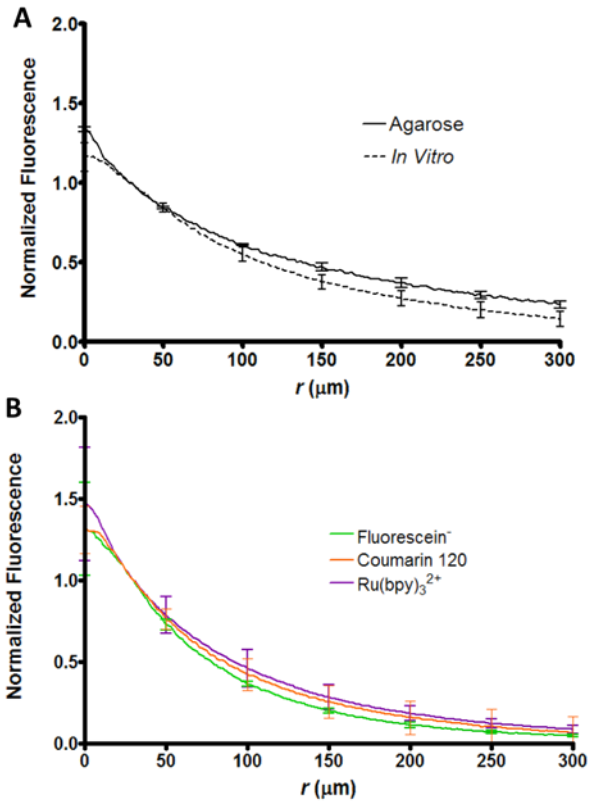

Figure 2.5 Fluorescence distribution for iontophoretic ejections into rat brain slices. To minimize *Pe*, ejections were performed using moderate ejection currents (<85 nA) and normalized 30 μm from the origin. (A) Comparison of the steady-state fluorescence intensity for ejections of coumarin 120 into agarose (solid, n=12) and the rat cortex (dashed, n=6). (B) Fluorescence intensity for fluorophores of different charges after 2 minute ejections (n=6) into the rat cortex. Similar to the ejections in agarose, different charge states [$Ru(bpy)_3^{2+}$ (2+), coumarin 120 (0), and fluorescein (1-)] had no effect on the distribution.

a time of 300 s to ensure steady state conformation, Figure 2.6A displays the convolved profile assuming a diffusion coefficient of 2.0×10^{-6} cm^2/s, lowered to account for slower diffusion in the brain (Sykova and Nicholson, 2008). The validity of the model is confirmed by the overlay of the $1/r$ diffusion curve from Equation 2.10. To examine how the concentration will change over the time course of an ejection, ejections of 30, 60, and 300 s were simulated. The concentration 100 µm from the source is displayed in Figure 2.6B (lines), along with experimental data (dots) for $Ru(bpy)_3^{2+}$fluorescence intensity. Although not identical, the point source model approximates the experimentally observed formation of a steady state and its relaxation when the ejection is terminated. During ejection full steady state takes a long time to realize, but reaches approximately 90% of its value within 100 µm after just two minutes. To visualize the spatial distribution after terminating an ejection, steady state was achieved with $Ru(bpy)_3^{2+}$ in agarose and the ejection current was disabled (Figure 2.6C). When the fluorescence data were plotted similarly to figures 2.4 and 2.5, allowing time for relaxation from the steady state produced a more dilute and spatially uniform distribution. This experiment mimics the way iontophoresis has been used to introduce drugs to modulate dopamine release in the brain (Herr et al., 2010). The drug is locally introduced by iontophoretic ejection, the concentrations are allowed to relax for a finite period (120 s in our published work) and then the dopaminergic neurons are stimulated. Changes in amplitude of the evoked release relative to a predrug release profile indicate the drug action.

CONCLUSIONS

The velocity of solution ejected from the barrel scales proportionally with the ejection current. The impact of advection on the concentration distribution of solute from iontophoretic delivery has been demonstrated to be significant at high ejection currents, but can be minimized

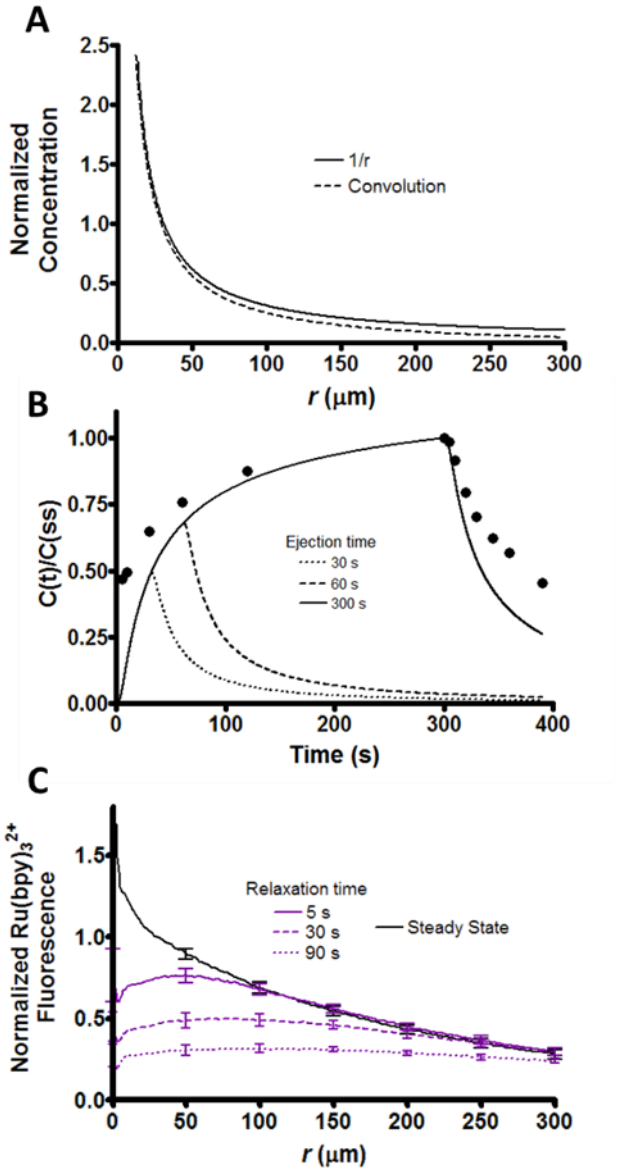

Figure 2.6 Time-dependent diffusion model and experimental applications. (A) Comparison of the 1/r curve from Equation 2.10 (solid) with a model of spherically divergent diffusion (dashed) for a 300 s ejection. (B) Concentration 100 μm from the origin versus time for simulated iontophoretic ejections of 30 (dotted), 60 (dashed), and 300 s (solid). All concentrations were normalized by the value at 300 s. Experimental data (dots) show that the model approximates the observed behavior. (C) Average (n=6) $Ru(bpy)_3^{2+}$ fluorescence distribution following termination of an ejection. Steady state was achieved in agarose (black) and the fluorescence intensity was recorded at 5 (purple, solid), 30 (purple, dashed), and 90 s (purple, dotted) after the ejection current was disabled. The intensity for each distribution was normalized by the intensity at steady state 30 μm from the barrel.

by using low to moderate ejection currents. In any case the distribution of solute further from the origin (>100 μm) is much less impacted by advection and is primarily diffusion-limited. Additionally, for small molecules such as those considered in this work, the mass transport of an ejected ion is independent of charge in brain tissue, indicating that migration outside of the barrel does not play a role on solute distribution. Lastly, diffusional relaxation from steady state produces a near uniform concentration bolus within 90 s of terminating the ejection, demonstrating how iontophoresis may be incorporated in future applications for more accurate quantification.

REFERENCES

Armstrong-James M, Millar J (1980) Quantification of noradrenaline iontophoresis. Nature 288:181-183.

Armstrong-James M, Fox K, Kruk ZL, Millar J (1981) Quantitative ionophoresis of catecholamines using multibarrel carbon fibre microelectrodes. J Neurosci Meth 4:385-406.

Bath B, D., Scott E, R., Phipps JB, White H, S. (2000) Scanning electrochemical microscopy of iontophoretic transport in hairless mouse skin. Analysis of the relative contributions of diffusion, migration, and electroosmosis to transport in hair follicles. J Pharm Sci 89:1537-1549.

Belle AM, Owesson-White C, Herr NR, Carelli RM, Wightman RM (2013) Controlled iontophoresis coupled with fast-scan cyclic voltammetry/electrophysiology in awake, freely moving animals. ACS Chem Neurosci 4:761-771.

Bevan P, Bradshaw CM, Pun RY, Slater NT, Szabadi E (1981) Electro-osmotic and iontophoretic release of noradrenaline from micropipettes. Experientia 37:296-297.

Bloom FE (1974) To spritz or not the spritz: the doubtful value of aimless iontophoresis. Life Sci 14:1819-1834.

Bucher ES, Fox ME, Kim L, Kirkpatrick DC, Rodeberg NT, Belle AM, Wightman RM (2014) Medullary norepinephrine neurons modulate local oxygen concentrations in the bed nucleus of the stria terminalis. J Cereb Blood Flow Metab 34:1128-1137.

Chen K, C., Nicholson C (2002) Measurement of diffusion parameters using a sinusoidal iontophoretic source in rat cortex. J Neurosci Meth 122:97-108.

Curtis DR (1964) Physical Techniques in Biological Research. New York: Academic Press.

Del Castillo J, Katz B (1955) On the localization of acetylcholine receptors. J Physiol 128:157-181.

Dionne VE (1976) Characterization of drug iontophoresis with a fast microassay technique. Biophys J 16:705-717.

Engstrom RC, Wightman RM, Kristensen EW (1988) Diffusional distortion in the monitoring of dynamic events. Anal Chem 60:652-656.

Guy Y, Faraji AH, Gavigan CA, Strein TG, Weber SG (2012) Iontophoresis from a micropipet into a porous medium depends on the zeta-potential of the medium. Anal Chem 84:2179-2187.

Herr NR, Kile BM, Carelli RM, Wightman RM (2008) Electroosmotic flow and its contribution to iontophoretic delivery. Anal Chem 80:8635-8641.

Herr NR, Daniel KB, Belle AM, Carelli RM, Wightman RM (2010) Probing presynaptic regulation of extracellular dopamine with iontophoresis. ACS Chem Neurosci 1:627-638.

Hicks TP (1984) The history and development of microiontophoresis in experimental neurobiology. Prog Neurobiol 22:185-240.

Johnson E, M., Deen W, M. (1996) Hydraulic permeability of agarose gels. AIChE J 42:1220-1224.

Kawagoe KT, Wightman RM (1994) Characterization of amperometry for i*n vivo* measurement of dopamine dynamics in the rat brain. Talanta 41:865-874.

Kruk ZL, Armstrong-James M, Millar J (1980) Measurement of the concentration of 5-hydroxytryptamine ejected during iontophoresis using multibarrel carbon fibre microelectrodes. Life Sci 27:2093-2098.

Norman RS (1975) Diffusional spread of iontophoretically injected ions. J Theor Biol 52:159-171.

Nowakowska M, Smoluch M, Sendor D (2001) The effect of cyclodextrins on the photochemical stability of 7-amino-4methylcoumarin in aqueous solution. J Incl Phenom Macro 40:213-219.

Overton P, Clark D (1992) Iontophoretically administered drugs acting at the n-methyl-d-aspartate receptor modulate burst firing in A9 dopamine neurons in the rat. Synapse 10:131-140.

Pierce RC, Rebec GV (1995) Iontophoresis in the neostriatum of awake, unrestrained rats: differential effects of dopamine, glutamate, and ascorbate on motor- and nonmotor-related neurons. Neuroscience 67:313-324.

Purves R (1976) The release of drugs from iontophoretic pipettes. J Theor Biol 67:789-798.

Purves R (1979) The physics of iontophoretic pipettes. J Neurosci Meth 1:165-178.

Purves R (1980a) Ionophoresis - progress and pitfalls. Trends Neurosci 3:245-247.

Purves R (1980b) Effect of Drug Concentration on Release from Ionophoretic Pipettes. J Physiol 300:72-73.

Sykova E, Nicholson C (2008) Diffusion in brain extracellular space. Physiol Rev 88:1277-1340.

Trubatch J, Van Harreveld A (1972) Spread of iontophoretically injected ions in a tissue. J Theor Biol 36:355-366.

West MO, Woodware DJ (1984) A technique for microiontophoretic study of single neurons in the freely moving rat. J Neurosci Meth 11:179-186.

Xu H, Guy Y, Hamsher A, Shi G, Sandberg M, Weber SG (2010) Electroosmotic sampling. Application to determination of ectopeptidase activity in organotypic hippocampal slice cultures. Anal Chem 82:6377-6383.

CHAPTER 3: QUANTITATIVE ANALYSIS OF IONTOPHORETIC DRUG DELIVERY FROM MICROPIPETTES[2]

INTRODUCTION

Iontophoresis describes delivery of molecular species by an electric field. Its use includes therapeutic treatment of the skin, eye, and nail, and has separately evolved into a tool for neurochemical investigations (Eljarrat-Binstock and Domb, 2006; Priya et al., 2006; Delgado-Charro, 2012). The latter approach utilizes drug delivery from micropipettes and is termed microiontophoresis. Originally developed for studies at the neuromuscular junction, this technique has since been incorporated to administer drugs to local regions of the brain (Suh et al., 1936; Nastuk, 1953; Rutherford et al., 1988; Windhorst and Johansson, 1999; Bucher et al., 2014). As a delivery method, microiontophoresis is advantageous due to the low solution volume required, the ability to bypass the blood brain barrier, rapid application time, and confined delivery regions (Kovács et al., 2005). Despite these benefits, general use has been limited because of difficulties verifying ejection progress and the inability to accurately determine ejected concentrations.

Microiontophoresis can be performed in either anodic or cathodic mode, which use positive and negative currents, respectively, to eject drugs from the pipette barrel. Anodic

[2] This chapter previously appeared as an article in *the Analyst*. The original citation is as follows:
Kirkpatrick DC, Walton, LR, Edwards, MA, Wightman, RM (2016) Quantitative Analysis of Iontophoretic Drug Delivery from Micropipettes. Analyst 141:1930-1938.

iontophoresis has traditionally been used to eject positive ions through electrostatic migration. More recently it has been demonstrated that this practice also generates an outward electroosmotic flow (EOF), which aids cation delivery and allows for the ejection of neutral molecules (Herr et al., 2008). In contrast, anodic iontophoresis is typically used for the delivery of anions.

Common practices in microiontophoresis involve scaling the ejection quantity by adjusting the magnitude of the ejection current, or simply using a current that results in a response (Buffalari and Grace, 2007; Invernizzi et al., 2007; Wang et al., 2011; Bronzi et al., 2015). However ejection quantities can vary between probes, and barrels may become damaged or clogged during experiments which alters ejection behaviour (Purves, 1980; Kirkpatrick et al., 2014). To obtain more certainty in ejection status, several technical advances have been developed which also help to address the quantitative shortcomings. Most notably, ejected solute can be monitored in real time by incorporation of a voltammetric microelectrode adjacent to the iontophoresis barrel (Herr et al., 2010). Ejection of electroactive drugs or markers is detected by the microelectrode upon ejection, confirming delivery, and can provide an estimate of the average local concentration (Armstrong-James and Millar, 1980; Kruk et al., 1980). Other techniques involve placing independent electrodes near the ejecting barrel and the incorporation of fluorescent markers in the ejection solution (Purves, 1979; Kaur et al., 2008; Ford et al., 2010). Theoretical approaches have also been applied in efforts to accurately determine ejection quantity (Purves, 1979; Bevan et al., 1981; Kasting, 1992; Lalley, 1999). These largely focus on the transport number, defined as the fraction of the ejection current accounted for by the target ion. Unfortunately such predictions are approximate because

transport numbers vary between barrels under similar ejection conditions, and predict no delivery of neutral species (Bradley and Candy, 1970).

Iontophoretic ejections typically involve application of a constant current through the barrel. If accurate, the transport number could be used determine the delivery rate and total quantity ejected for an ionic species. Importantly this concept only applies to ions, since neutral molecules do not contribute to the ejection current. Instead these species are more accurately represented by the transference number, defined as the amount of substance ejected per unit charge. Although this is the more complete term, distinction between transference and transport numbers is rarely reflected in current literature (Helfferich, 1962; Mudry et al., 2007).

Here we examine how barrel composition determines ejection rates in microiontophoresis. This includes a distinction between the delivery of ions and neutral molecules, accounting for their different mass transport mechanisms. We also examine how retaining currents (opposite in polarity to the ejection) may impact the reliability of such predictions on subsequent ejections. Separately the spatial distribution of ejected species in cathodic iontophoresis is examined and compared to anodic iontophoresis. Lastly, we exhibit the use of iontophoresis *in vivo* to demonstrate the principles described.

EXPERIMENTAL

Chemicals and Solutions

Chemicals were received from Sigma Aldrich (St. Louis, MO) unless otherwise noted. Phosphate buffered saline (140 mM NaCl, 3 mM KCl, 10 mM NaH_2PO_4) was diluted from a 10x stock and adjusted to pH=7.4 with 5 M NaOH on the day of use. All

iontophoresis solutions were made fresh from de-ionized water and filtered (0.45 µm Nylon, Nalgene, USA) prior to addition to the barrel. Their pH was measured to be between 5 and 7. For the purpose of mole fraction calculations, the following reagents were used to make iontophoretic solutions: dopamine hydrochloride (DA), 3,4-dihydroxyphenylacetic acid (DOPAC), L-glutamic acid monosodium hydrate (glutamate), hydroquinone (HQ), and disodium fluorescein (fluorescein).

Probe Fabrication, Iontophoretic Ejection, and Electrochemical Detection

Four-barreled pre-fused glass capillaries (Friedrich & Dimmock, Millville, NJ) were used to fabricate iontophoresis probes as previously described (Belle et al., 2013). Once pulled, inner barrel diameters ranged from 0.5 to 1 µm. Ejection currents were administered with a locally constructed current source (UNC Electronics Facility, Chapel Hill, NC) which was controlled with LabVIEW code (National Instruments, Austin, TX) using a NI-USB-6343 DAQ card (National Instruments). Ejections were facilitated through specification of a constant ejection current and the corresponding voltage was monitored. The ejection voltages as reported represent the average for the last 5 s of the ejection, which typically plateaued within seconds of initiation (Figure 3.1A, blue). For probes utilizing electrochemical detection, a carbon fiber was inserted into one of the barrels and the exposed tip was cut between 75-125 µm. This allowed ejection monitoring via fast-scan cyclic voltammetry (FSCV) (Figure 3.1A, green). Unless otherwise noted, a triangular waveform was applied at 10 Hz from -0.4 to +1.0 V and back at 400 V/s versus a Ag/AgCl pellet reference (World Precision Instruments, Sarasota, FL). Between scans, the potential was held at -0.4 V. For electrical connection to the carbon fiber, a 4 M CH_3COOK solution containing 0.15 M NaCl was placed in the

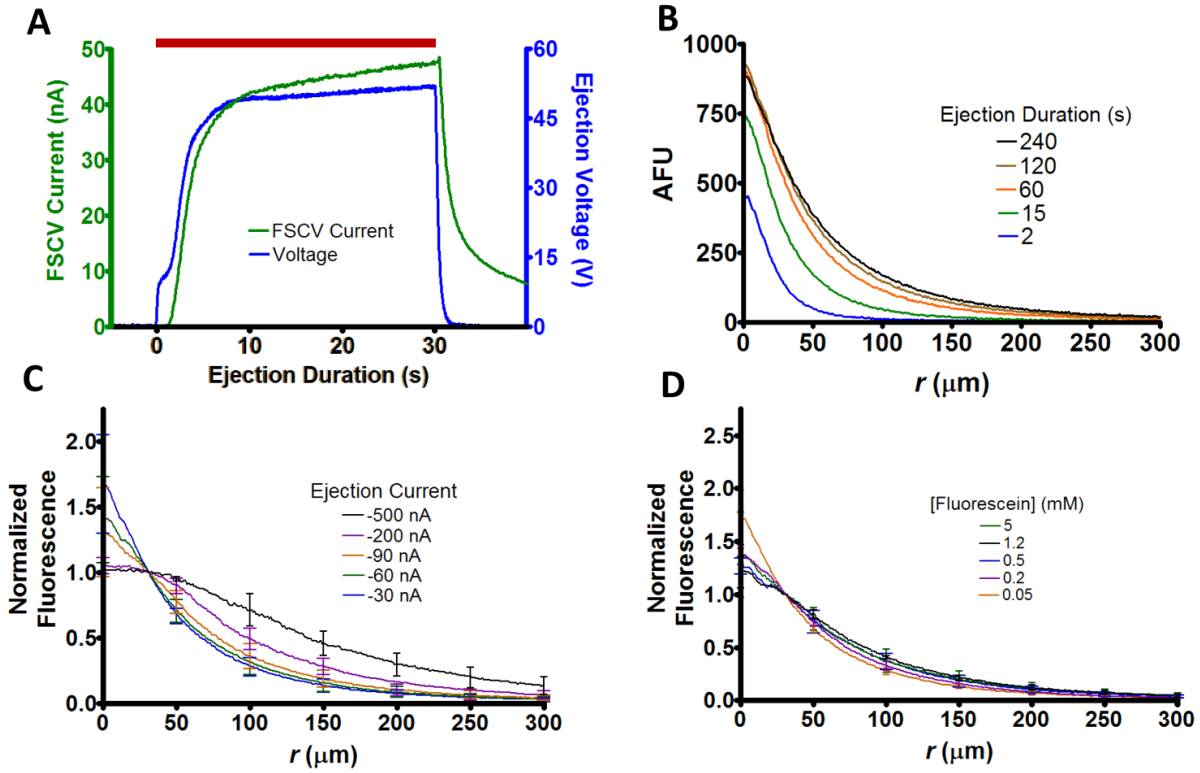

Figure 3.1 Quantitative methods and spatial characterization. (A) Temporal profile for 30 nA ejection of 5 mM hydroquinone in 5 mM NaCl. The background subtracted FSCV current (green) at a carbon-fiber microelectrode and the iontophoretic pump voltage (blue) both reach steady state shortly after initiation. The red bar represents the time of the ejection. (B) Representative temporal fluorescent profiles for an ejection of 5 mM fluorescein in 0.5 mM NaCl. The ejection was performed into the cortex of a rat brain slice at -90 nA. In all cases, r=0 represents the tip of the barrel. (C) Average normalized fluorescence distribution for ejections of 5 mM fluorescein in 0.5 mM NaCl (n=6). Here and elsewhere, profiles were recorded after 4 min of continuous ejection and n represents the number of probes used to perform ejections. Unless otherwise noted error bars represent ±1 SD. (D) Average normalized fluorescence distributions for ejected fluorescein solutions at -90 nA (n=6) from a 0.5 mM NaCl solvent.

microelectrode barrel and a stainless steel wire was inserted. Electrochemical data were collected using a locally built current transducer (UNC Chemistry Electronics Facility, Chapel Hill, NC), digitized (PCIe-6363, National Instruments), and analyzed after background subtraction, signal averaging, and filtering (2-10 kHz) with HDCV software (Bucher et al., 2013).

Liquid Chromatography Sample Collection and Analysis

Samples were collected for liquid chromatography by microiontophoretic ejection into 100 µL aliquots of PBS contained in a 0.5 mL Eppendorf polyethylene tube as previously described (Kirkpatrick et al., 2014). A chloridized Ag wire served as a pseudo-reference electrode. A liquid chromatograph (HP Series 1050, Hewlett Packard, Palo Alto, CA) was used to separate analytes within each aliquot. The column consisted of a C18 reverse phase (5 µM particle diameter, 4.6 x 250 mm, Phenomenex, Torrance, CA), and 20 µL samples were injected. The mobile phase contained 100 mM citric acid, 1 mM sodium hexyl sulfate (Research Plus, Barnegat, NJ), and 0.1 mM EDTA adjusted to pH=3 and was 8/92% (v/v) methanol/H_2O. Amperometric detection employed a thin layer glassy carbon electrode (Bioanalytical Systems, West Lafayette, IN) with an applied potential of +0.8 V vs. a Ag/AgCl reference electrode. The detector was controlled by homebuilt electronics and customized LabVIEW software (Jorgenson Lab, UNC). Aliquot concentrations were determined by comparison to calibration curves prepared from integrated peak areas.

Animal Care and Use

Adult male Sprague-Dawley rats (Charles River, Wilmington, MA) were used for the duration of the study. Animals were dually housed with food and water provided *ad libitum*. All procedures were approved by the Institutional Animal Care and Use Committee at the University of North Carolina at Chapel Hill. Care was given to minimize the number of animals used and to reduce any suffering.

Brain Slice Protocol

Rats were anesthetized with urethane (1.5 g/kg) and brains were quickly removed after decapitation and submerged into oxygenated (95% O_2, 5% CO_2) chilled artificial cerebral spinal fluid (aCSF) consisting of 126 mM NaCl, 2.5 mM KCl, 1 mM NaH_2PO_4, 26 mM $NaHCO_3$, 2 mM $MgSO_4$, 2 mM $CaCl_2$, and 11 mM glucose (pH=7.4). Coronal slices (300 μM thick) were made containing the striatum and cortex using a vibratome (VF-200, Precisionary Instruments, San Jose, CA) with stainless steel feather blades (Fendrihan, USA). Slices were immediately placed in room temperature (20 °C) aCSF and allowed to recover for at least 1 hour. For measurements slices were moved into a perfusion chamber (RC-22, Warner Instruments, Hamden, CT), anchored (SHD-22KIT, Warner Instruments) and perfused with 37 °C oxygenated aCSF at 2 mL/min on the stage of an Eclipse FN1 microscope (Nikon Instruments). Slices were allowed a 30 min equilibration period before investigation.

Fluorescence

The microscope was equipped for epifluorescence measurements with a xenon excitation source (X-Cite 120, EXFO) and a GFP bandpass filter cube (Ex: 450-490 nm, DCM: 495 nm, Em: 500-550 nm, Nikon Instruments) to select wavelengths for

fluorescein. The iontophoresis barrel tip was inserted ~30 µm under the slice surface using a micromanipulator (MPC-200-ROE, Sutter Instruments, Novato CA). To ensure steady state, ejections were performed for 4 min before imaging (Figure 3.1B). The voltage was monitored at all times to ensure clogging did not occur, signified by the absence of abrupt increases in potential. During imaging aCSF perfusion was temporarily suspended so that profiles were free from convection. Fluorescence images were recorded using a Retiga Exi camera (QImaging, Surrey, BC, Canada) with QCapture software (QImaging) at a pixel resolution of 1 µm. Radial profiles were evaluated using a Matlab (Mathworks, Natick, MA) script (Kirkpatrick et al., 2014). This was done by averaging 11 background subtracted cross-sectional radial profiles in the image plane. Due to the proximity of fluorescein's pK_a (6.4) to the barrel solution pH (5-6), only ejections performed on the same day and prepared from the same stock were compared.

In Vivo Single Unit Recording

Rats were anesthetized with urethane (1.5 g/kg). After placement in a stereotaxic frame, an iontophoretic probe with a carbon-fiber electrode was surgically implanted in the dorsal striatum using positioning from a stereotaxic atlas (coordinates relative to bregma were anterior-posterior (AP) +1.5 mm, medial-lateral (ML) +1.8 mm, AP +0.2 mm, ML +2.5 mm, each dorsal-ventral -4.0 to -6.0 mm) (Watson and Paxinos, 2006). Following insertion into the brain the potential of the microelectrode was cycled for 30 minutes to achieve a stable voltammetric response. The voltage was scanned from -0.4 V to +0.8 V and down to -1.4 V to detect oxygen at 400 V/s. Cyclic voltammograms were generated at a repetition rate of 5 Hz. The three iontophoretic barrels contained 100, 10, and 0.5 mM glutamate (drug) with equimolar 3,4-dihydroxyphenylacetic acid (DOPAC).

Solutions also contained 5, 0.5, 0.025 mM NaCl, respectively. DOPAC served as an electroactive marker for ejections and allowed estimation of average, local concentrations (Zare et al., 2009). Barrels were primed by ejecting for ~30 s above the targeted location. Electrochemical measurements employed a homemade current transducer (UNC Chemistry Electronics Facility, Chapel Hill, NC) and HDCV (Bucher et al., 2013). The electrode alternated between voltammetric mode and voltage measurements of single unit spikes as previously described (Takmakov et al., 2011). Between waveforms, the electrophysiological signal was amplified (x10,000), bandpass filtered (0.3-3 kHz), and digitized (Digitizer, Plexon, Dallas, TX). Single units were sorted off-line (Offline Sorter, Plexon) and activity that was time-locked to the iontophoretic ejections was evaluated (Neuroexplorer, Plexon). For each ejection, the glutamate concentration was calculated from the DOPAC electrochemical signal. To accomplish this, the average DOPAC concentration upon ejection was determined by comparison of the oxidation current to a flow analysis calibration (Herr et al., 2010). Since glutamate was equimolar with DOPAC in the barrel and has a similar charge and mobility, this value approximates the average ejected glutamate concentration.

RESULTS AND DISCUSSION

Spatial Characterization

In a prior paper, we demonstrated a variety of methods to quantitate microiontophoretic ejections (Kirkpatrick et al., 2014). Fast scan cyclic voltammetry (FSCV) with a carbon-fiber electrode adjacent to the iontophoretic barrel allows determination of the time course of ejections for electroactive species (Figure 3.1A,

green). Additionally, the total amount ejected over a time period can be quantitated by ejections into small volumes (~100 µL) that are analyzed by liquid chromatography with electrochemical detection. Lastly, the spatial distribution of ejected species can be visualized by fluorescence microscopy. Using this approach, we showed that ejected species have a spherical concentration distribution centered at the ejecting barrel. The radial profiles obtained during a prolonged ejection reveal the limit of the spatial range obtained with microiontophoresis (Figure 3.1B). The fluorescence temporal profiles reveal that a steady-state condition is achieved within 2 min of the start of ejection.

To evaluate the spatial distribution of cathodic iontophoresis, we examined the radial distribution of the monoanion fluorescein (pH=5) using different ejection currents. All profiles were examined at steady-state, which was chosen to be 4 min after continuous ejection to ensure complete formation. Because the receiving medium can influence the ejected distribution, all ejections were made into the cortex of rat brain slices (Sykova and Nicholson, 2008; Guy et al., 2012). To account for differences in ejection quantity, profiles were normalized by the intensity 30 µm from the barrel tip. The normalized spatial distributions for ejections using currents < 200 nA were nearly identical (Figure 3.1C). This was also the case in our prior studies for ejections with anodic current for positive and neutral species, owing to diffusion as the dominant mass transport mechanism (Kirkpatrick et al., 2014). Likewise, the fluorescein profiles follow a *1/r* distribution at distances beyond 100 µm from the barrel tip for currents up to 500 nA, indicating diffusion is the dominant mass transport mechanism beyond this distance regardless of ejection current magnitude.

To determine if the barrel concentration impacted the distribution, steady states were compared for -90 nA ejections of different fluorescein solutions (Figure 3.1D). When normalized to account for concentration differences, the responses were not statistically different (2-Way ANOVA, p=0.504). Taken together with our prior published work, these results indicate that distributions for ejections are identical regardless of current polarity or barrel concentration.

Modulating Transport Number with Ionic Mole Fraction

Ejection quantities were then examined to determine how well predicted transport numbers matched observed values. A theoretical value for the transport number (t_i) can be calculated for an ion from Equation 3.1, where z_i is the unit charge, u_i is the mobility in an electric field, C_i is concentration, and the sum is over all ions in solution, j.

$$t_i = \frac{|z_i| u_i C_i}{\sum |z_j| u_j C_j} \qquad \text{Equation 3.1}$$

Importantly this method assumes only transport through migration and does not account for electroosmotic flow (EOF). According to this equation, if ionic species have similar mobilities then the transport number for a given ion scales with the percentage of charge it makes up in the barrel solution. We denote this term the ionic mole fraction, which accounts for both concentration and charge of an ionic species relative to the whole. The ionic mole fraction should provide a means to predictably modulate the transport number by adjusting the relative percentage of ions in the barrel solution. To examine this, ejections of 5 mM dopamine (DA), a monocation at pH=6, were performed from solutions with different NaCl concentrations. Barrels also contained the neutral species

hydroquinone (HQ) at the same concentration of DA. The mobility of an ionic species, u_i, can be determined from the Nernst-Einstein equation (Equation 3.2) where D_i is the

$$u_i = \frac{q_e D_i}{k_B T} \qquad \text{Equation 3.2}$$

diffusion coefficient, q_e is the elementary charge ($1.6 \times 10^{-19} C$), k_B is Boltzmann's constant ($1.38 \times 10^{-23} J \cdot K^{-1}$),and T is temperature. For DA this value, $2.3 \times 10^{-4} cm^2 V^{-1} s^{-1}$, is similar in magnitude with reported mobility values for Na^+ and Cl^- (5.9×10^{-4} and $7.9 \times 10^{-4} cm^2 V^{-1} s^{-1}$, respectively), which should allow modulation of the transport number via the concentration (MacInnes, 1961). To test this, the observed transport number was calculated from the fraction of the ejection current accounted for by DA. This was done using Equation 3.3, where n_{DA} is the ejected DA quantity determined from LC analysis, t_{ej} is the ejection time, F is Faraday's constant ($96{,}485\ C/mol$) and i_{ej} is the ejection current. As predicted, the observed transport number yielded a direct

$$t_{DA} = \frac{\left(n_{DA}/t_{ej}\right) \times F}{i_{ej}} \qquad \text{Equation 3.3}$$

relationship ($r^2 = 0.991$) with the DA ionic mole fraction. The data (Figure 3.2, green) was then compared with the predicted transport number (dotted blue line), calculated from Equation 3.1. For all solutions, the observed transport number was greater than the predicted value. To determine whether this was due to EOF, the amount of HQ ejected was subtracted from that of DA for each ejection. Recall HQ is neutral and can thus be used to quantitate EOF, so the DA amount ejected after HQ subtraction was due only to migration. The transport number for this new DA amount was then recalculated using Equation 3.3 (blue squares) and displayed better agreement with the predicted values.

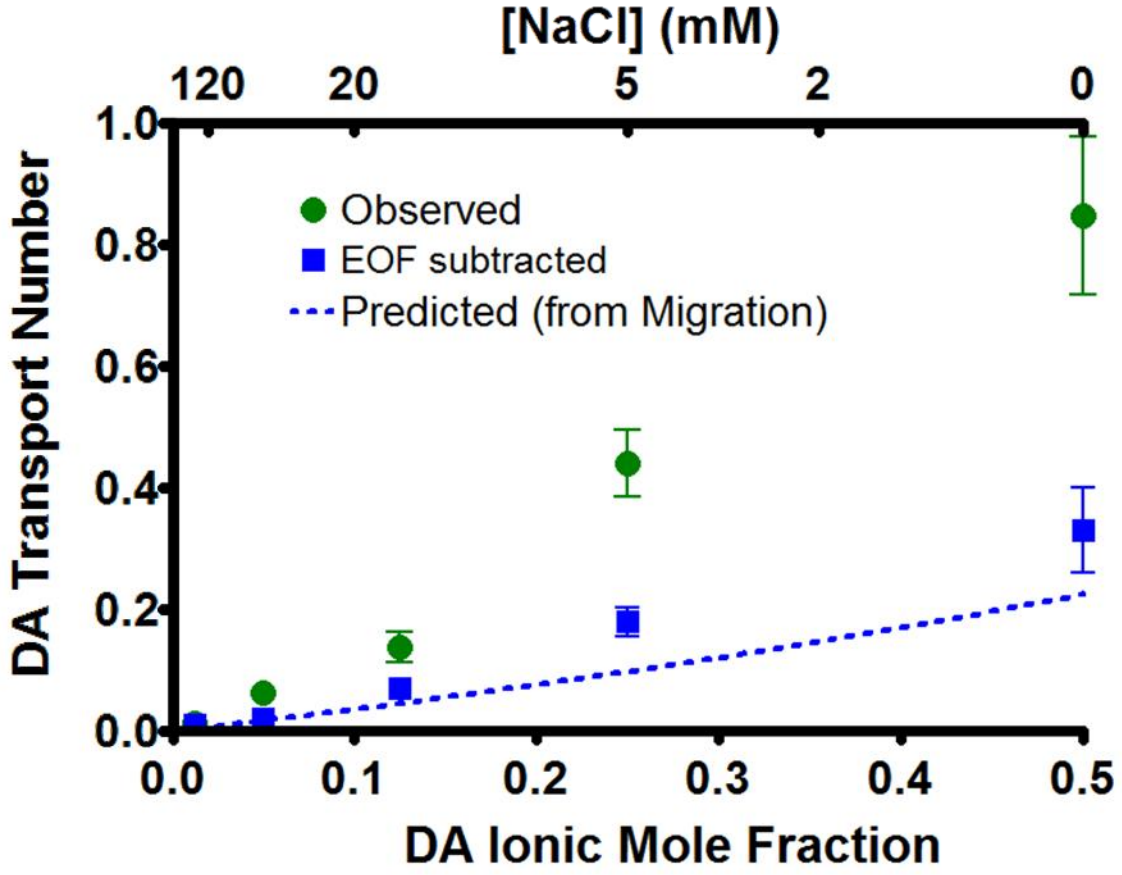

Figure 3.2 Transport number dependence on ionic mole fraction. Ejections of 5 mM DA and 5 mM HQ in NaCl (n=6) were performed at 150-2000 nA and ejection quantities were determined by liquid chromatography. The observed transport number was calculated by the fraction of the ejection current accounted for by the ejection of DA (green circles). After subtracting the DA ejected due to EOF, transport numbers were recalculated (blue squares). The predicted transport number due to migration (Equation 1) is represented by the dotted blue line.

Thus most of the discrepancy between the observed and predicted DA transport numbers is accounted for by EOF. Additionally the visible reduction of the transport number variance for the migration quantity indicates that much of the difference in ejection quantity between barrels containing identical solutions was attributable to different rates of EOF.

Next, ejections of solutions with different DA concentration in 5 mM NaCl were performed. To monitor EOF, solutions contained HQ at the same concentration as DA. Again, the observed transport number was strongly correlated with the ionic mole fraction (Figure 3.3A, green, $r^2 = 0.987$) and the predicted transport number underestimated experimental values. Once the amount of DA ejected due to EOF was subtracted (blue squares), the transport numbers matched those predicted by migration (dotted blue line). Just as in Figure 3.2, the discrepancy in the variance between the two cases suggests that barrels displayed a greater inconsistency in the EOF rate compared to migration.

These cases demonstrate several important factors regarding the transport number in microiontophoresis. First, it is predictably altered by the ionic mole fraction, observations which have also been reported in transdermal iontophoresis (Marro et al., 2001; Mudry et al., 2006). Importantly this provides a way to modify or predict changes in the ejection rate of a target ion. Secondly, the calculated transport number systematically underestimated the observed values, as larger quantities of DA were ejected than predicted from migration. This can mostly be explained by EOF, which is not accounted for in the prediction of transport numbers.

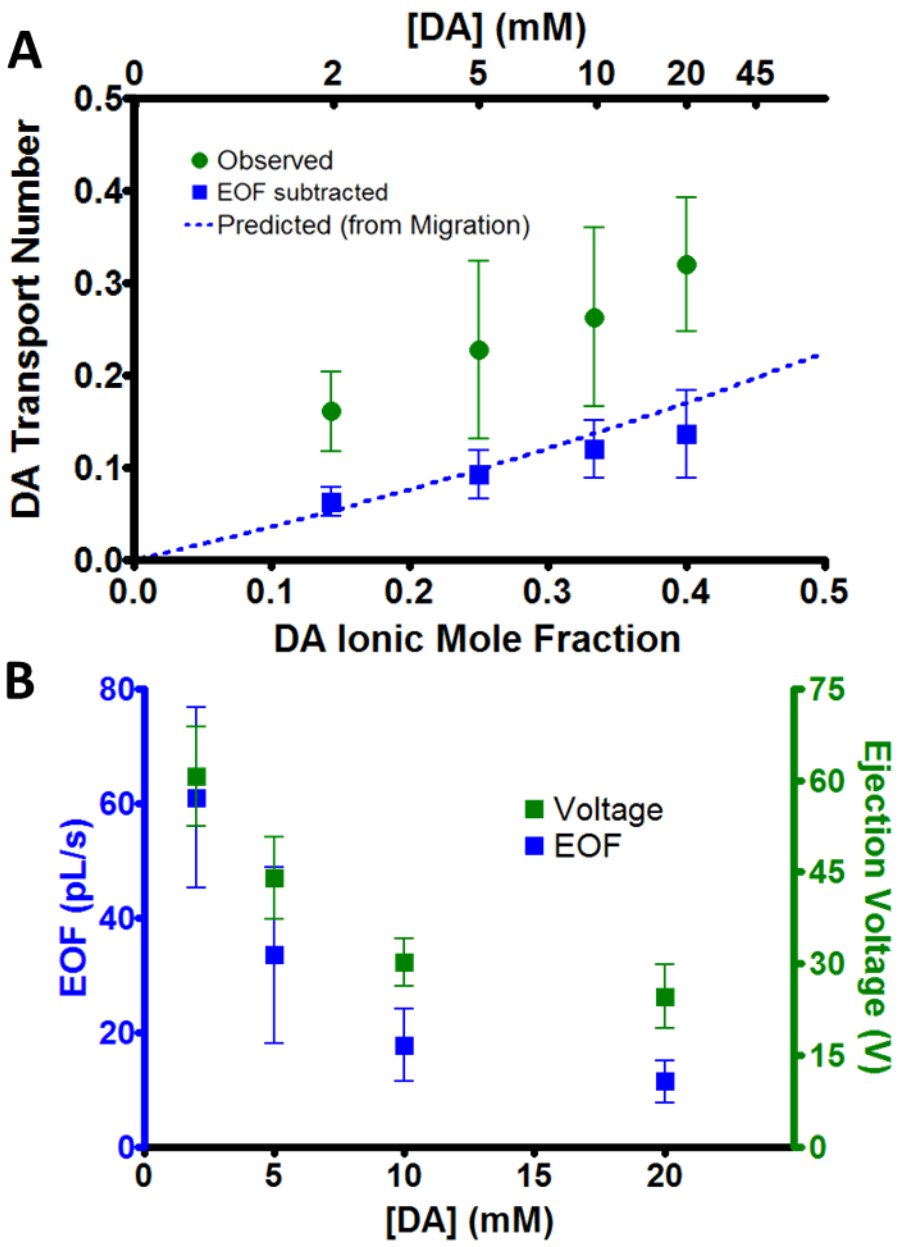

Figure 3.3. Effect of ion concentration on transport number and EOF. (A) DA observed transport numbers (green circles) for 120 nA ejections of equimolar DA and HQ in 5 mM NaCl (n=6). The transport numbers were recalculated after subtracting the DA amount ejected due to EOF (blue squares). The predicted transport number (dotted blue line) from Equation 1 is shown for comparison. (B) The iontophoretic pump voltage (green) and EOF (blue) for ejections in part A.

EOF Velocity Corresponds with Ejection Voltage

The EOF in the experiments of Figure 3.3A was calculated using the ejected HQ quantity and is shown in Figure 3.3B (blue). Barrels higher in DA concentration displayed reduced EOF, which coincided with a drop in the iontophoresis pump voltage required to facilitate the ejections (green). This drop in voltage can be precisely attributed to the increase in solution conductivity at higher concentrations (r^2 = 0.98 between voltage and solution resistivity, calculated from mobility and concentration).

As in capillary electrophoresis, the EOF velocity (v_{ep}) appears related to the electric field (E) by the EOF mobility (μ_{ep}), where $v_{ep} = \mu_{ep}E$. However, the electric field, proportional with the applied potential, does not decrease quite as rapidly as the EOF. This suggests that part of the decrease in the EOF may be independent of the voltage. This could be due to a reduced double layer around the barrel wall with increased ionic strength, a phenomenon that is well established in capillary electrophoresis.

Ejection Rates of Neutral Molecules

Next we studied the ejection rate of neutral molecules ejected at a constant ionic strength. Neutral substances do not contribute to the ejection current so the transport number and ionic mole fraction do not apply. Instead the transference number, amount ejected per unit charge, provides a better comparison for ejection quantities. Here we examined the molar ejection rate of neutral substances, which is proportional to the transference number when ejections are performed at a constant current.

The molar ejection rate should correspond directly to the barrel concentration if EOF is the dominant ejection mechanism. To determine if this was the case, 120 nA ejections of different HQ concentrations in 5 mM NaCl were performed and quantities were once again analyzed by LC. A linear relationship (r^2 = 0.999) was found between the barrel concentration and the molar ejection rate (Figure 3.4A, blue). Additionally the EOF (green) and ejection voltage (not shown) did not differ between barrels (P=0.673, P=0.120, respectively). Thus in contrast to ions, the ejection rate for a neutral species corresponds to barrel concentration rather than the mole fraction.

The previous results illustrate EOF in microiontophoresis at low ionic strength (~5 mM). However the double layer thickness adjacent to the glass wall is reduced at higher ion concentrations, which could ultimately inhibit EOF and prevent the delivery of neutral molecules. Additionally, if ejecting multiple substances from the same barrel, a change in the ejection mechanism could lead to a different ejection ratio dependent on the barrel composition.

To examine if this occurred, ejections of 5 mM DA and HQ in different NaCl solutions were performed. Since DA is transported by migration and EOF, an increase in its ejection rate compared to HQ would indicate an increased migration component compared to EOF. However, for ionic strengths up to 200 mM, this was not observed (Figure 3.4B). Similar observations of significant EOF at high ionic strength in capillary electrophoresis and transdermal iontophoresis have also been reported (Pikal, 1990; VanOrman et al., 1990). Thus EOF occurs to an appreciable extent in microiontophoresis even under highly ionic conditions, facilitating the ejection of bulk solution and permitting the delivery of neutral molecules.

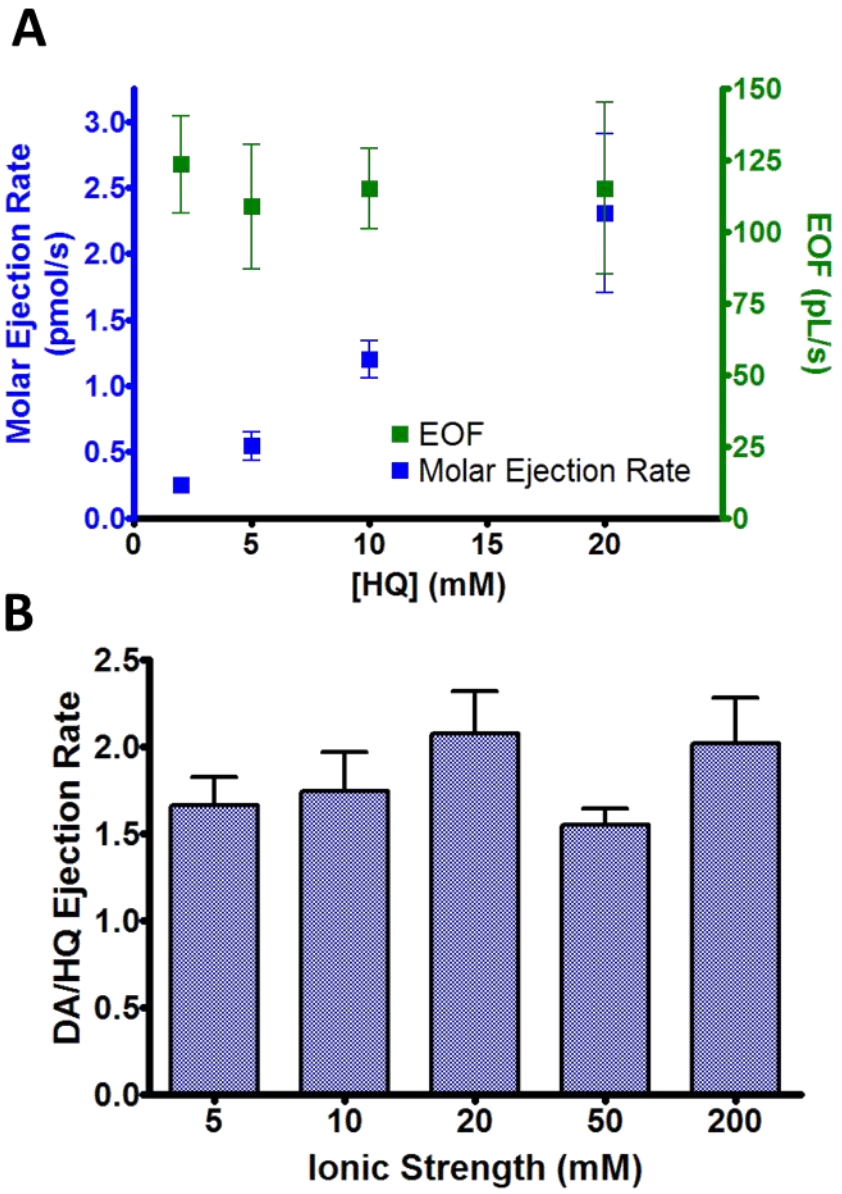

Figure 3.4 EOF and ejection rates for neutral molecules. (A) Molar ejection rate (blue) and EOF (green) for 120 nA ejections of HQ in 5 mM NaCl (n=6). (B) Relative ejection rates of DA and HQ at different ionic strengths (n=6). Barrels contained 5 mM DA and HQ and the remaining ionic strength was due to NaCl. Ejections were performed at a near constant voltage (100 V) for which currents ranged from 150-2500 nA

Cathodic Iontophoresis Ejection Rate Characterization

To determine if similar principles concerning ejection rates extend to cathodic iontophoresis, ejections of the monoanion fluorescein (pH=5) were performed from 0.5 mM NaCl using current of a negative polarity. Ejection rates were compared by the total fluorescence at steady state, determined by spherical integration of the radial fluorescence profile taken after 4 min of applying the ejection current. Just as we have previously demonstrated in anodic iontophoresis, cathodic ejections also show a linear relationship between the ejection rate and current (Figure 3.5A). To determine if the ionic mole fraction likewise determined the ejection rate, average intensities for -90 nA ejections were plotted versus the fluorescein ionic mole fraction (Figure 3.5B). As in anodic iontophoresis, this resulted in the predicted linear ($r^2 = 0.965$) relationship.

As additional confirmation, ejections from barrels of a fixed fluorescein mole fraction (0.15) were performed to determine if they displayed similar delivery rates when ejected at a constant current (-90 nA). These barrels had different fluorescein concentrations while the NaCl concentration was adjusted to maintain a constant ionic mole fraction. Unlike ejections of different fluorescein mole fractions (5B), these barrels resulted in similar fluorescence intensities (P=0.160) after ejection (Figure 3.5C). Thus we conclude that ion ejection rates for both cathodic and anodic microiontophoresis are similarly governed by the ionic mole fraction.

Retaining Currents Compromise Ejection Integrity

We have thus far demonstrated how changes to ejection rates can be predicted from initial barrel concentrations. Next we examine a common practice that may

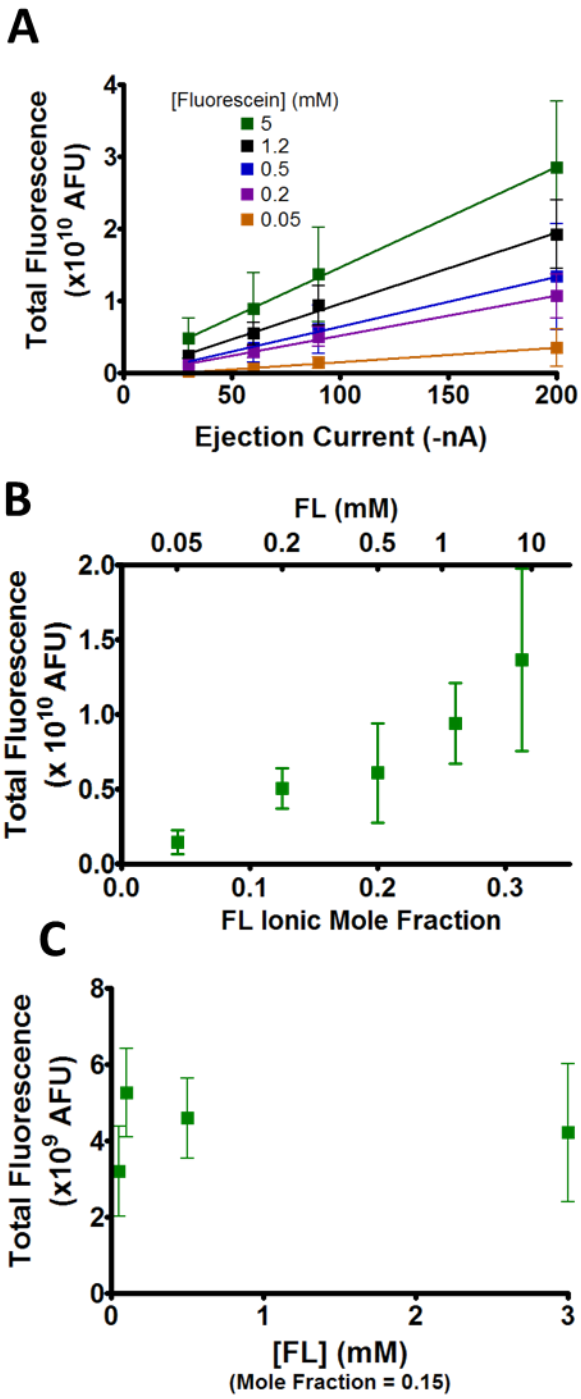

Figure 3.5 Cathodic iontophoresis ejection rate characterization for ejections into brain tissue. (A) Average total fluorescence at steady state for ejections of different fluorescein solutions (n=6). All barrels contained 0.5 mM NaCl. (B) Total fluorescence for -90 nA ejections. (C) Total fluorescence for ejections of fluorescein solutions at a fixed ionic mole fraction of 0.15 (n=5). The remainder of the charge was due to NaCl.

compromise such predictions. Some experiments utilize retaining currents to reduce leakage from the barrel (Gerhardt and Palmer, 1987; Harding and Felix, 1987). However, it also draws some ions into the barrel from the ejection medium and drives out oppositely charged ions, all of which will alter the barrel solution composition. To examine this, 30 s ejections of 5 mM HQ in 5 mM NaCl, which were monitored electrochemically with a carbon-fiber microelectrode in an adjacent barrel, were performed after applying different retaining currents over 5 min intervals. Controls (30 s ejections initiated 15 s after a 1 min priming ejection) were taken before each trial for comparison. Ejections following no retaining current displayed slightly less HQ current compared to the controls, likely due to diffusional exchange at the tip interface (Figures 3.6A, 3.6C). Following retaining currents, ejections resulted in a significant reduction of the HQ current, i_{ox} (P=0.0038). Additionally, the voltage required to facilitate the ejection also decreased, indicating greater solution conductivity (Figure 3.6B).

Although a retaining current mitigates diffusion from the barrel, it also compromises subsequent ejections. The change in the barrel solution composition alters the transport and transference numbers between ejections. Rather than applying a retaining current, alternative approaches to reduce these problems such as smaller barrel diameters or less concentrated solutions could be adopted. Electrochemical monitoring as used in this work enables detection of these problems in experimental systems.

Comparison of Ejection Quantity with Markers

The microiontophoretic principles demonstrated above were determined under ideal conditions. In practice, factors such as variable ejection duration and current

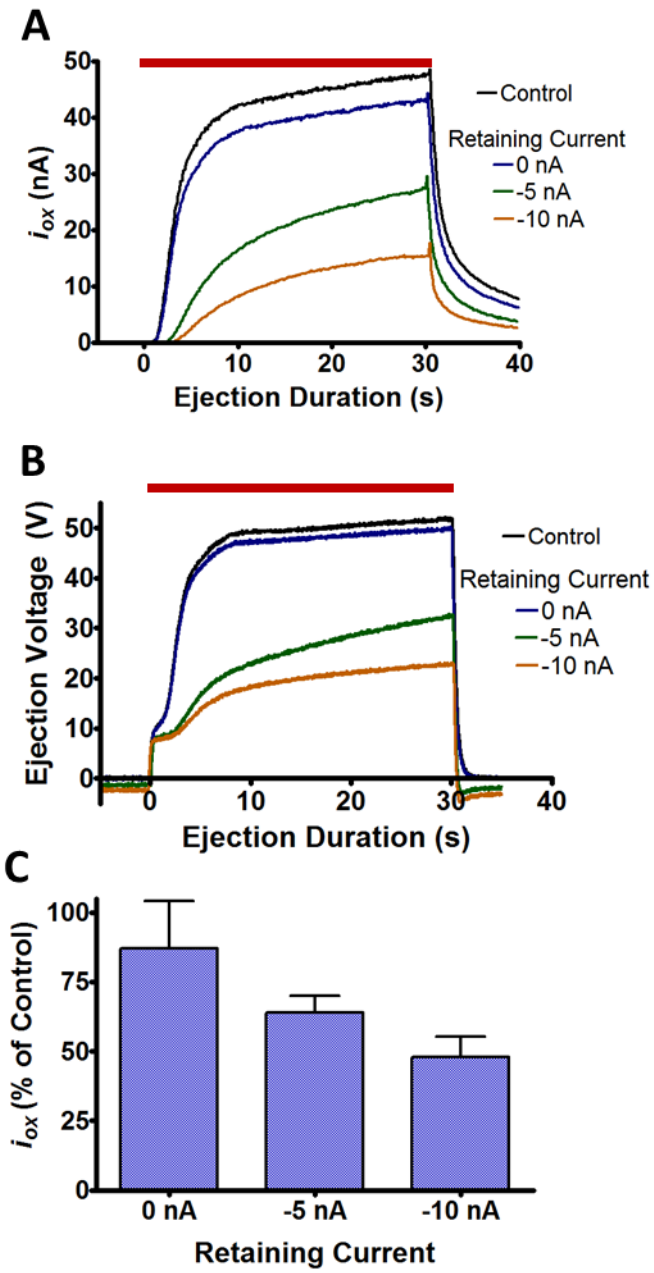

Figure 3.6 Effects of retaining currents on subsequent ejections. (A) Oxidation current at a carbon-fiber electrode for ejections of 5 mM HQ and NaCl. +30 nA ejections were performed following a 5 min waiting period at the designated retaining current. This was repeated four times with characterization occurring on the last ejection of the series. (B) Iontophoretic pump voltage for the ejections in part A. (C) Decline in HQ oxidation current of HQ after waiting periods (n=6). Control ejections were performed prior to the start of the series described above. This was compared to the HQ oxidation current of the final ejection. The current value was recorded as the average oxidation current during the last 5 s of the ejection.

magnitude, along with barrel obstruction from biological media may cause deviations. To evaluate practical application in a physiological process, glutamate was ejected in anesthetized rats into the dorsal striatum. Glutamate is an excitatory neurotransmitter that induces striatal cell firing and is heavily involved in modulating activity (Gerfen and Surmeier, 2011). It is a monoanion and was iontophoretically introduced from barrels that also contained 3,4-dihydroxyphenylacetic acid (DOPAC) as an monoanionic electroactive marker. DOPAC was separately determined to have no impact on cell firing in the region. Its ejection was monitored electrochemically by FSCV repeated at 5 Hz with an attached carbon-fiber electrode. Cell firing rate was monitored in the 180 ms interval between scans at the same carbon fiber (Takmakov et al., 2011). The three iontophoretic barrels contained 0.5, 10, and 100 mM glutamate with an equimolar concentration of DOPAC and a proportional amount of NaCl. For each barrel, 2 s ejections at 3 min intervals were used while increasing the ejection current until the threshold for cell firing was found. During ejection, the FSCV response for DOPAC was clearly observed (Figure 3.7A).

The minimum ejection current required to evoke cell firing for each of the barrels is shown in Figure 3.7B. Higher ejection currents were required for less concentrated solutions despite each solution having the same ionic mole fraction for glutamate. However, the glutamate concentration in the extracellular fluid that evoked firing, as assessed by the electrochemical marker (DOPAC), was equal across each of the barrel concentrations examined (Figure 3.7C). The apparent discrepancy between these results is explained by recalling that ions can diffuse into the barrel even without a retaining current (Figure 3.6), altering the true mole fraction at the end of the barrel. Since

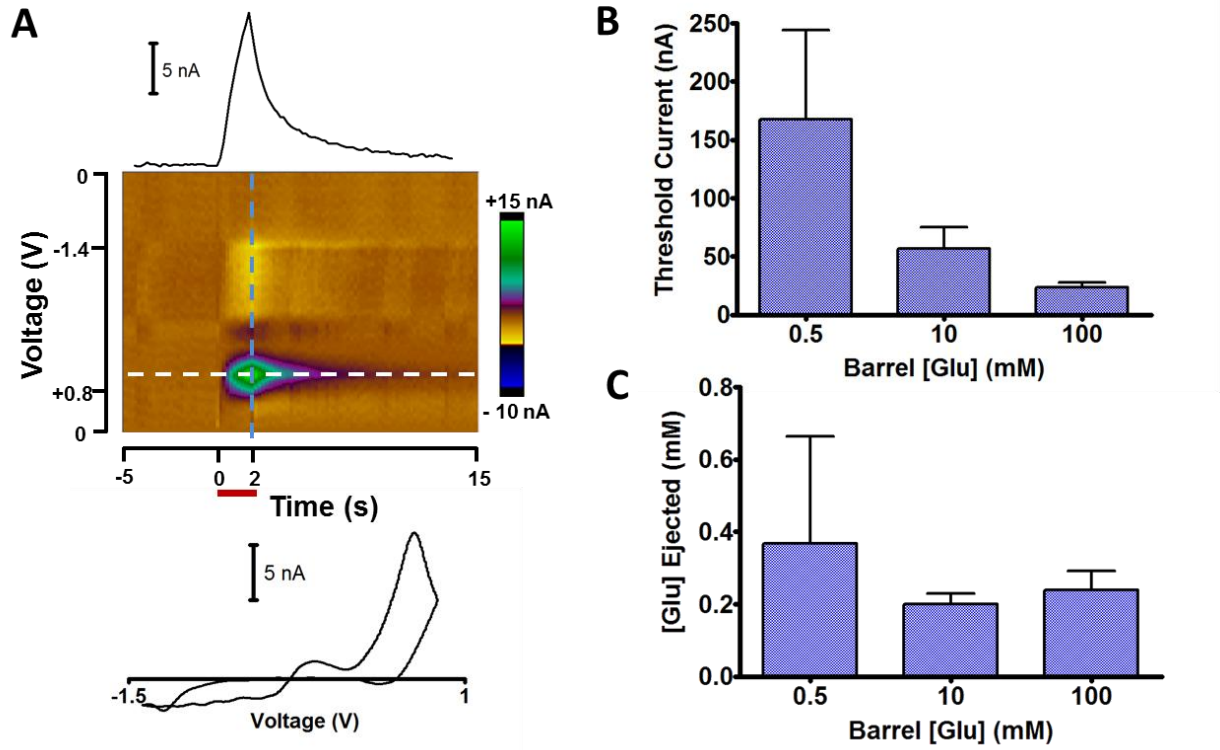

Figure 3.7 Deviation from ideal behavior in vivo. Barrels containing equimolar glutamate and DOPAC were used to evoke activity from medium spiny neurons in the dorsal striatum of an anesthetized rat. The iontophoresis probe contained 3 barrels of different concentrations and a carbon-fiber electrode to simultaneously monitor ejections through FSCV and record electrophysiology. (A) Electrochemical response for a 2 s ejection of 100 mM glutamate/DOPAC. The false color plot shows the background subtracted current. A horizontal cross-section (white dash) results in a current versus time trace (above) and the vertical cross section (blue dash) returns the DOPAC cyclic voltammogram (below). (B) Average ejection current magnitude required of each solution to initiate cell firing. Error bars represent the SEM (n=5). (C) Average local glutamate concentration for ejections in B. Concentrations were determined from the DOPAC signal with comparison to flow injection analysis calibration.

approximately equal quantities would be expected to diffuse into all barrels, this would most dramatically lower the fraction for the lowest concentration. In turn, this requires a larger current to eject the same quantity of the drug. Slight differences in EOF due to different applied voltages may also occur. Applications with short ejection times and long intervals between ejections are particularly susceptible to errors due to mixing. These experiments demonstrate the crucial role of electrochemical monitoring and its ability to correct for this effect.

Although the threshold extracellular glutamate concentration estimated from the electroactive marker was similar for all barrels, this estimate may not be precise. The NMDA, AMPA, and kainate receptors which bind glutamate are activated at low µM levels, while excitotoxicity in striatal cells occurs around 100 µM (Patneau and Mayer, 1990; Chen et al., 1995; Kew and Davies, 2010). The likely source of error is the calibration procedure for the electroactive marker, DOPAC. Calibration was done with flow injection analysis that results in a steady-state response to concentration. However, with 2 s ejections a steep concentration gradient exists across the electrode (Figure 3.1B). Thus, while the DOPAC response during these short ejections represents the average concentration across the electrode, it does not report the concentration at the microscopic site where the response was evoked by glutamate. Despite this, the ejected amounts which initiated cell firing resulted in similar responses to the electrochemical marker. Therefore, the oxidation current provided a reliable determination of the relative glutamate concentration at sites near iontophoresis probes, which demonstrates it can be an effective procedure for comparing relative ejection quantities. This is preferable to

reliance on the ejection current and a theoretical transport number, which as we have shown, are susceptible to experimental conditions.

CONCLUSIONS

We have demonstrated principles enabling greater control of microiontophoretic ejections. The concentration distribution of ejected species is diffusion limited 100 μm from the barrel tip for ejections <500 nA, and the ejection rate increases proportionally with the current. Both properties are independent of the ejection current polarity. Concerning ejection rates of molecular species, ions are ejected in proportion to ionic mole fraction of the barrel solution. For neutral substances, the transference number scales with the barrel concentration. To best maintain barrel composition between ejections, retaining currents should be avoided. In practice, diffusional exchange between the barrel solution and the ejection medium will occur. Electrochemical or fluorescent markers can be incorporated into the barrel solution to monitor ejection progress and correct for variability in ejected quantities.

REFERENCES

Armstrong-James M, Millar J (1980) Quantification of noradrenaline iontophoresis. Nature 288:181-183.

Belle AM, Owesson-White C, Herr NR, Carelli RM, Wightman RM (2013) Controlled iontophoresis coupled with fast-scan cyclic voltammetry/electrophysiology in awake, freely moving animals. ACS Chem Neurosci 4:761-771.

Bevan P, Bradshaw CM, Pun RY, Slater NT, Szabadi E (1981) Electro-osmotic and iontophoretic release of noradrenaline from micropipettes. Experientia 37:296-297.

Bradley PB, Candy JM (1970) Iontophoretic release of acetylcholine, noradrenaline, 5-hydroxytryptamine and d-lysergic acid diethylamide from micropipettes. Br J Pharmacol 40:194-201.

Bronzi D, Licata F, Li Volsi G (2015) Noradrenergic modulation of glutamate-induced excitatory responses in single neurons of the red nucleus: An electrophysiological study. Neuroscience 300:360-369.

Bucher ES, Fox ME, Kim L, Kirkpatrick DC, Rodeberg NT, Belle AM, Wightman RM (2014) Medullary norepinephrine neurons modulate local oxygen concentrations in the bed nucleus of the stria terminalis. J Cereb Blood Flow Metab 34:1128-1137.

Bucher ES, Brooks K, Verber MD, Keithley RB, Owesson-White C, Carroll S, Takmakov P, McKinney CJ, Wightman RM (2013) Flexible Software Platform for Fast-Scan Cyclic Voltammetry Data Acquisition and Analysis. Anal Chem 85:10344-10353.

Buffalari DM, Grace AA (2007) Noradrenergic Modulation of Basolateral Amygdala Neuronal Activity: Opposing Influences of α-2 and β Receptor Activation. J Neurosci 27:12358-12366.

Chen Q, Harris C, Brown CS, Howe A, Surmeier DJ, Reiner A (1995) Glutamate-Mediated Excitotoxic Death of Cultured Striatal Neurons Is Mediated by Non-NMDA Receptors. Exp Neurol 136:212-224.

Delgado-Charro MB (2012) Iontophoretic drug delivery across the nail. Expert Opin Drug Deliv 9:91-103.

Eljarrat-Binstock E, Domb AJ (2006) Iontophoresis: a non-invasive ocular drug delivery. J Control Release 110:479-489.

Ford CP, Gantz SC, Phillips PEM, Williams JT (2010) Control of extracellular dopamine at dendrite and axon terminals. J Neurosci 30:6975-6983.

Gerfen CR, Surmeier DJ (2011) Modulation of striatal projection systems by dopamine. Annu Rev Neurosci 34:441-466.

Gerhardt GA, Palmer MR (1987) Characterization of the techniques of pressure ejection and microiontophoresis using in vivo electrochemistry. J Neurosci Methods 22:147-159.

Guy Y, Faraji AH, Gavigan CA, Strein TG, Weber SG (2012) Iontophoresis from a micropipet into a porous medium depends on the zeta-potential of the medium. Anal Chem 84:2179-2187.

Harding JW, Felix D (1987) Quantification of angiotensin iontophoresis. Journal of Neuroscience Methods 19:209-215.

Helfferich FG (1962) Ion Exchange: McGraw-Hill.

Herr NR, Kile BM, Carelli RM, Wightman RM (2008) Electroosmotic flow and its contribution to iontophoretic delivery. Anal Chem 80:8635-8641.

Herr NR, Daniel KB, Belle AM, Carelli RM, Wightman RM (2010) Probing presynaptic regulation of extracellular dopamine with iontophoresis. ACS Chem Neurosci 1:627-638.

Invernizzi RW, Pierucci M, Calcagno E, Di Giovanni G, Di Matteo V, Benigno A, Esposito E (2007) Selective activation of 5-HT2C receptors stimulates GABA-ergic function in the rat substantia nigra pars reticulata: A combined in vivo electrophysiological and neurochemical study. Neuroscience 144:1523-1535.

Kasting GB (1992) Theoretical models for iontophoretic delivery. Adv Drug Deliv Rev 9:177-199.

Kaur G, Hrabetova S, Guilfoyle DN, Nicholson C, Hrabe J (2008) Characterizing molecular probes for diffusion measurements in the brain. J Neurosci Methods 171:218-225.

Kew JNC, Davies CH (2010) Ion channels from structure to function, 2nd Edition. Oxford: Oxford University Press.

Kirkpatrick DC, Edwards MA, Flowers PA, Wightman RM (2014) Characterization of Solute Distribution Following Iontophoresis from a Micropipet. Anal Chem 86:9909-9916.

Kovács P, Dénes V, Kellényi L, Hernádi I (2005) Microiontophoresis electrode location by neurohistological marking: Comparison of four native dyes applied from current balancing electrode channels. J Pharmacol Toxicol Methods 51:147-151.

Kruk ZL, Armstrong-James M, Millar J (1980) Measurement of the concentration of 5-hydroxytryptamine ejected during iontophoresis using multibarrel carbon fibre microelectrodes. Life Sci 27:2093-2098.

Lalley P (1999) Microiontophoresis and Pressure Ejection. In: Modern Techniques in Neuroscience Research (Windhorst U, Johansson H, eds), pp 193-212: Springer Berlin Heidelberg.

MacInnes DA (1961) The Principles of Electrochemistry. New York: Dover.

Marro D, Kalia YN, Delgado-Charro MB, Guy RH (2001) Optimizing iontophoretic drug delivery: Identification and distribution of the charge-carrying species. Pharm Res 18:1709-1713.

Mudry B, Guy RH, Delgado-Charro MB (2006) Transport numbers in transdermal iontophoresis. Biophys J 90:2822-2830.

Mudry B, Carrupt PA, Guy RH, Delgado-Charro MB (2007) Quantitative structure-permeation relationship for iontophoretic transport across the skin. J Control Release 122:165-172.

Nastuk WL (1953) Membrane potential changes at a single muscle end-plate produced by transitory application of acetylcholine with an electrically controlled microjet. Fed Proc 12:120.

Patneau DK, Mayer ML (1990) Structure-Activity Relationships for Amino Acid Transmitter Candidates Acting at N-Methyl-D-Aspartate and Quisqualate Receptors. J Neurosci 10:2385-2399.

Pikal MJ (1990) Transport Mechanisms in Iontophoresis. I. A Theoretical Model for the Effect of Electroosmotic Flow on Flux Enhancement in Transdermal Iontophoresis. Pharm Res 7:118-126.

Priya B, Rashmi T, Bozena M (2006) Transdermal iontophoresis. Expert Opin Drug Deliv 3:127-138.

Purves R (1979) The physics of iontophoretic pipettes. J Neurosci Meth 1:165-178.

Purves R (1980) Ionophoresis - progress and pitfalls. Trends Neurosci 3:245-247.

Rutherford A, Garcia-Munoz M, Arbuthnott GW (1988) An afterhyperpolarization recorded in striatal cells 'in vitro': effect of dopamine administration. Exp Brain Res 71:399-405.

Suh TH, Wang CH, Lim RKS (1936) The effect of intracisternal application of acetylcholine and the localization of the pressor centre and tract. Chin J Physiol 10:61-78.

Sykova E, Nicholson C (2008) Diffusion in brain extracellular space. Physiol Rev 88:1277-1340.

Takmakov P, McKinney CJ, Carelli RM, Wightman RM (2011) Instrumentation for fast-scan cyclic voltammetry combined with electrophysiology for behavioral experiments in freely moving animals. Rev Sci Instrum 82:074302.

VanOrman BB, Liversidge GG, McIntire GL, Olefirowicz TM, Ewing AG (1990) Effects of buffer composition on electroosmotic flow in capillary electrophoresis. J Microcolumn Sep 2:176-180.

Wang Y, Liu J, Gui ZH, Ali U, Fan LL, Hou C, Wang T, Chen L, Li Q (2011) α2-Adrenoceptor regulates the spontaneous and the GABA/glutamate modulated firing activity of the rat medial prefrontal cortex pyramidal neurons. Neuroscience 182:193-202.

Watson C, Paxinos G (2006) The Rat Brain in Stereotaxic Coordinates, 6 Edition. London: Academic Press.

Windhorst U, Johansson H (1999) Modern Techniques in Neuroscience Research, 1 Edition: Springer Berlin Heidelberg.

Zare HR, Namazian M, Coote ML (2009) Experimental and theoretical studies of electrochemical characteristics of 3,4-dihydroxyphenylacetic acid (DOPAC). Electrochim Acta 54:5353-5357.

CHAPTER 4: EVALUATION OF DRUG CONCENTRATIONS DELIVERED BY MICROIONTOPHORESIS[3]

INTRODUCTION

Microiontophoresis describes the ejection of solute from a capillary by an electric current. This technique has been widely used in neuroscience to deliver drugs, neurotransmitters, and labeling agents to specific areas of the brain (Ni et al., 2001; Staak and Pape, 2001; Beckstead et al., 2004; Kovács et al., 2005). While offering advantages over conventional delivery methods, the inability to determine ejection quantity or confirm drug delivery has impeded microiontophoresis from having greater impact. Indeed, the modern use of microiontophoresis is primarily for qualitative investigations (Leiras et al., 2010; Herr and Wightman, 2013; Wang et al., 2013; Patel and Zhang, 2014; Ayala and Malmierca, 2015). Commonly the ejection quantity is varied by adjusting the magnitude of the ejection current, but such methods are usually carried out without confirmation of the delivered amount (Invernizzi et al., 2007; Lipski and Grace, 2013; Bronzi et al., 2015). Because similar ejection conditions can result in different delivery rates, most users do not make precise claims of their ejection concentrations.

Theoretical attempts to determine ejection quantities have assigned transport numbers to specific analytes (Purves, 1980b). However slight variations in barrel geometries result in different transport numbers between similarly fabricated probes (Bloom, 1974). Additionally,

[3] This chapter is currently under review as an article in *Analytical Chemistry*. The citation will read follows:
Kirkpatrick DC, Walton, LR, Edwards, MA, Wightman, RM (2016) Quantitative Analysis of Iontophoretic Drug Delivery from Micropipettes. Anal Chem (submitted).

the ejection medium may influence the concentration distribution, rendering estimates of concentration from the ejection quantity meaningless (Trubatch and Van Harreveld, 1972; Guy et al., 2012). Measurement strategies for ejected solutions have shown more promise, as electrodes positioned near or adjacent to the barrel can detect the delivery of electroactive substances, as can fluorescence measurements for fluorophores, without affecting their delivery to the adjacent region (Dionne et al., 1978; Havey and Caspary, 1980; Kaur et al., 2008; Inagaki et al., 2009; Ford et al., 2010). These methods have the advantage of providing simultaneous information regarding the ejection progress with locally collected physiological data (Kruk et al., 1980; Haidarliu et al., 1995; Bucher et al., 2013). One technique for monitoring ejections, controlled iontophoresis, employs a carbon-fiber microelectrode incorporated into a multibarreled probe, with the remaining barrels used for ejections (Armstrong-James and Millar, 1979; Fu and Lorden, 1996). Ejection of an electroactive substance can be detected, quantified, and its concentration related to that of a co-ejected inactive compound if the relative mobilities are known (Belle et al., 2013). For use in brain tissue, the electroactive species, or marker, must be inert to the neurochemical processes under investigation (Herr et al., 2010).

We have previously shown that ejection rates of markers and drugs are consistent and can be determined from their mobilities in capillary electrophoresis because the same mass transport mechanisms, electroosmotic flow and migration, are operant in both techniques (Herr et al., 2008). In this study, ejections of quinpirole (QP), a D2 receptor agonist, were performed with an electrochemical marker to estimate the drug delivery quantity. QP inhibits dopamine (DA) release in a dose-dependent manner by binding to the autoreceptor on pre-synaptic DA terminals (Kennedy et al., 1992). Using the diminished stimulated DA release quantity following QP ejections and the electrochemical signal from the marker, we determined the accuracy of

calculated ejected drug concentrations. Our initial results had large discrepancies between the calculated concentrations and the observed effects. We then determined the causes of the poor predictions by evaluating the factors that govern evaluations of ejected concentrations. Through this, it is shown how optimized methods can improve assessments of drug concentrations in controlled iontophoresis.

EXPERIMENTAL

Chemicals and Solutions

All chemicals were received from Sigma Aldrich (St. Louis, MO). Artificial cerebral spinal fluid (aCSF) consisted of 126 mM NaCl, 2.5 mM KCl, 1 mM NaH_2PO_4, 26 mM $NaHCO_3$, 2 mM $MgSO_4$, 2 mM $CaCl_2$, and 11 mM glucose and adjusted to pH 7.4. Iontophoretic solutions were made fresh daily from deionized water and the pH consistently measured between 6 and 7. To prevent clogging, solutions were filtered (0.45 µm Nylon, Nalgene, USA) before addition to the barrel.

Iontophoresis with Fast-Scan Cyclic Voltammetry

Four-barreled iontophoresis probes (0.5 – 1 µm tip diameter) were fabricated from pre-fused glass capillaries (Friedrich & Dimmock, Millville, NJ) as previously described (Belle et al., 2013). One of the barrels held a capillary containing a carbon fiber (7 µm diameter) cut to approximately 100 µm while the other barrels were available for ejections. A homemade current source (UNC Electronics Facility, Chapel Hill, NC) was used in combination with customized LabVIEW code (National Instruments, Austin, TX) to control ejections through an NI-USB-6343 DAQ card (National Instruments). For each ejection, a constant current was applied to the barrel and the corresponding voltage data was recorded. A single Ag/AgCl reference electrode (World

Prescision Instruments, Sarasota, FL) held at ground potential was used as the return for iontophoretic ejections and for voltammetry experiments.

As the ejection proceeded, ejected electroactive species were detected by fast-scan cyclic voltammetry (FSCV) at the carbon-fiber microelectrode using a locally constructed instrument (UNC Chemistry Electronics Facility). HDCV software was used to control the potential during voltammetry and to collect data (Bucher et al., 2013). For detection of 2-(4-nitrophenoxy) ethanol (NPE) with DA or acetaminophen (AP), waveform parameters were chosen so that each species could be resolved (Herr et al., 2008). The waveform began from a -0.7 V holding potential, was scanned to -1.3 V, then to 1.0 V, and finally returned to the holding potential. This was done at a scan rate of 200 V/s and repeated at 10 Hz. For dose-response experiments, a waveform was used which optimized the DA signal (Heien et al., 2003). This utilized a holding potential of -0.4 V, which was then scanned to an upper limit of 1.0 V before returning to the holding potential. The scan rate was 600 V/s and the waveform was repeated at 10 Hz.

Fluorescence Microscopy

Iontophoretic barrels were filled with a 10 mM tris(2,2' – bipyridyl)dichlororuthenium(II) ($Ru(bpy)_3Cl_2$) and 5 mM NaCl solution. A micromanipulator (MPC-200-ROE, Sutter Instruments, Novato, CA) was used to insert the barrel tip ~50 µm beneath the surface of a 1% agarose block made from aCSF, which was positioned in a holding chamber on the stage of an Eclipse FN1 microscope (Nikon Instruments). Additional aCSF was added around the agarose in which the Ag/AgCl reference electrode was placed. The microscope was equipped with a xenon halide illumination source (X-Cite 120, EXFO) and filter cubes were used to select the excitation (450-490 nm) and emission (500-550 nm) wavelengths. Images were captured with a Retiga Exi

camera (QImaging, Surrey, BC, Canada) at a resolution of 1 pixel/μm and recorded with QCapture software (QImaging).

Ejections of $Ru(bpy)_3Cl_2$ (120 nA) were performed for 5, 15, or 60 s, and images were recorded every 3-10 s. Additional images were recorded for 1 min following ejection termination. A Matlab script (Mathworks, Natick, MA) was used to determine the average radial $Ru(bpy)_3^{2+}$ distribution of each image by averaging the fluorescence intensity along 11 background subtracted cross-sectional lines spanning from the barrel tip (Kirkpatrick et al., 2014).

Animal Care and Use

Sprague-Dawley male rats (250 – 350 g, Charles River, Wilmington, MA) were used for all *in vitro* experiments. Prior to use rats were dually housed and provided with food and water *ad libitum*. Procedures were approved by the Institutional Animal Care and Use Committee at the University of North Carolina at Chapel Hill. Special care was taken to limit the number of animals used and to reduce their suffering.

Brain Slice Preparation

Following urethane (1.5 g/kg) anesthesia, brains were quickly removed and placed in chilled oxygenated (95/5% O_2/CO_2) aCSF. A vibratome (VF-200, Precisionary Instruments, San Jose, CA) equipped with a stainless steel feather blade (Fendrihan, USA) was used to cut 300 μm thick coronal slices containing the anterior dorsal striatum. After cutting, slices were allowed to recover for at least 1 hour in 20 ˚C aCSF. For recordings slices were anchored (SHD-22KIT, Warner Instruments, Hamden, CT) in a perfusion chamber (RC-22, Warner Instruments) on the microscope stage. A continuous (2 mL/min) stream of 37 ˚C oxygenated aCSF was perfused

through the chamber. A 30 min equilibration period in the perfusion chamber was assigned for each slice prior to measurements.

Dose-Response Curves

A bipolar tungsten electrode with 250 □m spacing (MicroProbes, Gaithersburg, MD) was used to evoke DA release. It was inserted ~50 □m below the surface of a brain slice in the dorsal striatum. Release was evoked by a single 350 □A biphasic pulse (2 ms/phase) and detected using FSCV at a carbon-fiber microelectrode positioned midway between the stimulating electrodes. To avoid electrical interference the stimulation was applied 10 ms before the FSCV waveform. Release was evoked at 4 min intervals. After an initial conditioning phase of approximately 30 min, DA release was stable, changing by less than 10% between stimulations (Limberger et al., 1991; Kennedy et al., 1992). To apply QP via perfusion, the standard aCSF stream was switched to aCSF containing a known concentration of the drug. Stimulation continued every 4 min until released DA stabilized at a new concentration, typically achieved within 20-30 min (Jones et al., 1995). This value was taken as the effect of the drug and was compared to pre-drug release. Dosages were applied in increasing order, with no more than four concentrations per slice.

For iontophoretic experiments the carbon-fiber microelectrode was incorporated in a multibarreled probe, positioned in the dorsal striatum at a location similar to those in the perfusion experiments. Identical biphasic electrical stimulations were used, and co-ejections (5, 15, or 60 s) of QP and an electrochemical marker were performed after consistent DA release was established. Stimulation occurred at precise times after the ejection (3, 15, or 60 s). The amount of DA released from stimulation after the ejection was recorded as the post-drug release

quantity. Ejections were timed so that a 4 min stimulation rate was maintained. To allow recovery from previous administration, two stimulations were performed between successive ejections. AP and DHBA were used independently as markers to monitor ejections via oxidation on the carbon-fiber electrode. For AP trials, a 1 mM solution of the marker, 0.3 µM QP, and 5 mM NaCl was ejected. For DHBA, the concentrations of the marker, QP, and NaCl were chosen based on the ejection duration and time before stimulation to allow for complete coverage of the dose-response curve, and to assure for detection of the marker within the linear calibration range. Exact barrel concentrations are reported individually for each case.

Statistical Analysis of Dose-Response Data

Regression curves and parameters for dose-response data were determined in Prism (GraphPad Software, La Jolla, CA) using a sigmoidal dose-response (variable slope) model, which employs a four parameter logistic Hill equation to fit data. Constraints were applied for the maximum equal to 1.0 and the bottom less than or equal to 0.2. These were required for several iontophoresis datasets (AP and DHBA with 3 s wait time) which displayed highly varied responses, and were chosen based off perfusion results. All P-values reported for the best-fit parameters were calculated using the comparison method with an F test.

RESULTS AND DISCUSSION

Advantages of Microiontophoretic Drug Delivery

Quantitative drug application is challenging in neurochemical investigations. Doses administered *in vivo* are typically based on the animal's mass, but uptake and metabolism ultimately determine the effective concentration at the region of interest. *In vitro* experiments can more reliably perfuse known concentrations throughout a brain slice, but long application

times are required to attain equilibrium. The perfusion procedure we employed is illustrated in Figure 1A. A carbon-fiber microelectrode was used to detect DA by FSCV in the dorsal striatum of a rat brain slice. The DA signal increased directly following electrical stimulation and returned to baseline shortly after. Failure to return to the exact baseline could be due to chemical interferences or electrode drift (Schultz et al., 2015). After the pre-drug release stabilized , 30 nM QP was administered. Evoked DA release gradually decreased during perfusion until a new stable release quantity was achieved. Due to the time required for the drug to diffuse into the slice, its full inhibitory effect was not realized until nearly 20 min after its application.

In contrast, locally delivered drugs from microiontophoresis take effect in seconds which allows for more rapid investigations. To illustrate this, Figure 4.1B shows a controlled iontophoresis ejection in which the oxidation current of a co-ejected marker, DHBA, was monitored by FSCV on a carbon-fiber microelectrode during QP delivery. The inhibitory effect of QP on stimulated DA release was observed 15 s after the ejection (Figure 4.1C).

Concentration Evaluations of Controlled Ejections

To determine concentrations of ejected species from controlled iontophoresis, Equation 4.1 was used where i_m is the marker current at the end of the ejection, A_m is a flow-analysis

$$[D] = i_m \times A_m \times \frac{[M]_b}{[D]_b} \times \frac{v_D}{v_M} \times DF \qquad \text{Equation 4.1}$$

calibration factor, $[M]_b$ and $[D]_b$ are the respective marker and drug barrel concentrations, $\frac{v_D}{v_M}$ is their mobility ratio in an electric field, and DF is a dilution factor (Herr et al., 2010). The marker current, calibration factor, barrel concentrations, and electric mobility ratio provide the average concentration of the marker at the end of the ejection. The dilution factor adjusts for the amount

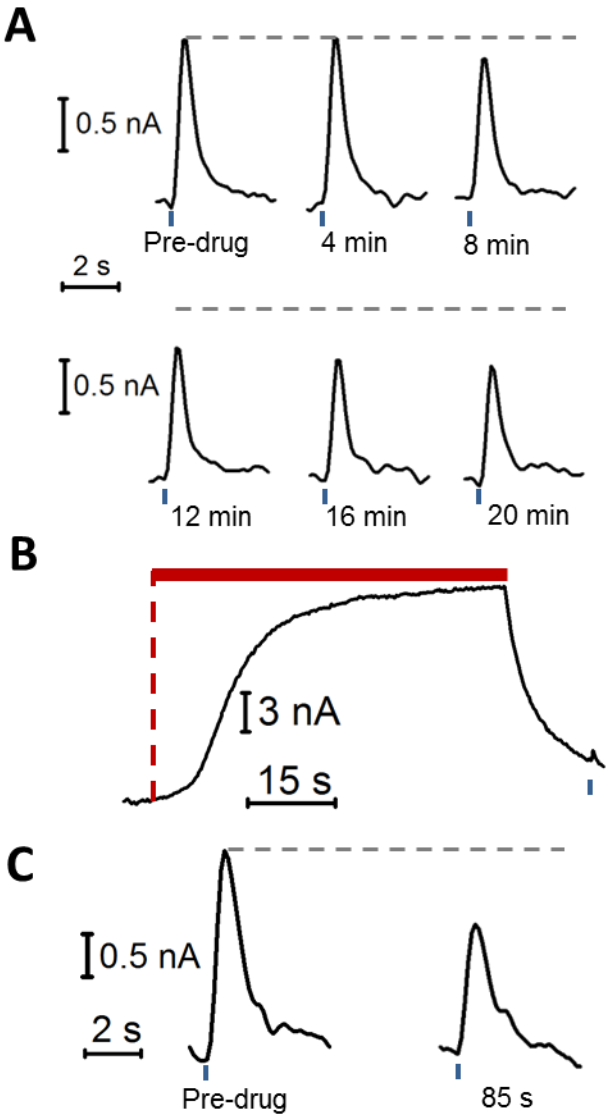

Figure 4.1 Comparison of drug administration by perfusion and controlled iontophoresis in the dorsal striatum of a brain slice. (A) Electrically evoked DA release was monitored with a microe-lectrode during perfusion of 30 nM QP. The released amount before drug (termed baseline, dashed grey line) was established and the perfusion stream was switched to aCSF containing QP; this time was taken as t = 0. Stimulation continued every 4 min (blue bars) until the new release quantity was stable. (B) Controlled iontophoretic delivery of QP. An iontophoretic probe containing a carbon-fiber microelectrode was used to eject a solution of QP, DHBA, and NaCl (0.4, 0.2, 5 mM, respectively) at 15 nA for 60 s (red bar). The oxidation of DHBA upon ejection was detected by FSCV performed on the electrode. DA release was elicited 15 s after the end of the ejection and was also detected by the carbon fiber. (C) Comparison of baseline and post-drug DA release following the ejection in B.

of drug remaining at the time of stimulation, typically 5-120 s after the ejection is terminated. This value is empirically determined by the fraction of the marker oxidation current at the stimulation time compared to its steady-state value (Figure 4.1B). The ability of Equation 4.1 to yield ejection concentrations was tested by comparing responses of controlled iontophoresis to those obtained from perfusion of QP, the standard drug delivery method for slice experiments. For perfusion, known QP concentrations were administered to the slice and the electrically evoked DA response was recorded after a new stable value was obtained. This quantity was compared to the pre-drug release amount, and as indicated by the error bars, results were highly reproducible (Figure 4.2, squares). Best-fit parameters from a four parameter Hill regression model yielded an IC_{50}, the drug concentration which inhibits maximal release by half, of 37 nM, a Hill slope, indicating the cooperativity at the binding site, of -1.28 (Table 4.1), and a reasonable value of the correlation coefficient (Khinkis et al., 2003). Each of these parameters agrees with previously reported values (Miller, 2008; O'Neill et al., 2009). Next, dose-response data were collected for controlled iontophoretic delivery of QP, a monocation at the pH values employed. In these initial experiments, AP, a neutral molecule, was used as the electroactive marker. Ejections were 15 s in length and DA release was evoked 15 s after the end of the ejection, with data obtained from 5 different iontophoretic probes due to barrel to barrel ejection variability (Purves, 1980a). Figure 4.2 (circles) shows the DA response to iontophoretic delivery of QP using Equation 4.1 to evaluate ejection concentrations. These data have two major differences compared to the perfusion data. First, as reflected by the low correlation coefficient, the data were highly scattered and displayed a considerable degree of variance. Second, concentration estimates systematically underestimated the effective value, as a significantly different IC_{50} ($P < 0.0001$) was determined between delivery modes. Thus controlled iontophoresis failed to

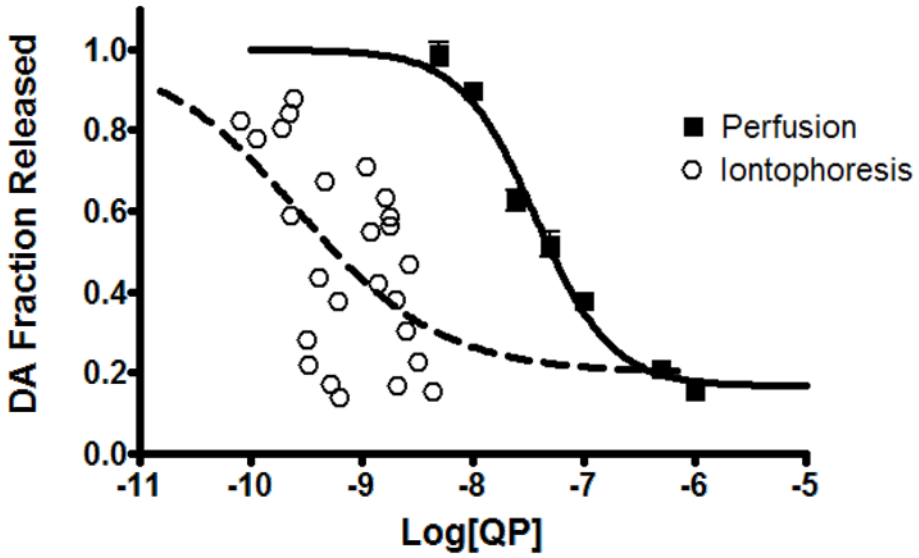

Figure 4.2 Dose-response data for the effect of QP on stimulated DA release in the dorsal striatum. QP was delivered by perfusion (squares, n=5 per concentration) or controlled iontophoresis (circles). Iontophoretic ejections (5 ejections from 5 unique probes) were monitored using AP and QP concentrations were evaluated using Equation 1. Error bars for perfusion represent the SEM.

	Perfusion	**Iontophoresis**
Log(IC_{50})	-7.43 ± 0.04	-9.57 ± 0.83
Hill slope	-1.28 ± 0.12	-0.68 ± 0.83
r^2	0.966	0.296

Table 4.1 Parameters of perfusion and iontophoretic dose-response data for QP administration and its effect on stimulated DA release. Parameters are from analysis of data shown in Figure 4.2 using a four parameter Hill model. Perfusion trials utilized 5 measurements at each concentration. Iontophoretic data was obtained by 5 ejections from 5 different probes. AP was used as the electro-chemical marker and concentrations were evaluated using Equation 1. Entries indicate the value and SEM.

produce either accuracy or precision in evaluation of ejected concentrations.

Initial Ejection Behavior Influenced by Molecular Charge

To understand the failure of Equation 4.1 to reliably predict concentrations, the behavior of co-ejected species was further examined by ejecting a solution of DA, a protonated monocation at physiological pH, and the neutral molecule NPE into aCSF. These two compounds can be individually detected by FSCV during their co-ejection. Since mass transport in iontophoresis is a consequence of electroosmotic flow (EOF) and migration, ejection rates are dependent upon molecular charge and size (Mudry et al., 2006; Mudry et al., 2007; Herr et al., 2008). Because these molecules are similarly sized, variation in their transport is primarily due to their charge difference, with EOF acting equally on both molecules while only DA is affected by migration. Temporal ejection profiles revealed a clear delay in NPE ejection compared to DA (Figure 4.3A). This indicates that initiation of mass transport by EOF lags that of migration.

The delayed action of EOF is due to the time required to eject the interfacial layer from the barrel tip. The interfacial layer is a heterogeneous region created by exchange between the barrel solution and the ejection medium during the time between ejections (Bradshaw and Szabadi, 1974). When the ejection was initiated, the voltage increased step-wise and rose more gradually as time progressed (Figure 4.3B). More voltage was required to maintain a constant ejection current because the highly ionic interfacial layer in the barrel tip was first ejected, increasing the total resistance of the barrel solution. Once this layer was cleared, the voltage approached steady state, and EOF was initiated.

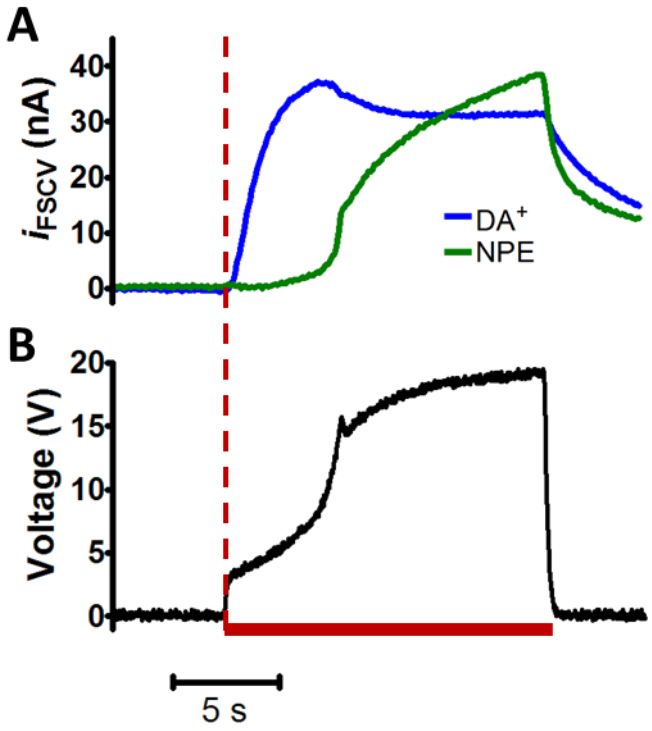

Figure 4.3 Combined delivery of differently charged species. (A) Faradaic current versus time traces for DA (blue) and NPE (green) during co-ejection. A solution of 1 mM DA, 11 mM NPE, and 5 mM NaCl was ejected (red bar) into aCSF while a carbon-fiber microelectrode was used to monitor delivery. (B) Ejection voltage required to supply 30 nA for the ejection in A.

Ejection Current Affects Interfacial Layer Clearance Time

To further characterize combined delivery, the experiment was repeated using different ejection currents that followed 3 min waiting periods. Differences in the ejected quantities of DA and NPE were more apparent at lower ejection currents (Figure 4.4A, upper). Further, the ratio of the faradaic current between the two species at the end of ejections was dependent on the ejection current (Figure 4.4B, right, ANOVA, P=0.0016). This is because larger currents more quickly cleared the interfacial layer from the tip, which afterwards allowed for the ejection of bulk barrel solution. For weaker ejections the interfacial layer took longer to eject, and in some instances, was not cleared.

The problem of differential ejection rates was remedied by ejecting species of similar charge (Figure 4.4A, lower). When DA was replaced with AP, ejected quantities of the two neutral species were similar regardless of the ejection current (Figure 4.4B, right, ANOVA, P=0.090). These experiments explain why the neutral AP marker failed to reliably track the ejection of positively charged QP in the controlled iontophoresis dose-response experiment. Delayed EOF at the onset of ejections resulted in the delivery of the drug without the marker, leading to inconsistent and underestimated concentrations. Although we have previously documented significant EOF in barrels of high ionic strength (200 mM), these measurements were made for ejections lasting multiple minutes from barrels which were fully primed beforehand (Kirkpatrick et al., 2016). Continuous ejections of this sort prohibit the formation of an interfacial layer, and indeed are often employed specifically for this purpose (Rice and Nicholson, 1991; Rice et al., 1993). Additional work comparing DA and NPE ejection rates involved rapidly alternating between ejection and rest periods, conditions which similarly minimize the interfacial layer (Herr et al., 2008). The key difference in the current study is that

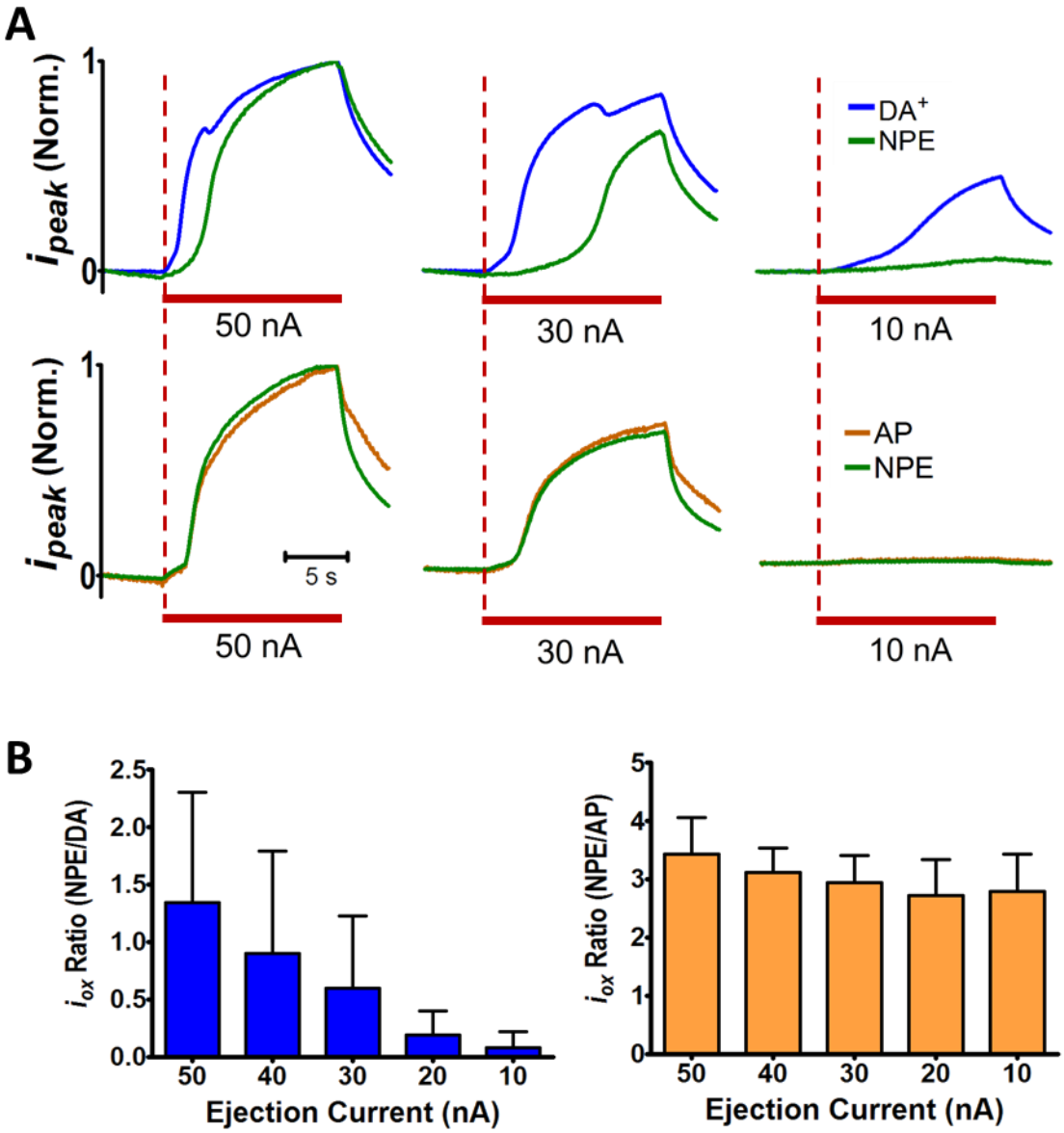

Figure 4.4 Variation in delivery profiles of co-ejected species with ejection current. (A) Representative current versus time traces for co-ejected species when ejected using different currents. Delivery from barrels containing 1 mM DA (blue) and 11 mM NPE (green) reveal differential ejection amounts with the ejection current magnitude (upper). Solutions of 5 mM AP (orange) and 11 mM NPE (green) resulted in similar delivery profiles (lower). All profiles were normalized to the maximum value obtained during the 50 nA ejection. Solutions also contained 5 mM NaCl. (B) Ratio of the maximum faradaic current of co-ejected species for NPE/DA (left) and NPE/AP (right).

an interfacial layer was allowed to form during a 3 min waiting period prior to ejections, which caused the delay in EOF. Thus the electric mobility term of Equation 4.1 $\left(\frac{v_D}{v_M}\right)$ correcting for different ejection rates between dissimilarly charged species is dependent on the time required to eject the interfacial layer. However, as demonstrated, this term can be disregarded when the charge and molecular size of ejected species are similar because analytes of comparable mobility exhibit similar ejection behavior.

Reevaluating Ejection Concentrations with Modified Approaches

To further examine the failure of Equation 4.1 to properly evaluate concentrations from controlled iontophoresis, the solute distribution of ejections was studied using fluorescence microscopy. $Ru(bpy)_3^{2+}$, a cationic fluorophore, was ejected into a 1% agarose gel which produces a similar distribution as ejections in brain tissue (Kirkpatrick et al., 2014). A color plot of the fluorescence intensity after 15 s of continuous ejection is shown in Figure 4.5A, which demonstrates how the maximum intensity occurs at the barrel tip and decays with spherical symmetry. Following a 15 s period with the ejection current turned off, the same distribution becomes much more uniform (Figure 4.5B). The time-course of the intensity at different locations during and following 15 s ejections is shown in Figure 4.5C. Due to the symmetrical nature of the distribution, these intensities represent the concentration on a sphere of radius *r* around the ejection point. Reduced concentrations after the ejection show the importance of the dilution factor (DF) in Equation 4.1, which to this point was determined by the ratio of the marker current at stimulation compared to the steady state value. However due to solute adsorption, concentration heterogeneity, and capacitive drift of the electrode, we feared this method was susceptible to error (Johnson et al., 2016). Instead, DF was determined from the

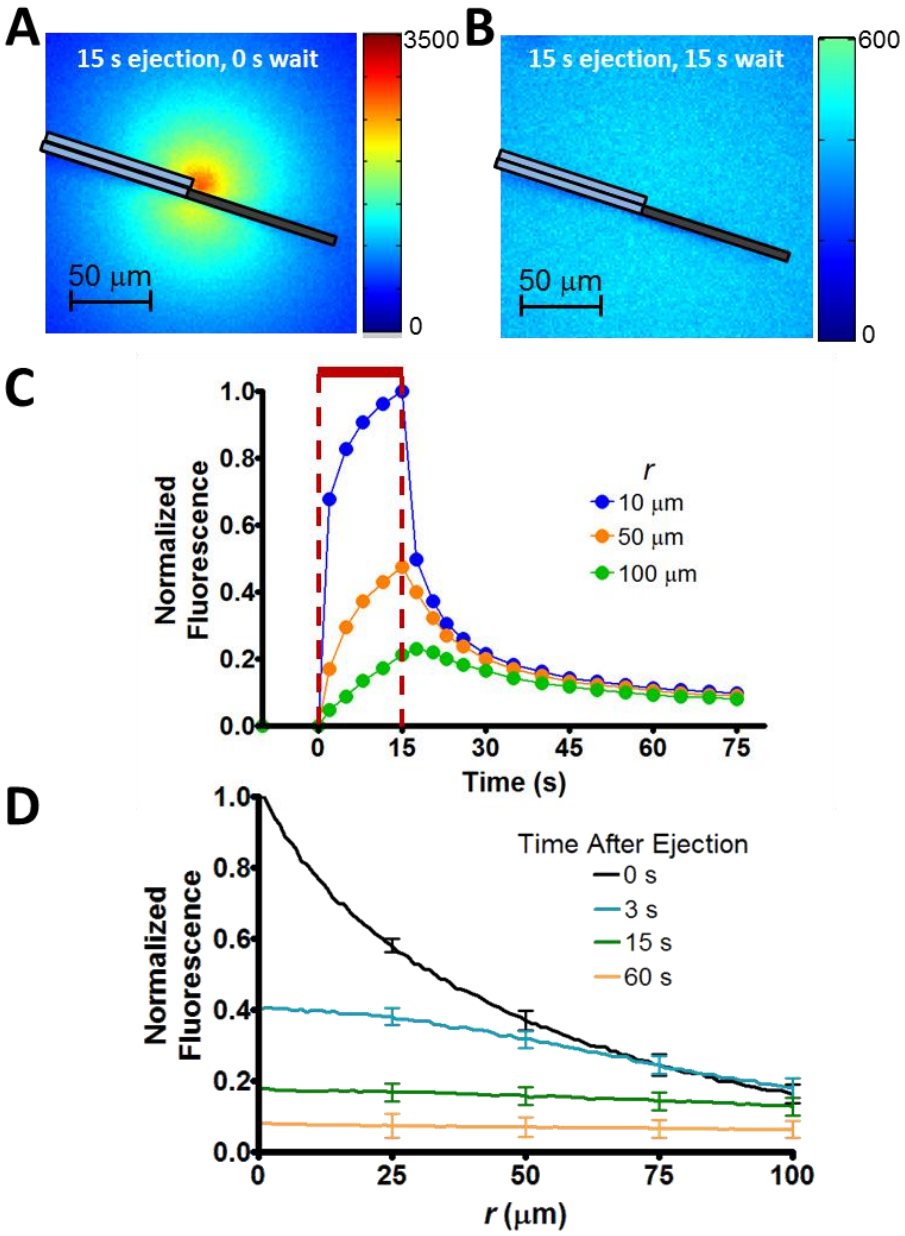

Figure 4.5 Distribution of ejected solute during and after iontophoretic delivery. (A) Color plot of $Ru(bpy)_3^{2+}$ fluorescence intensity at the end of a 15 s ejection and (B) the same distribution after a 15 s waiting period during which the ejection current was disabled. The location of the carbon-fiber electrode (black) and iontophoretic barrel (light blue) are indicated by the overlaid representation. (C) Fluorescence intensity on a sphere of radius r centered at the ejection origin during and following ejection (n=8). All values were normalized to the maximum intensity 10 µm from the ejection point. The red bar represents the ejection time and the dashed vertical lines indicate the initiation and termination of the ejection. (C) Distribution of ejected solute along the length of the carbon-fiber electrode at select time points following 15 s iontophoretic delivery.

fluorescence data. Figure 4.5D shows the average fluorescence intensity as a function of distance along the carbon fiber at the end of 15 s ejections, and again for various waiting periods after the ejection was terminated. Each profile was integrated over a sphere to reveal the total amount of solute present. The ratio of the quantity after the waiting period compared to at the end of the ejection gave the new fraction for DF. This value for the 15 s waiting period, 0.55, was larger than that obtained using the electrochemical estimate, 0.14, which resulted in the underestimated concentrations.

To study the ability of controlled iontophoresis to determine ejection concentrations with the updated dilution and mobility factor corrections, dose-response data were obtained for QP using DHBA as the electrochemical marker. Like QP, DHBA is a monocation, but it is electroactive and was found not to affect DA release in the striatum. Figure 4.6A shows that unlike the results obtained with AP as the electroactive marker (Figure 4.2), evaluations using DHBA had a good correlation across multiple barrels and ejection current magnitudes (r^2 = 0.887). Thus, the imprecision of the data in Figure 4.2 was greatly improved by the use of a marker with an identical charge as the drug. However neither this nor the new method for DF resolved the issue of inaccuracy, as the IC_{50} was overestimated by more than an order of magnitude (Table 4.2).

Drug Dilution to a Uniform Distribution Improves Precision

The waiting period between the end of the ejection and stimulation was next examined to determine its role on concentration evaluations. Dose-response data were generated using 15 s ejections with DHBA as the marker for waiting periods of 3 and 60 s (Figure 4.6B). The difference between IC_{50} values was insignificant, indicating that the duration of the waiting

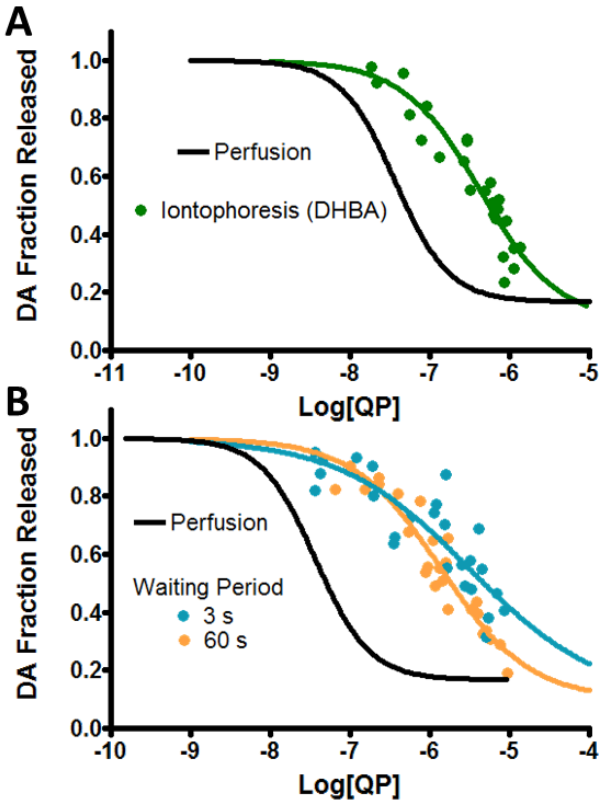

Figure 4.6 Controlled iontophoretic dose-response data for QP administration using DHBA to monitor ejections. (A) Responses following 15 s ejections with a 15 s waiting period. (B) Dose-response data for 3 and 60 s waiting periods following 15 s ejections. For all ejections, Equation 4.1 was used to evaluate concentrations using the fluorescence dilution factor (DF = 0.94, 0.55, and 0.25 for the 3, 15, and 60 s waiting periods, respectively). Barrels contained 0.2 mM DHBA and 0.05 mM QP for the 3 and 15 s waiting periods. For 60 s, this was increased to 0.4 mM DHBA and 0.2 mM QP. All barrels contained 5 mM NaCl, and each dataset is comprised of 5 ejections from 5 unique probes.

	3 s	**15 s**	**60 s**
$Log(IC_{50})$	-5.32 ± 0.99	-6.25±0.42	-5.72 ± 0.31
Hill slope	-0.51 ± 0.26	-0.83 ± 0.24	-0.71 ± 0.16
r^2	0.723	0.887	0.906

Table 4.2 Parameters of iontophoretic dose-response data for QP administration on stimulated DA release following different waiting periods. The time indicates the duration between the end of the ejection and DA stimulation. Parameters reflect data displayed in Figures 4.6A and 4.6B, which were obtained by 5 ejections from 5 different probes. DHBA was used to monitor ejections, and concentrations were evaluated using Equation 1 with the updated fluorescence DF method. A four parameter Hill model was used to evaluate parameters and entries indicate the value and SEM.

period did not affect accuracy (Table 4.2, P=0.774). However data for the 3 s waiting period were more weakly correlated compared to 15 s and 60 s intervals. Thus, we concluded that an insufficient waiting period before stimulation can decrease precision, which could be due to several factors. First, shorter waiting periods result in a less uniform concentration across the electrode at the time of stimulation (Figure 4.5D). Terminals with D2 receptors are densely populated and released DA diffuses only a few micrometers in the extracellular space before its uptake back into neurons (Garris et al., 1994; Venton et al., 2003). This means that homogeneous DA release across the electrode necessitates a uniform drug concentration along the length of the carbon fiber, which can only be achieved with longer waiting periods. Secondly, the drug concentration around the electrode is less variable with longer times (Figure 4.5C). The half-life for dissociation of QP to D2 receptors is ~0.15 s (Levant et al., 1992; Lepiku et al., 1997), so waiting periods spanning multiple half-lives allows more time for the drug and receptor to equilibrate at diluted concentrations.

Interestingly dilution to a nearly uniform and stable conformation occurs relatively quickly once ejections are terminated. This is because the highest concentrated region accounts for only a fraction of the solute delivered during the ejection. Indeed, spherical integration of the fluorescence data for the 0 s profile in 5D reveals that just 0.3% of ejected species are found within 10 µm of the ejection origin, while more than 77% is located outside of 50 µm. Due to the spherical nature of the distribution, by which the volume increases with the third power of the radius, regions further away contain the majority of drug and more strongly influence the concentration upon dilution. Thus a moderate wait time (15 s) after ejections is sufficient to form a homogeneous and stable concentration along the electrode.

Ejection Time Affects Accuracy of Concentration Evaluations

The effect of the ejection time was next examined by comparing QP dose-response data for 5 and 60 s ejections. Delivery was monitored with DHBA and DA stimulation occurred following a 15 s waiting period. Concentration evaluations grew more accurate with longer ejection times, and the IC_{50} better matched the perfusion standard (Figure 4.7A, Table 4.3). To determine why this occurred, the solute distribution for each duration was examined using fluorescence microscopy. As shown in Figure 4.7B, both distributions resulted in a gradient along the electrode at the end of ejections. These gradients are problematic because the average concentration of the ejection bolus, which the marker current is intended to represent, does not equal the average concentration along the electrode, which the marker current actually measures. Again this is explained by the spherical distribution of ejected species, whose volume is not appropriately weighted by the marker current. For example, according to the 5 s profile 25% of the marker current is produced within the first 10 μm of the electrode, despite this region containing just 0.5% of the total ejected species. Thus smaller, more concentrated centers of spherical distributions disproportionately contribute to the marker current, leading to overestimated values of the average concentration.

The reason longer ejection durations resulted in more accurate IC_{50} evaluations is because they resulted in less severe gradients at the end of ejections. Since regions further away from the origin become more concentrated with ejection time, they are better represented by the concentration near the ejection point that dominates the marker signal. However even the 60 s ejections overestimated the IC_{50} of perfusion ($P < 0.0001$), which we attribute to several factors. First, after 60 s of continuous delivery, the ejection concentration profile was still non-uniform along the electrode. Ideally the distribution would be homogeneous to match the flow-injection

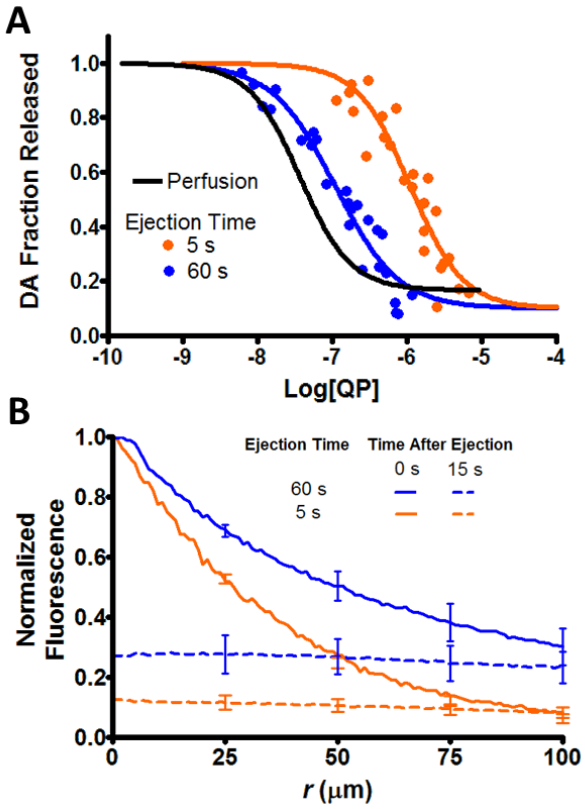

Figure 4.7 Ejection length increases accuracy of concentration evaluations. (A) Dose-response data for 5 and 60 s controlled iontophoretic ejections with a 15 s waiting period. Ejections were monitored using DHBA and Equation 1 was used to evaluate ejection concentrations (DF was 0.63 and 0.62 for 5 and 60 s ejection periods, respectively). Barrels performing 5 s ejections contained 0.4 mM DHBA and 0.1 mM QP in 5 mM NaCl, which was changed to 0.2 mM DHBA and 0.0125 mM QP in 10 mM NaCl for 60 s ejections. Each dataset includes 5 ejections from 5 unique probes. (B) Solute distribution following ejections and a 15 s waiting period. Ejections of $Ru(bpy)_3^{2+}$ were performed into agarose for 5 and 60 s (n=8). For each case the fluorescence was normalized to the maximum value at the end of the ejection.

	3 s	**15 s**
$Log(IC_{50})$	-5.96 ± 0.14	-6.84 ± 0.15
Hill slope	-1.25 ± 0.27	-0.90 ± 0.16
r^2	0.876	0.941

Table 4.3 Parameters of iontophoretic dose-response data for QP administration on stimulated DA release following different ejection durations. The time indicates the ejection duration, which was followed with a 15 s waiting period before DA stimulation. Parameters represent data in Figure 4.7A, obtained by 5 ejections from 5 different probes. Concentrations were evaluated from Equation 1 using the DHBA marker current and updated DF term. Entries indicate the value and SEM, determined from a four parameter Hill model.

analysis calibration conditions, but this is not achievable using extended ejections. Secondly, biofouling on the surface of untreated carbon-fiber electrodes reduces sensitivity (Ewing et al., 1981; Vreeland et al., 2015). In fact, calibration following a 45 min incubation period in a slice revealed a decreased response of up to 80% in the current study. Lastly, some receptors may desensitize with prolonged exposure to drug, resulting in unreliable responses at the time of stimulation. However this was unlikely the case in the current study, as D2 receptors are resilient to persistent exposure of QP (Drukarch et al., 1991; Van Muiswinkel et al., 1994; Nimitvilai and Brodie, 2010).

Even when optimized, there exists more quantitative uncertainty in concentrations determined from controlled iontophoresis than perfusion. However, in certain circumstances the benefits of iontophoresis could well be worth this small sacrifice. This is because drugs can be administered more quickly by iontophoresis, with the combined ejection and waiting period lasting only 85 s for the most accurate parameter set (Figure 7A). In contrast, drugs delivered by perfusion require 10-20 min before their full effect is observed. Not only does faster administration increase throughput, it also preserves slice health and receptor sensitization which are susceptible to prolonged application periods. Ultimately the choice of a delivery method will depend upon the demands of the application, but as shown, controlled iontophoresis can provide a reliable drug delivery alternative for neurochemical investigations.

CONCLUSIONS

We have demonstrated methods to improve the accuracy and precision of concentration evaluations in controlled iontophoresis. To decrease uncertainty in the ejection status of a drug, markers should be used which share a similar molecular size and charge. For greater consistency

in evoked responses, a moderate 15 s waiting period between the end of the ejection and stimulation allows the drug concentration to become more uniform. Finally, longer ejection times increase the accuracy of evaluations by decreasing the concentration gradient along the electrode, which allows regions further away to become more concentrated and better reflect the marker current generated near the origin. While concentration evaluations determined from controlled iontophoresis are still imperfect, these improvements, coupled with the benefits of quick and highly localized application, offer significant advantages for studies requiring rapid drug delivery.

REFERENCES

Armstrong-James M, Millar J (1979) Carbon fibre microelectrodes. J Neurosci Methods 1:279-287.

Ayala YA, Malmierca MS (2015) Cholinergic Modulation of Stimulus-Specific Adaptation in the Inferior Colliculus. J Neurosci 35:12261-12272.

Beckstead MJ, Grandy DK, Wickman K, Williams JT (2004) Vesicular Dopamine Release Elicits an Inhibitory Postsynaptic Current in Midbrain Dopamine Neurons. Neuron 42:939-946.

Belle AM, Owesson-White C, Herr NR, Carelli RM, Wightman RM (2013) Controlled iontophoresis coupled with fast-scan cyclic voltammetry/electrophysiology in awake, freely moving animals. ACS Chem Neurosci 4:761-771.

Bloom FE (1974) To spritz or not the spritz: the doubtful value of aimless iontophoresis. Life Sci 14:1819-1834.

Bradshaw CM, Szabadi E (1974) The measurement of dose in microelectrophoresis experiments. Neuropharmacology 13:407-415.

Bronzi D, Licata F, Li Volsi G (2015) Noradrenergic modulation of glutamate-induced excitatory responses in single neurons of the red nucleus: An electrophysiological study. Neuroscience 300:360-369.

Bucher ES, Brooks K, Verber MD, Keithley RB, Owesson-White C, Carroll S, Takmakov P, McKinney CJ, Wightman RM (2013) Flexible Software Platform for Fast-Scan Cyclic Voltammetry Data Acquisition and Analysis. Anal Chem 85:10344-10353.

Dionne VE, Steinback JH, Stevens CF (1978) An analysis of the dose-response relationship at voltage-clamped frog neuromuscular junctions. J Physiol 281:421-444.

Drukarch B, Schepens E, Stoof JC (1991) Sustained activation does not desensitize the dopamine D2 receptor-mediated control of evoked in vitro release of radiolabeled acetylcholine from rat striatum. Eur J Pharmacol 196:209-212.

Ewing AG, Dayton MA, Wightman RM (1981) Pulse voltammetry with microvoltammetric electrodes. Anal Chem 53:1842-1847.

Ford CP, Gantz SC, Phillips PEM, Williams JT (2010) Control of extracellular dopamine at dendrite and axon terminals. J Neurosci 30:6975-6983.

Fu J, Lorden JF (1996) An easily constructed carbon fiber recording and microiontophoresis assembly. J Neurosci Methods 68:247-251.

Garris P, Ciolkowski E, Pastore P, Wightman R (1994) Efflux of dopamine from the synaptic cleft in the nucleus accumbens of the rat brain. J Neurosci 14:6084-6093.

Guy Y, Faraji AH, Gavigan CA, Strein TG, Weber SG (2012) Iontophoresis from a micropipet into a porous medium depends on the zeta-potential of the medium. Anal Chem 84:2179-2187.

Haidarliu S, Shulz D, Ahissar E (1995) A multi-electrode array for combined microiontophoresis and multiple single-unit recordings. J Neurosci Methods 56:125-131.

Havey DC, Caspary DM (1980) A simple technique for constructing 'piggy-back' multibarrel microelectrodes. Electroencephalogr Clin Neurophysiol 48:249-251.

Heien MLAV, Phillips PEM, Stuber GD, Seipel AT, Wightman RM (2003) Overoxidation of carbon-fiber microelectrodes enhances dopamine adsorption and increases sensitivity. Analyst 128:1413-1419.

Herr NR, Wightman RM (2013) Improved techniques for examining rapid dopamine signaling with iontophoresis. Front biosci (elite edition) 5:249-257.

Herr NR, Kile BM, Carelli RM, Wightman RM (2008) Electroosmotic flow and its contribution to iontophoretic delivery. Anal Chem 80:8635-8641.

Herr NR, Daniel KB, Belle AM, Carelli RM, Wightman RM (2010) Probing presynaptic regulation of extracellular dopamine with iontophoresis. ACS Chem Neurosci 1:627-638.

Inagaki K, Heiney SA, Blazquez PM (2009) Method for the construction and use of carbon fiber multibarrel electrodes for deep brain recordings in the alert animal. J Neurosci Methods 178:255-262.

Invernizzi RW, Pierucci M, Calcagno E, Di Giovanni G, Di Matteo V, Benigno A, Esposito E (2007) Selective activation of 5-HT2C receptors stimulates GABA-ergic function in the rat substantia nigra pars reticulata: A combined in vivo electrophysiological and neurochemical study. Neuroscience 144:1523-1535.

Johnson JA, Rodeberg NT, Wightman RM (2016) Failure of Standard Training Sets in the Analysis of Fast-Scan Cyclic Voltammetry Data. ACS chemical neuroscience.

Jones SR, Garris P, Wightman RM (1995) Different effects of cocaine and nomifensine on dopamine uptake in the caudate-putamen and nucleus accumbens. J Pharmacol Exp Ther 274:396-403.

Kaur G, Hrabetova S, Guilfoyle DN, Nicholson C, Hrabe J (2008) Characterizing molecular probes for diffusion measurements in the brain. J Neurosci Methods 171:218-225.

Kennedy RT, Jones SR, Wightman RM (1992) Dynamic Observation of Dopamine Autoreceptor Effects in Rat Striatal Slices. J Neurochem 59:449-455.

Khinkis LA, Levasseur L, Faessel H, Greco WR (2003) Optimal Design for Estimating Parameters of the 4-Parameter Hill Model. Nonlinearity Biol Toxicol Med 1:363-377.

Kirkpatrick DC, Edwards MA, Flowers PA, Wightman RM (2014) Characterization of Solute Distribution Following Iontophoresis from a Micropipet. Anal Chem 86:9909-9916.

Kirkpatrick DC, Walton LR, Edwards MA, Wightman RM (2016) Quantitative analysis of iontophoretic drug delivery from micropipettes. the Analyst.

Kovács P, Dénes V, Kellényi L, Hernádi I (2005) Microiontophoresis electrode location by neurohistological marking: Comparison of four native dyes applied from current balancing electrode channels. J Pharmacol Toxicol Methods 51:147-151.

Kruk ZL, Armstrong-James M, Millar J (1980) Measurement of the concentration of 5-hydroxytryptamine ejected during iontophoresis using multibarrel carbon fibre microelectrodes. Life Sci 27:2093-2098.

Leiras R, Velo P, Martín-Cora F, Canedo A (2010) Processing Afferent Proprioceptive Information at the Main Cuneate Nucleus of Anesthetized Cats. J Neurosci 30:15383-15399.

Lepiku M, Rinken A, Järv J, Fuxe K (1997) Modulation of [3H]quinpirole binding to dopaminergic receptors by adenosine A2A receptors. Neurosci Lett 239:61-64.

Levant B, Grigoriadis DE, DeSouza EB (1992) Characterization of [^{3}H] quinpirole binding to D2-like dopamine receptors in rat brain. J Pharmacol Exp Ther 262:929-935.

Limberger N, Trout SJ, Kruk ZL, Starke K (1991) “Real time” measurement of endogenous dopamine release during short trains of pulses in slices of rat neostriatum and nucleus accumbens : role of autoinhibition. Naunyn-Schmiedeberg's Arch Pharmacol 344:623-629.

Lipski WJ, Grace AA (2013) Activation and Inhibition of Neurons in the Hippocampal Ventral Subiculum by Norepinephrine and Locus Coeruleus Stimulation. Neuropsychopharmacology 38:285-292.

Miller C (2008) Improving Brain Slice Methodology. In: Chemistry, p 133. North Carolina: University of North Carolina Chapel Hill.

Mudry B, Guy RH, Delgado-Charro MB (2006) Transport numbers in transdermal iontophoresis. Biophys J 90:2822-2830.

Mudry B, Carrupt PA, Guy RH, Delgado-Charro MB (2007) Quantitative structure-permeation relationship for iontophoretic transport across the skin. J Control Release 122:165-172.

Ni Z, Gao D, Bouali-Benazzouz R, Benabid A-L, Benazzouz A (2001) Effect of microiontophoretic application of dopamine on subthalamic nucleus neuronal activity in normal rats and in rats with unilateral lesion of the nigrostriatal pathway. Eur J Neurosci 14:373-381.

Nimitvilai S, Brodie MS (2010) Reversal of prolonged dopamine inhibition of dopaminergic neurons of the ventral tegmental area. J Pharmacol Exp Ther 333:555-563.

O'Neill C, Evers-Donnelly A, Nicholson D, O'Boyle KM, O'Connor JJ (2009) D2 receptor-mediated inhibition of dopamine release in the rat striatum in vitro is modulated by CB1 receptors: studies using fast cyclic voltammetry. J Neurochem 108:545-551.

Patel CR, Zhang H (2014) Local Application of Sodium Salicylate Enhances Auditory Responses in the Rat's Dorsal Cortex of the Inferior Colliculus. Front Neurol 5:235.

Purves R (1980a) Ionophoresis - progress and pitfalls. Trends Neurosci 3:245-247.

Purves R (1980b) Effect of Drug Concentration on Release from Ionophoretic Pipettes. J Physiol 300:72-73.

Rice ME, Nicholson C (1991) Diffusion characteristics and extracellular volume fraction during normoxia and hypoxia in slices of rat neostriatum. J Neurophysiol 65:264-272.

Rice ME, Okada YC, Nicholson C (1993) Anisotropic and heterogeneous diffusion in the turtle cerebellum: implications for volume transmission. J Neurophysiol 70:2035-2044.

Schultz W, Carelli RM, Wightman RM (2015) Phasic dopamine signals: from subjective reward value to formal economic utility. Current Opinion in Behavioral Sciences 5:147-154.

Staak R, Pape H-C (2001) Contribution of GABAA and GABAB Receptors to Thalamic Neuronal Activity during Spontaneous Absence Seizures in Rats. J Neurosci 21:1378-1384.

Trubatch J, Van Harreveld A (1972) Spread of iontophoretically injected ions in a tissue. J Theor Biol 36:355-366.

Van Muiswinkel FL, Drukarch B, Steinbusch HWM, Stoof JC (1994) Dopamine D-2 Autoreceptors Regulating the Release of Dopamine from Cultured Rat Fetal Dopaminergic Neurons Do Not Desensitize upon Sustained Activation: Implications for the Combined Pharmaco- and Grafting Therapy in Parkinsonian Patients. Exp Neurol 125:218-227.

Venton BJ, Zhang H, Garris PA, Phillips PEM, Sulzer D, Wightman RM (2003) Real-time decoding of dopamine concentration changes in the caudate–putamen during tonic and phasic firing. J Neurochem 87:1284-1295.

Vreeland RF, Atcherley CW, Russell WS, Xie JY, Lu D, Laude ND, Porreca F, Heien ML (2015) Biocompatible PEDOT:Nafion Composite Electrode Coatings for Selective Detection of Neurotransmitters in Vivo. Anal Chem 87:2600-2607.

Wang T, Rusu SI, Hruskova B, Turecek R, Borst JGG (2013) Modulation of synaptic depression of the calyx of Held synapse by GABA(B) receptors and spontaneous activity. J Physiol 591:4877-4894.

CHAPTER 5: EXPANDING NEUROCHEMICAL INVESTIGATIONS WITH MULTI-MODAL RECORDING: SIMULTANEOUS FAST-SCAN CYCLIC VOLTAMMETRY, IONTOPHORESIS, AND PATCH CLAMP MEASUREMENTS [4]

INTRODUCTION

Neurochemical systems are analyzed by a variety of methods, which can characterize distinct events such as cell firing, neurotransmitter release, and changes in blood flow (Michael and Borland, 2007; Vertes and Stackman, 2011). Information collected simultaneously from multiple domains, termed multi-modal recording, helps to reveal relationships between variables that may be otherwise too difficult to surmise from isolated or independent measurements. This is beneficial for studies that need to link events between domains, such as the relationship between cellular activity and exocytosis, the influence of neurotransmitters on vascular coupling, or the behaviors of interconnected cells (Oberhauser et al., 1996; Galarreta and Hestrin, 1999; Henze et al., 2000; Sheth et al., 2004; Lu et al., 2005; Phongphanphanee et al., 2008; Yamamoto et al., 2010; Cepeda et al., 2013). Two popular domains which have recently undergone rapid growth in neurochemical studies are the electrophysiological, which provides information about cellular activity, and the electrochemical, used to study the local chemical environment. These can be combined using distinct sensors, or both executed at a single electrode (Takmakov et al., 2011).

[4] This chapter is currently under review as an article in *the Analyst*. The citation will read follows:
Kirkpatrick DC, McKinney CJ, Manis PB, Wightman, RM (2016) Expanding Neurochemical Investigations with Multi-Modal Recording: Simultaneous Fast-Scan Cyclic Voltammetry, Iontophoresis, and Patch Clamp Measurements. Analyst (submitted).

The whole-cell patch clamp is a commonly employed electrophysiological method that uses a micropipette to manipulate and record cell behavior (Sakmann and Neher, 1992). It has two modes of operation: voltage clamp, typically used to study ion channels, and current clamp, which records the cell membrane potential. Patch clamp electrophysiology has been successfully incorporated in multi-modal investigations with amperometry, which provides information in the chemical domain (Moser et al., 1995; Oberhauser and Fernandez, 1996; Galli et al., 1998). Although simple to incorporate, amperometry limits information about the chemical environment since it only allows for the detection of a singular analyte, and does not provide information about the identity of the detected chemical. In comparison, fast-scan cyclic voltammetry (FSCV), which utilizes a triangular potential waveform scanned rapidly across a carbon-fiber microelectrode, can differentiate between multiple electroactive species and offers qualitative information regarding their identities (Bucher and Wightman, 2015). In addition, carbon-fiber electrodes can be used to detect a broad range of neurochemical events, such as changes in pH, single unit activity, and even ionic changes (Takmakov et al., 2010; Takmakov et al., 2011). Incorporation of FSCV with patch clamp electrophysiology would improve the ability of neurochemical investigations to obtain and relate information spread over multiple domains.

In this work we demonstrate a method to combine patch clamp and FSCV instrumentation. Since both techniques require precise current and voltage measurements, a model circuit is first developed to determine the anticipated electrical crosstalk between instruments. Upon analysis both methods were predicted to operate without interference, and the experimental results largely confirmed this. Once validated,

whole-cell current clamp measurements were performed to monitor cellular activity in the presence of exogenously applied FSCV potential. Although currents generated during FSCV could theoretically excite or damage cells if coupled into the membrane, no change in cell behavior was observed. Additionally, currents administered during iontophoresis, a drug delivery method which uses an electric current to eject a solution from a glass capillary, were also determined not to impact nearby cells. Lastly, application of combined measurements is demonstrated by monitoring cell behavior during iontophoresis of glutamate, an excitatory neurotransmitter. In all, we exhibit the feasibility and utility of multi-modal patch and FSCV measurements.

EXPERIMENTAL

Chemicals and solutions

All chemicals were used as received from Sigma Aldrich (St. Louis, MO). Recording artificial cerebral spinal fluid (aCSF) consisted of 126 mM NaCl, 2.5 mM KCl, 1 mM NaH_2PO_4, 26 mM $NaHCO_3$, 2 mM $MgSO_4$, 2 mM $CaCl_2$, and 11 mM glucose. After oxygenation (95% O_2, 5% CO_2) the pH was adjusted to 7.4. Iontophoretic solutions were made daily from filtered (0.45 μm Nylon, Nalgene, USA) DI water. Their pH measured between 6 and 7.

Animal care and use

Male Sprague-Dawley rats (250-300 g, Charles River, Wilmington, MA) were used for all experiments. Rats were dually housed on a 12/12 hour day/night cycle and provided with food and water *ad libitum*. Special care was given to minimize the number of animals and to reduce their suffering. All procedures were approved by the

Institutional Animal Care and Use Committee at the University of North Carolina at Chapel Hill.

Brain slice preparation

Following anesthesia with urethane (1.5 g/kg), brains were quickly removed and submerged into oxygenated (95% O_2, 5% CO_2) chilled sucrose-based aCSF (185 mM sucrose, 2.5 mM KCl, 1.2 mM KH_2PO_4, 25 mM $NaHCO_3$, 25 mM glucose, 10 mM $MgSO_4$, and 0.5 mM $CaCl_2$, adjusted to pH=7.4). A vibratome (VF-200, Precisionary Instruments, San Jose, CA) fitted with a stainless steel blade (Fendrihan, USA) was used to obtain 300 µm thick coronal slices containing the nucleus accumbens (NAc). After cutting, these were immediately transferred to room temperature (20 ˚C) recording aCSF and allowed 1 hour to recover. During experiments, slices were anchored (SHD-22KIT, Warner Instruments, Hamden, CT) in a perfusion chamber (RC-22, Warner Instruments) on the stage of an Eclipse FN1 microscope (Nikon Instruments, Melville, NY), which sat atop a vibration free table (TMC, Peabody, MA). A 30 min period of continuous perfusion (2 mL/min) with 37 ˚C recording aCSF was given prior to analysis.

Patch clamp electrophysiology

Patch pipettes were fabricated from borosilicate capillaries (1.5/0.86 mm O.D./I.D., Sutter Instruments) using a PC-84 micropipette puller (Sutter Instruments). Pipettes were filled with an intracellular solution consisting of 126 mM K-gluconate, 6 mM KCl, 2 mM NaCl, 10 mM HEPES, 1 mM EGTA, 10 mM phosphocreatine, 4 mM Mg-ATP, and 0.3 mM Na_2-GTP which was adjusted to pH=7.2 and measured between 260 and 290 mOsm. An Ag wire coated with AgCl was used to connect the pipette to the

headstage. The pipette resistance was determined using a 0-10 mV potential step, and consistently measured between 6 and 9 MΩ. Visualization of cells in the NAc core was achieved using asymmetric illumination (Kachar, 1985). Images were obtained through a 40x immersion objective (Nikon Instruments), captured on a CMOS camera (Rolera Bolt, QImaging, Surrey, BC), and displayed with associated software (Q-Capture Pro 7, QImaging). Medium spiny neurons (MSNs) were distinguished from interneurons based on size. Once identified, a micromanipulator (MP-285 with MPC-200-ROE and controller, Sutter Instruments, Novato, CA) was used to position the patch pipette near the cell. Following formation of a GΩ seal, a whole-cell patch was obtained by applying suction to the pipette. Recordings were made with an Axopatch 200B patch clamp amplifier (Axon Instruments, Foster City, CA). Cell parameters were determined from a 10 mV step applied from a -75 mV potential. Membrane resistance (69 ± 4 MΩ, SEM, n=39) and capacitance (78 ± 3 pF, SEM, n=39) were used in conjunction with the response to intracellular current steps to confirm correct identification of cells (Kawaguchi, 1993; Gustafson et al., 2006; Ibáñez-Sandoval et al., 2010; Lepora et al., 2011). Only trials where the pipette access resistance measured below 35 MΩ and changed less than 25% during experiments were included. A Ag/AgCl electrode (World Precision Instruments, Sarasota, FL) was used as a reference, and also served as the iontophoresis current return electrode. Whole-cell currents and voltages were low-pass filtered at 2 kHz, digitized at 10 kHz (Digidata 1320A Axon Instruments), and recorded using Clampex 10.3 software (Molecular Devices, Silicon Valley, CA). Pipette offset potential and pipette capacitance compensation controls were adjusted prior to forming a

GΩ seal. Whole cell capacitance and series resistance were 75% compensated in voltage clamp. For current clamp measurements, series resistance was fully compensated.

Fast-scan cyclic voltammetry

Multibarreled iontophoresis probes containing a T-650 carbon-fiber electrode were constructed from pre-fused borosilicate capillaries (Friedrich & Dimmock, Millville, NJ) as previously described (Belle et al., 2013). The carbon fiber was cut to 100 µm and served as the FSCV electrode. Connection to the headstage was made with a stainless steel wire inserted into the electrode barrel, which contained a 4 M CH_3COOK and 0.15 mM NaCl solution. A micromanipulator (MPC-200-ROE, Sutter Instruments) was used to position the probe near visually identified cells. Measurements were obtained using a triangular waveform and applied from a homemade instrument (UEI, UNC Chemistry Electronics Facility, UNC Chapel Hill). Unless otherwise stated, the waveform consisted of a -0.4 V holding potential with an upper limit of 1.0 V, scanned at 600 V/s, and repeated at 5 Hz. For detection of DOPAC, the holding potential was lowered to -0.8 V. Waveform parameters and data collection were accomplished with HDCV software through a PCIe-6363 DAQ card (National Instruments) (Bucher et al., 2013). Prior to analysis, data underwent filtering (2-16 kHz), background subtraction, and signal averaging.

Initial simultaneous FSCV and patch clamp measurements yielded significant 60 Hz noise. To address this, different Ag/AgCl reference electrodes were used for each instrument (Ott, 1988). Signals were further isolated by connecting the FSCV return electrode to a negative battery terminal, while the patch reference electrode remained at AC power ground (Figure 5.1A). This required battery operation of the UEI, which generated the FSCV waveform applied

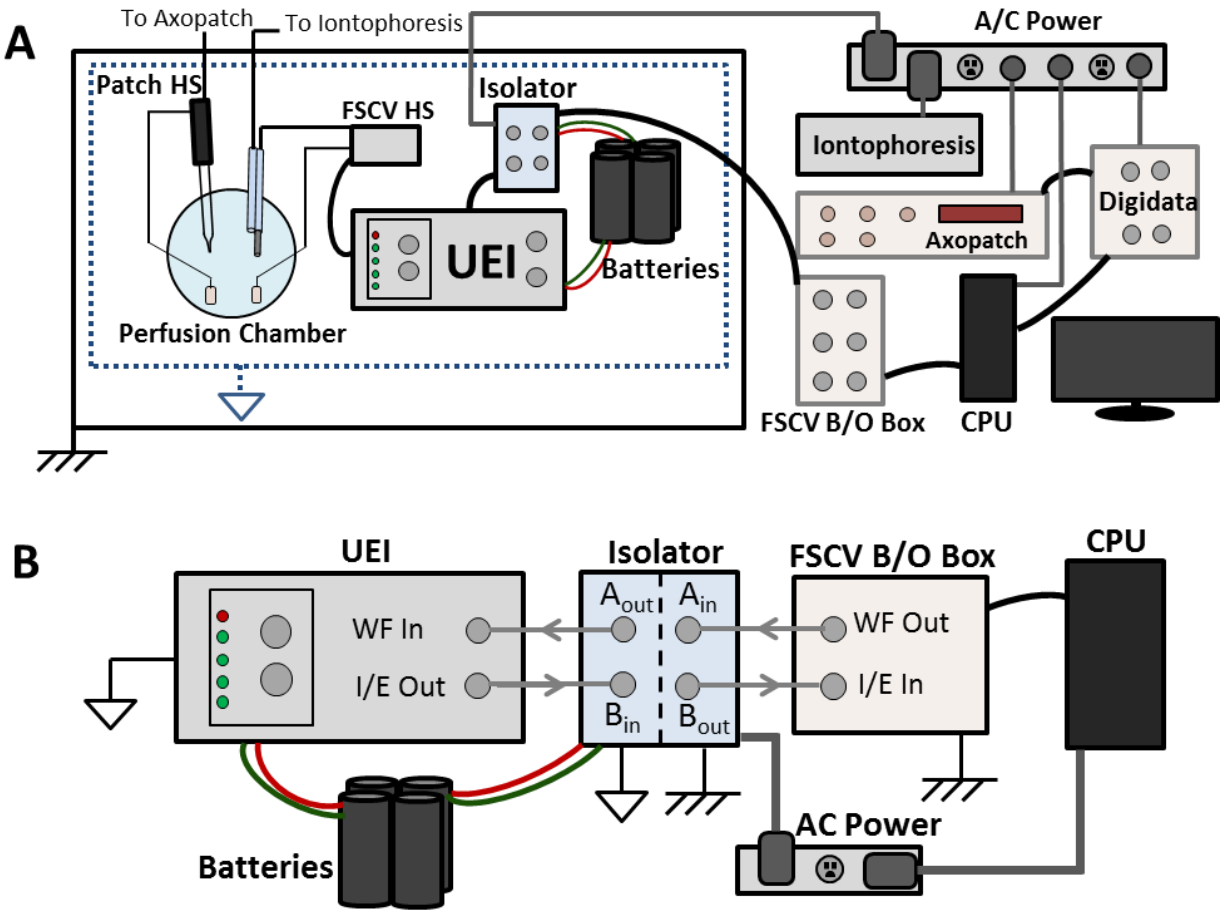

Figure 5.1 Instrumentation for combined recordings. (A) Block diagram of FSCV, patch clamp, and iontophoresis instruments. Patch clamp commands are generated at the CPU, amplified (Digidata, Axopatch), and applied at the patch headstage. All components are referenced to AC ground. Similarly, iontophoresis currents are AC ground-referenced. For FSCV, commands originate at the CPU referenced to AC ground. These are amplified (B/O Box) and transduced (Isolator) to a battery-referenced potential. The UEI, powered by the battery, receives the command and applies the waveform at the electrode. (B) Transduction of FSCV signals. The waveform command is sent from the CPU to the isolator ('WF Out' to 'A_{in}'), and arrives at the UEI after transduction ('A_{out}' to 'WF In'). FSCV current is transduced through the isolator ('I/E Out' to 'B_{in}') and recorded by the CPU ('B_{out}' to 'I/E In').

at the electrode. Additionally, since all commands originated at the AC ground-referenced CPU of a personal computer, an optical isolator (UNC Chemistry Electronics Facility) was used to transduce FSCV command signals to the battery-referenced potential prior to reaching the UEI (Figure 5.1B). Current generated at the carbon-fiber electrode underwent the reverse process prior to recording. The FSCV current was measured by the UEI, transduced to AC power ground, and recorded at the CPU.

Iontophoresis

The remaining barrels on the multibarreled carbon-fiber probes were used for iontophoretic ejections. After pulling, drug barrels had diameters of 0.5 to 1.0 µm. Ejection currents were administered from a locally constructed instrument (UNC Chemistry Electronics Facility), which was controlled using customized LabVIEW software (National Instruments, Austin, TX) and an NI-USB 6343 DAQ card (National Instruments). A Ag/AgCl electrode (World Precision Instruments, Sarasota, FL) held at AC power ground was used as the counter electrode.

RESULTS AND DISCUSSION

Modeling the Collective Use of Patch Clamp, FSCV, and Iontophoresis Instrumentation

A model circuit was developed which simulated concurrent FSCV and patch clamp measurements. This is depicted in Figure 5.2, in which a cell is patched in whole-cell mode with the corresponding circuit components detailed in Table 5.1. Here, we focus specifically on the current clamp method for patch measurements. In this configuration, the cell membrane voltage is recorded by the patch amplifier, which is also used to administer intracellular current injections. Chemical changes around the cell are detected

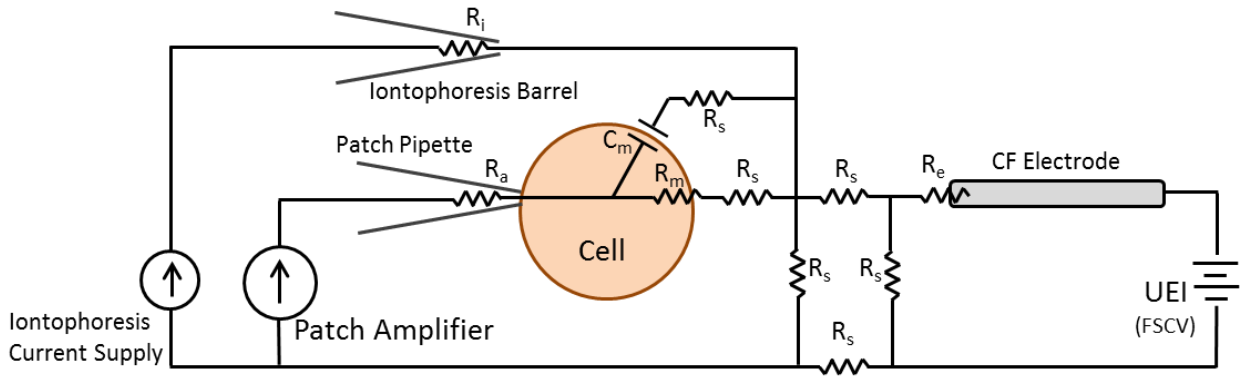

Figure 5.2 Model circuit for combined operation of FSCV, patch clamp, and iontophoresis instruments. The patch pipette is controlled by the patch amplifier, operating in whole-cell mode. FSCV is performed on the carbon-fiber electrode, which is connected to a potentiostat (UEI). Iontophoretic ejections are administered by a constant current source.

Symbol	Description	Value
$\mathbf{R_s}$	Extracellular Solution Resistance	~100 Ω
$\mathbf{R_a}$	Pipette/Membrane Access Resistance	10 – 35 MΩ
$\mathbf{R_m}$	Cell Membrane Resistance	30 – 300 MΩ
$\mathbf{R_i}$	Iontophoresis Barrel Resistance	0.1 – 1 GΩ
$\mathbf{C_m}$	Cell Membrane Capacitance	50 – 200 pF
$\mathbf{R_e}$	FSCV Electrode Resistance	~1 MΩ

Table 5.1 Description and values for Figure 5.2 circuit components

by the FSCV current on a carbon-fiber microelectrode, which is controlled by the universal electrochemical instrument (UEI). Also included is iontophoresis, a drug delivery method which uses an electrical current applied from a constant source to eject solution from a micropipette. To determine if FSCV and patch measurements would be obscured by the incorporation of other methods, the amount of crosstalk, or electrical interference between instruments, was calculated. For example, in FSCV the maximum potential applied to the electrode rarely exceeds 1.4 V (Hafizi et al., 1990; Heien et al., 2003). From this voltage, the model predicts measurements of the membrane potential performed by the patch amplifier will be overestimated by 0.035 mV. Similarly a 1 µA iontophoretic ejection, the maximum current deliverable by many commercially available iontophoretic instruments, was calculated to increase measurements by 0.075 mV (2000; 2008; 2016). Since both of these values are below the 1 mV noise level common to most current clamp instruments, FSCV and iontophoresis were not expected to significantly impact recordings made of the membrane potential. For FSCV measurements, a 1 µA iontophoresis ejection was calculated to add 0.025 nA to the current at the carbon-fiber electrode. Similarly a 500 pA intracellular injection delivered by the patch amplifier was predicted to increase the FSCV current by 0.5 pA. Both of these values are below the noise in FSCV recordings, which rarely exceeds 0.3 nA (Keithley et al., 2009; Johnson et al., 2016). Thus no significant electrical coupling or crosstalk was anticipated between instruments.

FSCV Signal Unaffected by Patch and Iontophoretic Currents

To experimentally determine the effect of patch and iontophoretic currents on FSCV measurements, a carbon-fiber microelectrode contained in a multibarreled probe

was inserted into the nucleus accumbens (NAc) core of a rat brain slice. The three other barrels on the probe contained an NaCl solution for iontophoresis ejections. A patch pipette was positioned roughly 10 µm from the carbon fiber. For simplicity, the patch pipette in initial experiments was not attached to a cell, but was still operated in current clamp mode. First, the FSCV signal was examined by measuring elicited dopamine (DA) release, which was electrically evoked using a bipolar stimulating electrode. During this time, both the patch pipette and iontophoretic barrels maintained zero net current. Figure 5.3A displays a color plot showing the background subtracted FSCV current following evoked release (middle). A vertical cross-section (dashed blue line) taken just after stimulation reveals the cyclic voltammogram of DA (upper), which confirms the identity of the chemical signal. Similarly a horizontal cross-section along the DA oxidation potential (dashed white line) reveals the DA oxidation current versus time (lower), and shows the time-course of release. Inspection of the current in the absence of DA revealed ~0.1 nA of noise from the baseline, which compares favorably to FSCV measurements performed in isolation.

Next, current was delivered from the patch pipette to study its effect on the FSCV signal. Figure 5.3B displays the FSCV current along the DA oxidation potential during successive current steps. No effect was observed on the FSCV signal. This occurred despite no cell attached to the patch pipette, which should have amplified crosstalk between instruments. Thus as predicted from the model circuit, current administered from the patch pipette did not affect FSCV measurements. Subsequently, the effect of the iontophoresis ejection current on FSCV measurements was examined by ejecting NaCl solutions from the iontophoretic barrels. Figure 5.3C displays the current along the DA

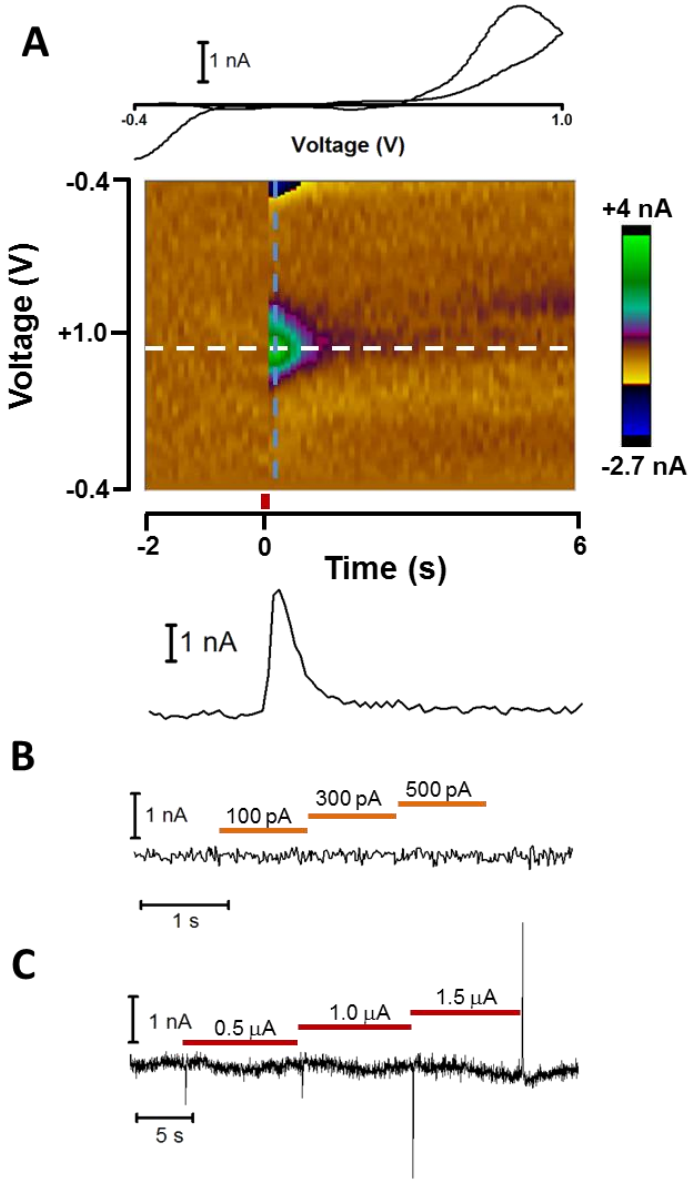

Figure 5.3 Effect of patch and iontophoresis instruments on FSCV measurements. (A) FSCV response to electrically evoked DA release. A carbon-fiber electrode detected electrically evoked DA release in the NAc core of a rat brain slice while a neighboring patch pipette and iontophoresis barrel maintained zero net current. The DA CV (upper) was obtained from the color plot (middle) using the current across the waveform just after stimulation (dashed blue line). A DA current versus time trace (lower) was generated from the current at the DA oxidation potential over the time-course of the measurement. Stimulation (red bar) occurred at t=0. (B) FSCV signal along the DA oxidation potential during current steps administered by the patch pipette. Orange bars represent the time of the applied current. (C) FSCV signal along the DA oxidation potential during iontophoretic ejection (red bars) of NaCl.

oxidation potential as iontophoretic current was applied step-wise between 0.5 and 1.5 μA. Rapid deflections were observed when the ejection current was changed to a new value. Since these deflections quickly returned to the baseline, they were attributed to capacitive coupling between the iontophoresis barrel and the carbon fiber. If caused by direct current flow between the iontophoresis barrel and carbon fiber, the signal would have shown a baseline shift sustained throughout the ejection. However this did not occur, as the FSCV current was unaffected shortly after the deflections subsided. Together, these experiments confirmed calculations from the model predicting neither patch nor iontophoretic current would interfere with FSCV measurements.

Effect of FSCV Waveform on Patch Recordings

Next, the ability to perform patch clamp recordings during FSCV was examined. To accomplish this, a medium spiny neuron (MSN) in the NAc core of a brain slice was patched in whole-cell mode. A multibarreled iontophoresis probe containing a carbon-fiber electrode was positioned approximately 10 μm from the cell body. For FSCV, a triangular waveform was applied to the carbon-fiber electrode between -0.4 to +1.0 V at 600 V/s, repeating at 5 Hz. Due to the lack of excitatory glutamatergic tone in the slice, MSNs resided in a down, or resting state, and required a depolarizing stimulus to initiate firing (Vergara et al., 2003; Azdad et al., 2008). Figure 5.4A shows a current clamp recording of the MSN membrane potential during FSCV at an adjacent carbon-fiber electrode, which shows repetitive transients centered on the resting potential. These transients occurred at an identical frequency to the FSCV waveform, and disappeared when the waveform was disabled. Additionally, their magnitude, which ranged between 2 - 4 mV from the baseline, was unaffected by the distance between the carbon fiber and

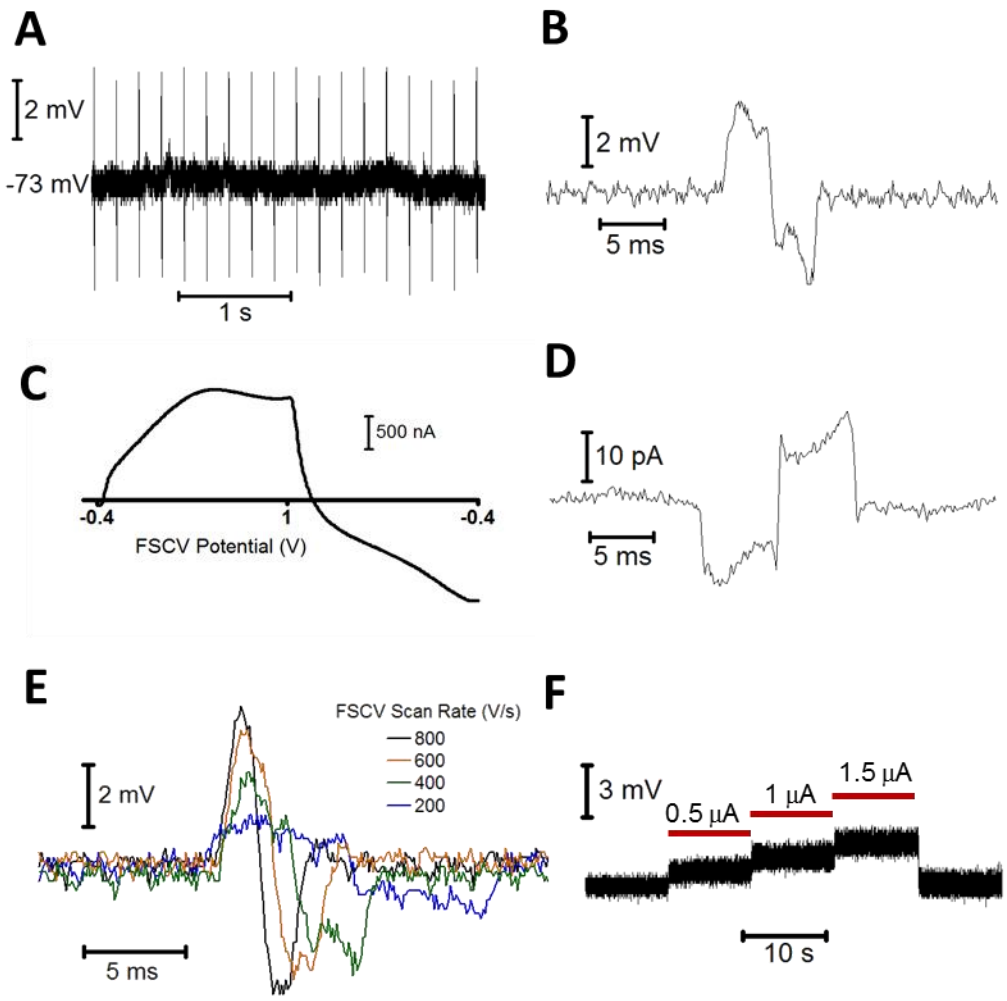

Figure 5.4 Effect of FSCV and iontophoresis instruments on patch clamp measurements. (A) Whole-cell current clamp recording of the spontaneous membrane potential of an MSN in the presence of a carbon-fiber electrode performing FSCV. (B) A magnified transient from A. (C) The unsubtracted FSCV current at the carbon-fiber electrode from A. (D) Whole-cell voltage clamp recording (v_m = -75 mV) of an MSN, made in the presence of a carbon fiber performing FSCV. (E) Transients recorded in a whole-cell current clamp for different scan rates at the FSCV electrode. The waveform maintained constant limits between -0.4 and 1.0 V. (F) Current clamp recording of the patch pipette voltage during iontophoretic ejections (red bars) of NaCl.

patch pipette. When further examined, transients had a similar appearance to the unsubtracted FSCV current at the carbon-fiber electrode (Figures 5.4B, 5.4C). Whole-cell voltage clamp measurements also contained transients, but these appeared as the inverse of the FSCV current (Figure 5.4D).

To determine the cause of transients, parameters of the FSCV waveform were varied while the effect on the current clamp signal was observed. First, the limits of the triangular waveform were lowered from -0.4 and +1.0 V to -0.7 and +0.7 V, while a consistent scan rate (600 V/s) was maintained. This had no effect on the transient magnitude, indicating they were not caused by direct current between the carbon fiber and patch pipette. Next, the scan rate of the waveform was varied while maintaining constant voltage limits. As shown in Figure 5.4E, the transient magnitude increased with the scan rate. These results indicated that transients were due to capacitive coupling of the FSCV waveform into the patch recordings. This is because capacitive current (i_c) is generated in proportion to the rate of change of a voltage, $i_c = C(dV/dt)$, and is independent of the magnitude of the potential. Since capacitive rather than direct current was the source of transients, recordings made when the FSCV potential was constant were not affected. This occurs between triangular ramps, when a holding potential is applied to promote analyte adsorption to the electrode surface (Heien et al., 2003; Swamy and Venton, 2007). During this period, measurements of the membrane potential were identical to those made with the waveform disabled.

Cell firing and shifts in the membrane potential can still be reliably monitored in the presence of an FSCV electrode because the holding potential accounts for a majority of the total voltammetric period. For example, during the 5 Hz waveform utilized in

Figure 5.4A, the triangular portion was applied just 2.3% of the time. However if recordings without capacitive transients are desired, there are several methods to minimize or remove them while still collecting electrochemical information. First, since capacitive coupling is proportional to dV/dt, a lower FSCV scan rate will reduce the size of transients (Figure 5.4E). Indeed at sufficiently low scan rates (<200 V/s), transients could be eliminated entirely. However this may not be desirable in certain cases because it is accompanied by a decrease in the FSCV electrode sensitivity (Keithley et al., 2011). Alternatively, some patch amplifiers are equipped with cross capacitance neutralization circuits, which may be used to eliminate transients from recordings without altering the FSCV waveform parameters.

Effect of Iontophoretic Current on Patch Recordings

We then investigated whether current clamp measurements were affected by iontophoretic current. To do this, the patch pipette voltage was monitored during iontophoretic ejections of NaCl. Experiments were performed in the absence of a cell to ensure that changes in the measured pipette potential were due to the iontophoretic current rather than cellular activity. Figure 5.4F reveals that the pipette potential increased proportionally with the iontophoretic current. Because the voltage offset was sustained throughout the ejection period, the change in potential could be attributed to direct current flow between the iontophoretic and patch pipettes. Measurements of the average error, 0.89 mV per μA of iontophoretic current (n=5), were similar to those made when a cell was attached, and were roughly an order of magnitude greater than the model predicted. Most likely this was due to polarization at the iontophoretic barrel tip during ejections, which altered the current flow predicted in the model (Yusko et al., 2010; Shi et

al., 2015). Nevertheless the observed offset was small compared to anticipated signals. In fact, since most iontophoretic ejections employ currents from the 10's to 100's of nA, errors incurred during ejections would still likely be contained within the noise (Herr and Wightman, 2013). Thus in practice, iontophoretic current was determined not to have a significant impact on current clamp measurements.

Cell Response to Exogenous Potential and Current

After establishing the ability to accurately perform current clamp measurements concurrently with FSCV and iontophoresis, we next examined how these techniques affected nearby cells. Since the behavior of many neuronal components is voltage dependent, cells neighboring the carbon-fiber probe may be affected by exogenous potential and current inherent to these methods. To study this, a carbon fiber contained in a multibarreled iontophoresis probe was positioned ~10 μm from the soma of an MSN. A whole-cell patch was performed and the membrane potential of the resting cell was examined while the FSCV waveform was alternated on and off. Figure 5.5A demonstrates that besides capacitive transients, no difference was observed between periods when the waveform was applied (red bars) and disabled. The cell maintained its resting potential and no firing was initiated. Next, the effect of the FSCV waveform on excited cells was examined. Using current steps administered from the patch pipette, cells were progressively depolarized until firing was achieved (Figure 5.5B). Consistent with well-established behavior, MSNs displayed strong inward rectification, a voltage ramp preceding firing, and a delayed initial action potential (Planert et al., 2010). Additionally both the rheobase, the current required to induce firing, and the threshold potential, the membrane voltage which must be reached to initiate firing, were unaffected

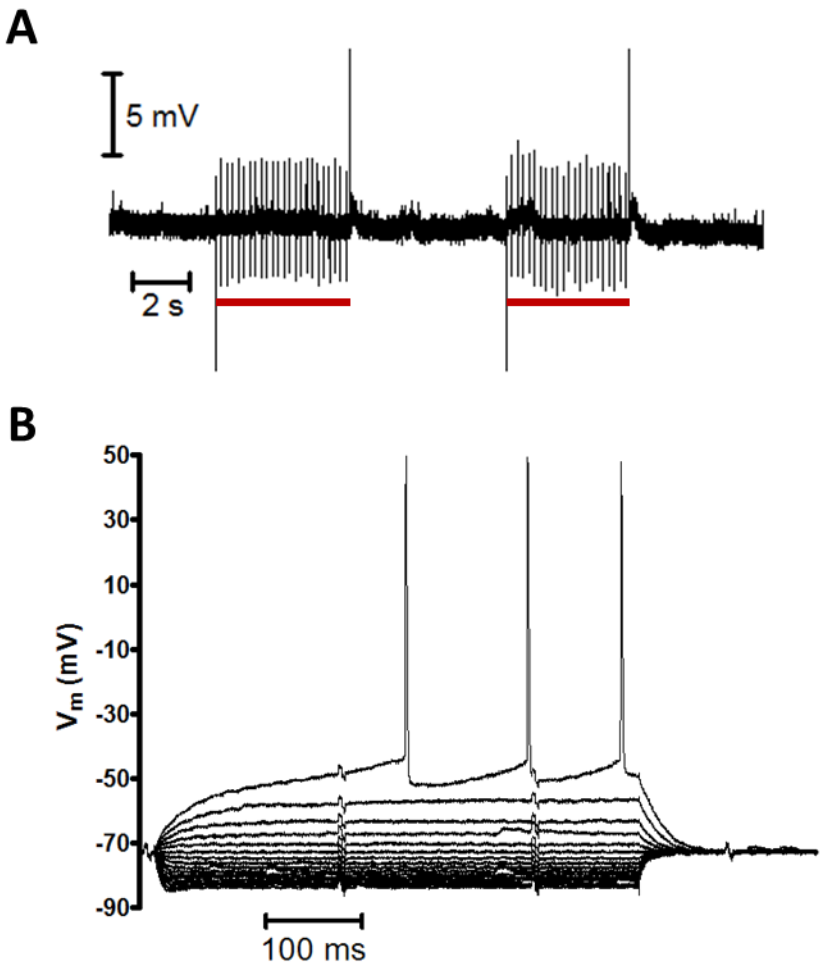

Figure 5.5 Effect of FSCV on neighboring cells. (A) Resting MSN membrane potential during application of FSCV waveform. A current clamp recording of the spontaneous activity of an MSN was obtained in the presence of a carbon fiber performing FSCV. The electrode was positioned adjacent to the cell and the waveform was alternated on (red bars) and off. (B) MSN response to intracellular current injections in the presence of a carbon fiber performing FSCV. Current injections began at -200 pA and increased stepwise by 20 pA until firing was observed. Note that the voltage scale in B is much less than in A.

by the FSCV waveform (paired t test, P=0.753, P=0.744 respectively, *n*=13). Thus no difference was observed in the resting or active state of cells due to exogenous FSCV potential.

Next, the effect of iontophoretic ejections on cell behavior was examined. Since iontophoretic currents are several orders of magnitude greater than the rheobase, it has been suggested that ejection currents may perturb nearby cells (Bloom, 1974). In fact, some commercial iontophoretic systems attempt to offset the ejection current with an equal and opposite balancing current applied through a separate barrel. To study how the iontophoretic current affected cells, MSN firing was observed during ejection of NaCl. First, a depolarizing current injection was applied from the patch pipette to transition cells into an active state, where firing occurred at a constant frequency (Figure 5.6). Next, an iontophoretic barrel located next to the cell delivered the ejection current. If the iontophoretic current impacted cells, the firing rate would have increased due to the additional excitatory stimulus. However, no change in the firing frequency was observed for ejection currents up to 40 µA, even without the use of balancing currents. The only effect was a slight offset in the voltage measured by the patch pipette, most visible during the 800 nA ejection, which as shown by Figure 5.4F occurs independently of cellular activity. Thus just as in FSCV, exogenous iontophoretic current did not affect cell behavior.

Applications of Combined Instrumentation

To demonstrate simultaneous patch and FSCV measurements, glutamate, an excitatory neurotransmitter, was iontophoretically applied to MSNs while cellular activity

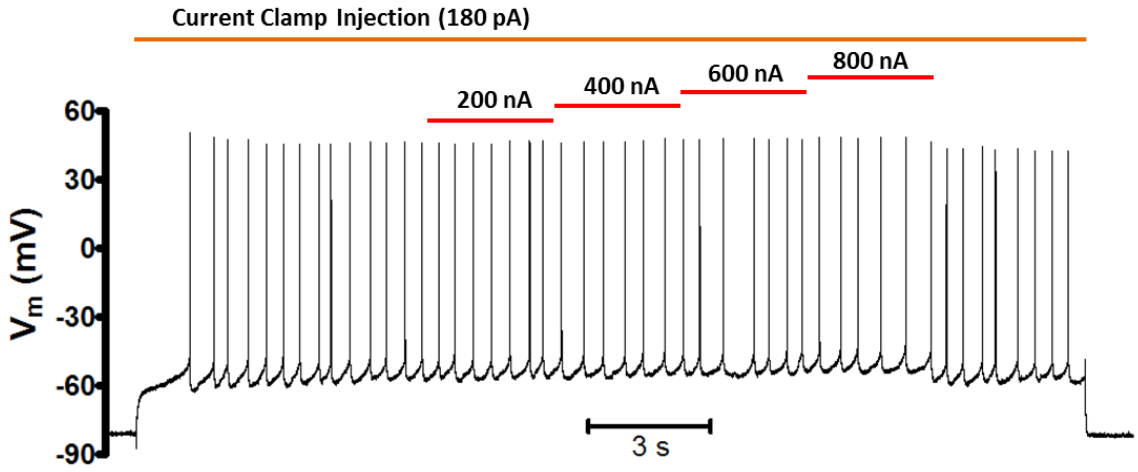

Figure 5.6 Effect of iontophoretic current on neighboring cells. An MSN was depolarized by an intracellular current injection (orange bar), and began firing at a constant frequency. An iontophoresis barrel positioned near the cell delivered the iontophoretic current (red bars).

was recorded. Ejections were monitored by FSCV using a method termed controlled iontophoresis, in which the ejection of an electroactive analyte is detected by the carbon fiber (Armstrong-James and Millar, 1980; Herr et al., 2008). Since glutamate is not electroactive, the iontophoretic solution also contained 3,4-dihydroxyphenylacetic acid (DOPAC). DOPAC had no effect on MSNs, but its oxidation on the carbon fiber served as an electrochemical marker for ejections (Kirkpatrick et al., 2016). This allowed the time-course of glutamate delivery and the relative ejection quantity to be determined.

Figure 5.7A displays the membrane potential of an MSN (black) during iontophoretic delivery (red bars). As the iontophoretic current was increased, the cell became increasingly depolarized and firing was initiated. This was due to a greater ejection concentration of glutamate, represented by the DOPAC oxidation current (7A, blue) and FSCV color plot in 7B. The time-course of the -30 nA ejection is shown in Figure 5.7C. Detection of the ejection marker occurred almost immediately after the iontophoretic current was initiated. Due to the time required for glutamate to reach the cell and act upon receptors, membrane depolarization was slightly delayed (Kirkpatrick et al., 2014). Cell firing occurred as the marker current peaked, and quickly ceased once it approached the pre-ejection quantity.

CONCLUSIONS

We have demonstrated how simultaneous patch clamp and FSCV measurements can be successfully incorporated into multi-modal investigations. Their combined use allows cell behavior to be examined concurrently with changes in the chemical, metabolic, and ionic environment. It was also determined that cells are not affected by

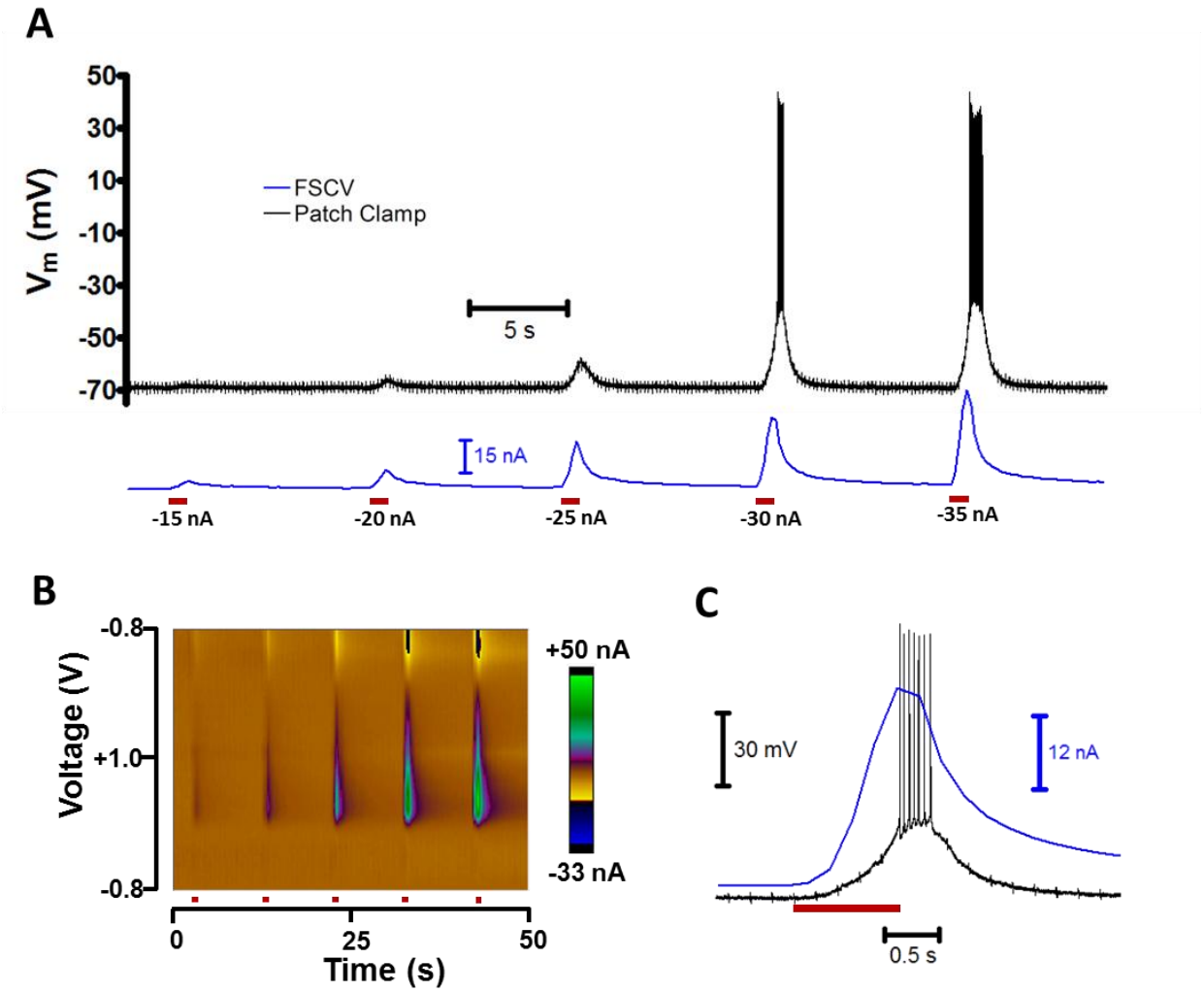

Figure 5.7 Concurrent FSCV and patch recordings during iontophoretic drug administration. (A) Physiological and chemical changes during iontophoretic ejections of glutamate and an electroactive marker. A multibarreled iontophoresis probe positioned ~10 µm from an MSN was used to perform 1 s ejections (red bars) of glutamate, an excitatory neurotransmitter, and DOPAC, the marker. A carbon-fiber electrode on the probe was used to perform FSCV, which detected the ejection of the marker (blue). The cell membrane potential (black) was recorded in a whole-cell current clamp. (B) Color plot of the FSCV current for ejections in A. (C) Time-course of -30 nA ejection in A.

exogenous electrical potentials and currents inherent to FSCV and iontophoresis. Collective use of these methods increases the power of neurochemical studies to correlate information across multiple domains.

REFERENCES

(2000) WPI Model 260 Instruction Manual. Sarasota, FL: World Precision Instruments.

(2008) 6400 Advanced Micro-Iontophoresis Current Generator Operating Manual. Minneapolis, MN: Dagan Corporation.

(2016) Neurophore BH-2 Micro-Iontophoresis System User's Manual. Hamden, CT: Harvard Apparatus.

Armstrong-James M, Millar J (1980) Quantification of noradrenaline iontophoresis. Nature 288:181-183.

Azdad K, Gall D, Woods AS, Ledent C, Ferre S, Schiffmann SN (2008) Dopamine D2 and Adenosine A2A Receptors Regulate NMDA-Mediated Excitation in Accumbens Neurons Through A2A-D2 Receptor Heteromerization. Neuropsychopharmacology 34:972-986.

Belle AM, Owesson-White C, Herr NR, Carelli RM, Wightman RM (2013) Controlled iontophoresis coupled with fast-scan cyclic voltammetry/electrophysiology in awake, freely moving animals. ACS Chem Neurosci 4:761-771.

Bloom FE (1974) To spritz or not the spritz: the doubtful value of aimless iontophoresis. Life Sci 14:1819-1834.

Bucher ES, Wightman RM (2015) Electrochemical Analysis of Neurotransmitters. Annu Rev Anal Chem 8:239-261.

Bucher ES, Brooks K, Verber MD, Keithley RB, Owesson-White C, Carroll S, Takmakov P, McKinney CJ, Wightman RM (2013) Flexible Software Platform for Fast-Scan Cyclic Voltammetry Data Acquisition and Analysis. Anal Chem 85:10344-10353.

Cepeda C, Galvan L, Holley SM, Rao SP, André VM, Botelho EP, Chen JY, Watson JB, Deisseroth K, Levine MS (2013) Multiple Sources of Striatal Inhibition Are Differentially Affected in Huntington's Disease Mouse Models. J Neurosci 33:7393-7406.

Galarreta M, Hestrin S (1999) A network of fast-spiking cells in the neocortex connected by electrical synapses. Nature 402:72-75.

Galli A, Blakely RD, DeFelice LJ (1998) Patch-clamp and amperometric recordings from norepinephrine transporters: Channel activity and voltage-dependent uptake. Proc Natl Acad Sci USA 95:13260-13265.

Gustafson N, Gireesh-Dharmaraj E, Czubayko U, Blackwell KT, Plenz D (2006) A Comparative Voltage and Current-Clamp Analysis of Feedback and Feedforward Synaptic Transmission in the Striatal Microcircuit In Vitro. J Neurophysiol 95:737-752.

Hafizi S, Kruk ZL, Stamford JA (1990) Fast cyclic voltammetry: improved sensitivity to dopamine with extended oxidation scan limits. J Neurosci Methods 33:41-49.

Heien MLAV, Phillips PEM, Stuber GD, Seipel AT, Wightman RM (2003) Overoxidation of carbon-fiber microelectrodes enhances dopamine adsorption and increases sensitivity. Analyst 128:1413-1419.

Henze DA, Borhegyi Z, Csicsvari J, Mamiya A, Harris KD, Buzsáki G (2000) Intracellular Features Predicted by Extracellular Recordings in the Hippocampus In Vivo. J Neurophysiol 84:390-400.

Herr NR, Wightman RM (2013) Improved techniques for examining rapid dopamine signaling with iontophoresis. Front biosci (elite edition) 5:249-257.

Herr NR, Kile BM, Carelli RM, Wightman RM (2008) Electroosmotic flow and its contribution to iontophoretic delivery. Anal Chem 80:8635-8641.

Ibáñez-Sandoval O, Tecuapetla F, Unal B, Shah F, Koós T, Tepper JM (2010) Electrophysiological and Morphological Characteristics and Synaptic Connectivity of Tyrosine Hydroxylase-Expressing Neurons in Adult Mouse Striatum. J Neurosci 30:6999-7016.

Johnson JA, Rodeberg NT, Wightman RM (2016) Failure of Standard Training Sets in the Analysis of Fast-Scan Cyclic Voltammetry Data. ACS Chem Neurosci 7:349-359.

Kachar B (1985) Asymmetric illumination contrast: a method of image formation for video light microscopy. Science 227:766-768.

Kawaguchi Y (1993) Physiological, morphological, and histochemical characterization of three classes of interneurons in rat neostriatum. J Neurosci 13:4908-4923.

Keithley RB, Mark Wightman R, Heien ML (2009) Multivariate concentration determination using principal component regression with residual analysis. TrAC, Trends Anal Chem 28:1127-1136.

Keithley RB, Takmakov P, Bucher ES, Belle AM, Owesson-White CA, Park J, Wightman RM (2011) Higher Sensitivity Dopamine Measurements with Faster-Scan Cyclic Voltammetry. Anal Chem 83:3563-3571.

Kirkpatrick DC, Edwards MA, Flowers PA, Wightman RM (2014) Characterization of Solute Distribution Following Iontophoresis from a Micropipet. Anal Chem 86:9909-9916.

Kirkpatrick DC, Walton LR, Edwards MA, Wightman RM (2016) Quantitative analysis of iontophoretic drug delivery from micropipettes. Analyst 141:1930-1938.

Lepora NF, Blomeley CP, Hoyland D, Bracci E, Overton PG, Gurney K (2011) A simple method for characterizing passive and active neuronal properties: application to striatal neurons. Eur J Neurosci 34:1390-1405.

Lu H, Hartmann MJ, Bower JM (2005) Correlations Between Purkinje Cell Single-Unit Activity and Simultaneously Recorded Field Potentials in the Immediately Underlying Granule Cell Layer. J Neurophysiol 94:1849-1860.

Michael A, Borland L (2007) Electrochemical Methods for Neuroscience. Boca Raton, FL: CRC Press.

Moser T, Chow RH, Neher E (1995) Swelling-induced catecholamine secretion recorded from single chromaffin cells. Pflügers Archiv 431:196-203.

Oberhauser AF, Fernandez JM (1996) A fusion pore phenotype in mast cells of the ruby-eye mouse. Proc Natl Acad Sci USA 93:14349-14354.

Oberhauser AF, Robinson IM, Fernandez JM (1996) Simultaneous capacitance and amperometric measurements of exocytosis: a comparison. Biophys J 71:1131-1139.

Ott H (1988) Noise Reduction Techniques in Electrochemical Systems, 2nd Edition. New York, NY: John Wiley & Sons, Inc.

Phongphanphanee P, Kaneda K, Isa T (2008) Spatiotemporal Profiles of Field Potentials in Mouse Superior Colliculus Analyzed by Multichannel Recording. J Neurosci 28:9309-9318.

Planert H, Szydlowski SN, Hjorth JJJ, Grillner S, Silberberg G (2010) Dynamics of Synaptic Transmission between Fast-Spiking Interneurons and Striatal Projection Neurons of the Direct and Indirect Pathways. J Neurosci 30:3499-3507.

Sakmann B, Neher E (1992) The Patch Clamp Technique. Sci Am 266:44-51.

Sheth SA, Nemoto M, Guiou M, Walker M, Pouratian N, Toga AW (2004) Linear and Nonlinear Relationships between Neuronal Activity, Oxygen Metabolism, and Hemodynamic Responses. Neuron 42:347-355.

Shi W, Sa N, Thakar R, Baker LA (2015) Nanopipette delivery: influence of surface charge. Analyst 140:4835-4842.

Swamy BEK, Venton BJ (2007) Subsecond Detection of Physiological Adenosine Concentrations Using Fast-Scan Cyclic Voltammetry. Anal Chem 79:744-750.

Takmakov P, McKinney CJ, Carelli RM, Wightman RM (2011) Instrumentation for fast-scan cyclic voltammetry combined with electrophysiology for behavioral experiments in freely moving animals. Rev Sci Instrum 82:074302.

Takmakov P, Zachek MK, Keithley RB, Bucher ES, McCarty GS, Wightman RM (2010) Characterization of Local pH Changes in Brain Using Fast-Scan Cyclic Voltammetry with Carbon Microelectrodes. Anal Chem 82:9892-9900.

Vergara R, Rick C, Hernandez-Lopez S, Laville JA, Guzman JN, Galarraga E, Surmeier DJ, Bargas J (2003) Spontaneous voltage oscillations in striatal projection neurons in a rat corticostriatal slice. J Physiol 553:169-182.

Vertes R, Stackman R (2011) Electrophysiological Recording Techniques, 1 Edition. New York City, NY: Humana Press.

Yamamoto K, Koyanagi Y, Koshikawa N, Kobayashi M (2010) Postsynaptic Cell Type–Dependent Cholinergic Regulation of GABAergic Synaptic Transmission in Rat Insular Cortex. J Neurophysiol 104:1933-1945.

Yusko EC, An R, Mayer M (2010) Electroosmotic Flow Can Generate Ion Current Rectification in Nano- and Micropores. ACS Nano 4:477-487.